Biotechnology Center

International Master's Program in Regenerative Biology and Medicine

Characterization of a novel *Nkx2-5* mutant mouse model for Congenital Heart Disease

A Thesis
By

Ricardo Moreno Traspas

Submitted in partial fulfillment of the requirements

for the degree of
Master of Science

Supervisor: Dr. Gonzalo del Monte Nieto

First Assessor: Prof. Dr. Richard P. Harvey

Second Assessor: Prof. Dr. med. Gerd Kempermann

Date of submission: 10/08/2017

Abstract

Nkx2-5 is a master transcription factor which plays important roles in gene regulatory networks controlling heart development, and whose mutations have been correlated with congenital heart defects in humans. This gene belongs to the NK-2 family of homeobox genes, characterized by the presence of the DNA-binding homeodomain. Whereas the function of the homeodomain has been deeply investigated, little attention has been paid to other conserved domains such as the NK2 Specific Domain (NK2SD). The Harvey Lab generated a novel transgenic mouse line in which the NK2SD domain was replaced by a glycine chain. Interestingly, NK2SD deletion in homozygosis resulted in embryonic lethality. Aiming to characterize the mutant phenotype of the defective embryos, we conducted an extensive study including wholemount embryonic phenotype analysis, and morphological, histological and molecular characterization of the cardiovascular defects. Our results showed a range of cardiac defects in the mutant embryos, including reduced heart size, atrioventricular and septal defects, and increased extracellular matrix. Moreover, results from the molecular analysis revealed aberrant gene expression affecting the right heart chambers and the interventricular septum. Overall, our study identified that the NK2SD mutant phenotype recapitulates some of the cardiac defects observed in *Nkx2-5*-related congenital heart disease patients, constituting a valid model for potential use in translational research.

Acknowledgments

Heartfelt thanks to Prof. Dr. Richard P. Harvey for giving me the great opportunity to join his research group and conduct my MSc thesis in a top Australian research center such as the Victor Chang Cardiac Research Institute (VCCRI), as well as for helpful discussions and suggestions.

I am profoundly grateful to Dr. Gonzalo del Monte Nieto for his brilliant supervision and guidance, his patience and time in teaching me the lab techniques and strategies used in this research, his expert advice and encouragement throughout the project, critical reading of the manuscript and all the support I received from him.

I would like to express my appreciation as well to Arne Adam for his invaluable help with the experiments and lab methodologies, all the rest of the Harvey lab members for their support and creating a nice working atmosphere which positively influenced my performance in the lab, Dr. Julie Moreau for kindly providing the *Nkx2*-5^{GFP} mouse line, and the BioCORE facility staff at the VCCRI for their essential and efficient animal work.

I would also like to acknowledge Prof. Dr. med. Gerd Kempermann for accepting being the second assessor of this thesis and his invaluable support to make my stay at the VCCRI possible.

Finally, this research would have been impossible without the unconditional support and love from my family and close friends, my sincere and big thanks to all of them.

This work was supported by funds from the VCCRI (Sydney, Australia), the Roland Ernst Foundation (Dresden, Germany), the Association of Friends and Sponsors from the Dresden University of Technology (Dresden, Germany) and the German Academic Exchange Service (DAAD) (Germany).

Table of Contents

List of Tables

List of Figures

Abbreviations

AP	Alkaline Phosphatase
ANF	ATRIAL NATRIURETIC FACTOR
AV	Atrioventricular
AVC	Atrioventricular Canal
BS	Blocking Solution
BSA	Bovine Serum Albumin
CHD	Congenital Heart Disease
ChIP	Chromatin Immunoprecipitation Assays
Csx	*Cardiac specific homeobox gene*
CX40	CONNEXIN40
DamID	DNA adenine methyltransferase identification
DIG	Digoxygenin
DNA	Deoxyribonucleic Acid
E	Embryonic Day
ECM	Extracellular Matrix
EMT	Epithelial-Mesenchymal Transition
EPDCs	Epicardial Derived Cells
ESCs	Embryonic Stem Cells
EtOH	Ethanol
GFP	Green Fluorescent Protein
Gja5	*Gap junction protein alpha 5*
Gly	Glycine

GRNs	Gene Regulatory Networks
HD	Homeodomain
Hey2	*Hairy/Enhancer-of-Split Related Protein 2*
H&E	Hematoxylin and Eosin
HRP	Horseradish Peroxidase
IAS	Interatrial Septum
ICM	Inner Cell Mass
IVS	Interventricular Septum
KO	Knockout
LA	Left Atria
LPM	Lateral Plate Mesoderm
LV	Left Ventricle
MABT	Maleic Acid Buffer Tween
Mest	*Mesoderm specific transcript*
MEST	MESODERM-SPECIFIC TRANSCRIPTION HOMOLOG PROTEIN
Mlc2v	*Myosin light chain 2v*
mRNA	Messenger Ribonucleic Acid
N1ICD	NOTCH1 Intracellular Domain
Neo	Neomycin
NK2SD	NK2-Specific Domain
NKE	NK Element
Nppa	*Natriuretic peptide A*
OFT	Outflow Tract
ON	Overnight

PBS	Phosphate Buffer Saline
PBT	PBS containing 0.1% Tween-20
PCR	Polymerase Chain Reaction
PHF	Primary Heart Field
PFA	Paraformaldehyde
RA	Right Atria
RT	Room Temperature
RT-qPCR	Real Time Quantitative Polymerase Chain Reaction
RV	Right Ventricle
RNA	Ribonucleic Acid
RNA_{seq}	Ribonucleic Acid Sequencing
SDS	Sodium Dodecyl Sulfate
SEM	Standard Error of Mean
SHF	Secondary Heart Field
SMA	Alpha Smooth Muscle Actin
SRF	SERUM RESPONSE FACTOR
SSC	Saline Sodium Citrate
TF	Transcription Factor
TN	*tin*/*Nkx2-5*
TSA	Tyramide Signal Amplification
VCCRI	Victor Chang Cardiac Research Institute
YRD	Tyrosine-Rich Domain
WT	Wild Type

1. Introduction

1.1. The Heart

The mammalian heart is a highly modified muscular vessel which pumps blood through the circulatory system, the most important transport system in vertebrates. The blood vessels not only provide tissues with oxygen and nutrients and assist in the removal of metabolic waste, but is also involved in hemostasis, defense against toxins and pathogens thanks to the humoral and cellular immune systems, transport of hormones and other relevant signaling molecules, and the regulation of the body temperature, water electrolytes, blood pH and mineral household. Therefore, the heart as the biological pump allowing blood circulation plays a crucial role in maintaining the proper homeostasis of the whole organism. Its importance is highlighted by the fact that defects in normal cardiac function have severe consequences in the well-being of the organism, which can be dramatic and life threatening in many cases.

Anatomically, the heart is located in the middle of the mediastinum, at the level of the thoracic vertebrae T5-T8 in humans. It lies between both lungs, above the diaphragm and underneath the sternum and the rib cartilages. The back surface of the heart sits near the vertebral column, but separated by the esophagus and the aorta. The heart is cone-shaped, with its base positioned upwards and tapering down to the apex. The left part of the heart is larger and slightly offset to the left side of the chest.

1.1.1. The Heart Chambers

In archosaurs (crocodilians and birds) and mammals, the heart is divided into four chambers: left (LA) and right (RA) atria, where the blood ingresses the heart, and left (LV) and right (RV) ventricles, involved in pumping the blood out of the heart (**Figure 1A**). The interatrial septum (IAS) separates the atria and the interventricular septum (IVS) is the boundary for the ventricles (**Figure 1A**). The IVS is thicker than the IAS since the ventricles generate a bigger pressure when they contract. Therefore, the heart is divided in two circuits in solitary confinement: the right heart, comprising the RA and the RV, and the left heart, comprising the LA and the LV (**Figure 1A**). The deoxygenated blood coming from the body's tissues reaches the RA through the superior and the inferior venae cavae, then enters the RV and is ejected to the lungs through the pulmonary trunk which branches into the left and the right pulmonary arteries. The LV receives

oxygenated blood from the lungs through the pulmonary veins, which then passes to the LV from where is pumped to the whole organism through the aorta [2].

The region between atria and ventricles is made by dense connective tissue, it not only separates the atria from the ventricles (**Figure 1A**), it also functions as an important boundary for the heart's electrical conduction system. Furthermore, it contains the atrioventricular (AV) valves, highly specialized cardiac tissue involved in the regulation of blood flow between atrium and ventricles. The AV valves separate the cardiac chambers of each heart region: the tricuspid valve in the right heart, and the mitral or bicuspid valve in the left heart. There are other two additional semilunar valves which sit at the exit of each of the ventricles associated to the main arterial vessels: the pulmonary valve at the base of the pulmonary artery in the RV, and the aortic valve at the base of the aorta in the LV. The cardiac valves ensure the unidirectional flow of the blood in the heart [2].

The four-chambered heart and its division in two completely isolated blood circuits allows archosaurs and mammals to have a double circulatory system in which oxygenated and deoxygenated bloods are not mixed. This complete separation between the systemic and the pulmonary circulation ensures body tissues to receive oxygen-saturated blood which facilitates sustained muscle movement and allows warm-blooded animals to achieve thermoregulation. Moreover, the blood is pumped from the heart to the organism at a higher pressure, what results in a faster blood flow [2].

1.1.2. The Pericardium

The heart is encapsulated inside the rib cage and protected by the pericardium, a double-membraned fibroserous sac, that ensures the anchoring of the heart in its proper position in the mediastinum. The fibrous pericardium is the most superficial layer, made up of dense and loose connective tissue, whereas the serous pericardium is fused to the fibrous pericardium and is formed by a single layer of connective tissue cells. The space in between the heart and the pericardium is called the pericardial cavity and contains the pericardial fluid, which provides lubrication as well as cushioning and protection [2].

1.1.3. The Heart Wall

The heart wall is formed by three layers: the inner layer called endocardium, the middle layer called myocardium, and the outer layer called epicardium (**Figure 1B**).

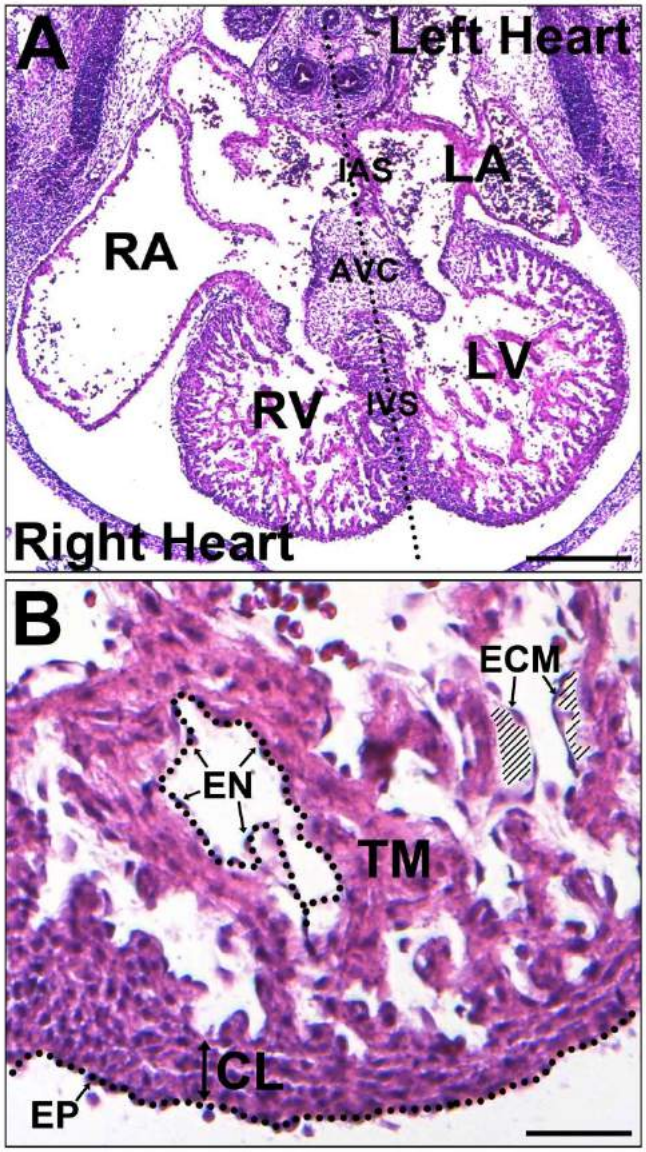

Figure 1. Basic Heart Histological Morphology.

(A) H&E section of a E12.5 mouse heart in low magnification (5x), in which the main cardiac regions are indicated. The dotted line delimitates the separation between the right and the left hearts. (B) H&E section of the cardiac wall in a E12.5 mouse heart in high magnification (10x), in which the different histological layers are indicated. The dotted lines highlight the contours of the endocardial and epicardial layers. The parallel black lines highlight the area between the endocardium and the myocardium full of ECM. AVC: atrioventricular canal; CL: compact layer; ECM: extracellular matrix; EN: endocardium; EP: epicardium; IAS: interatrial septum; IVS: interventricular septum; LA: left atria; LV: left ventricle; RA: right atria; RV: right ventricle; TM: trabecular myocardium. Scale Bar (A): 390 μm; Scale Bar (B): 5 μm.

The Epicardium

The epicardium, also known as the visceral layer of the pericardium in the medical field, lies in close contact with the myocardium (**Figure 1B**). It is formed by a monostratified layer of mesoepithelial cells overlying loose connective tissue, as well as elastic fibers and adipose tissue. Importantly, the nerves and blood vessels of the heart reach the cardiac tissue through the epicardium. The nerves are important for the of control of the heartbeat, whereas the cardiac blood vessels, known as coronary arteries, branch out from the base of the aorta and irrigate the cardiac tissue providing most part of the nutrients and the O_2 [2].

The Myocardium

The myocardium or cardiac muscle is an involuntary striated muscle formed by cardiomyocytes, mononuclear myocardial cells, contractile and ramified. Cardiomyocytes form what is known as cardiac syncytium: an electrochemical network of cells which enables the rapid transmission of the electrical impulses and, thus, the coordinated contraction of the myocardium. This is possible thanks to the intercalated discs, specialized structures which connect cells physically, chemically and electrically. They allow action potential to spread between adjacent cardiomyocytes by permitting the free passage of ions. There are two independent syncytiums in the heart separated by the isolating tissue of the atrioventricular canal (AVC): the atrial myocardial unit and the ventricular myocardial unit [2].

The myocardium also contains two other specialized cell types that form the heart electrical conduction system: the pacemaker cells and the cells from the specialized conduction tissue. The pacemaker cells are small cells located in the sinoatrial node which generate spontaneous action potentials that regulate the cardiac rate, but they do not contribute to the contractile force of the heart. On the other hand, the cells from the specialized conduction system form the AV node, the His bundle and the Purkinje fibers. They transmit fast and efficiently the electrical impulse generated by the pacemaker cells, from the atrium to the ventricles [2].

Histologically, the ventricular myocardium is organized in two clear regions: the compact layer and the trabecular myocardium (**Figure 1B**). The compact layer forms the outer wall of the RV and the LV and displays a relatively constant thickness. The trabecular myocardium, located in the luminal side of the ventricular wall, refers to the rounded or irregular sponge-like myocardial tissue that projects from the compact layer to the chamber lumen in the LV and the RV. The

trabecular myocardium morphology is important to avoid suction that would happen with a flat surface and thus improves the efficient pumping of blood from the heart [2].

The Endocardium

The endocardium is the innermost layer of the heart, made up of a lining of simple squamous epithelium which covers the luminal side of the myocardium in the four cardiac chambers and also the valves (**Figure 1B**). It can be in close contact with cardiomyocytes or separated by extracellular matrix (ECM) which varies in thickness (**Figure 1B**). The endocardial cells are biologically and embryologically similar to the endothelial cells lining the blood vessels of the body. Indeed, the endocardium is continuous with the endothelium of the veins and arteries of the heart. It acts as a barrier, provides a non-thrombogenic surface to avoid blood clotting in the heart and is also involved in controlling contractility and the electrophysiological environment of the myocardium by the secretion of endothelins [2].

1.2. Mouse Heart Development

The heart is the first organ to develop and function in the embryo highlighting its critical role in supplying the early developing embryo with the oxygen and nutrients to fulfill its fast increasing metabolic demand. Heart development in all vertebrates, from fish to humans, follows similar general processes. Much of the knowledge on this field has been generated using animal models. Most of the original research in the area of cardiac development was conducted and chicken embryos, mainly due to their easy manipulation inside the egg. However, the rapid progression of transgenic technologies has made the mouse (*Mus musculus*) and zebrafish the prominent model organisms in which to study normal and abnormal cardiovascular development.

Murine cardiovascular structure and physiology is similar to humans. Systematic comparative analysis of mouse and human fetal cardiovascular development has proved that cardiac developmental sequences in normal mouse and human embryos are comparable, with only minor differences in atrial and venous morphology [3]. This evidence strongly supports the suitability of the mouse as a good model to study heart development with the aim to extrapolate the knowledge generated to better understand human heart development. Other advantages of using mice in this research field include the fact that embryos, tissues and derived primary cells are accessible at all stages of embryonic development for detailed molecular, cellular, structural and physiological analysis. Moreover, there is a wide range of genetic manipulations that can be achieved in the

mouse, allowing the study of the consequences of single gene mutations in a uniform genetic background. Thanks to research using transgenic mouse models, important information has been collected about genetic regulatory networks (GRNs) governing cardiovascular development and the impact of genomic mutations in congenital heart defects in humans. Importantly, these studies are the first step for conducting translational research with potential applications in the clinical setting.

1.2.1. From Fertilization to Gastrulation (E0.0 – E7.5)

The zygote formed upon fertilization undergoes rapid rounds of cell division, progressing to morula (embryonic day (E) 2.0) and eventually to blastula (E3.0). The blastocyst is formed by 16-40 compacted cells in which it is possible to distinguish two main regions: the inner cell mass (ICM), formed by mesenchymal cells which will give rise to the whole organism, and the trophectoderm, which surrounds the ICM and is formed by epithelial polarized cells which will form extraembryonic structures. The implantation of the blastocyst in the endometrium of the uterus (E4.0) triggers the ICM cells to start dividing and proliferating to end up forming a bilaminar embryonic disc, composed of two cell layers: the hypoblast, which will give rise to the extraembryonic endoderm, and the epiblast, with a cap shape and formed by epithelial-like cells which will form the rest of the embryonic tissues.

After implantation the embryo undergoes gastrulation (E5.5-E6.5), a remarkable process which starts at the posterior region of the epiblast and ends up generating the trilaminar embryo. The first event in the gastrulation process is the formation of the primitive streak along the midline of the bilaminar embryonic disc, which expands to create the primitive node at its cranial end and defines the major body axis of the embryo. Epiblast epithelial cells undergo epithelial-mesenchymal transition (EMT) and migrate inwards towards the primitive streak, detaching from the epiblast and migrating beneath it. This process culminates with the formation of the 3 distinct primary germ layers of the embryo proper: endoderm, mesoderm and ectoderm. Importantly, each region of the primitive streak receives a specific morphogen signature coming from the node and the extraembryonic tissues. This differential signaling stimulation patterns the embryo along the rostro-caudal axis and determines the different tissues and structures which will be generated from the 3 germ layers. The heart is derived from the mesodermal germ layer, specifically from the splanchnic (ventral) lateral plate mesoderm (LPM) overlying the endoderm [4, 5].

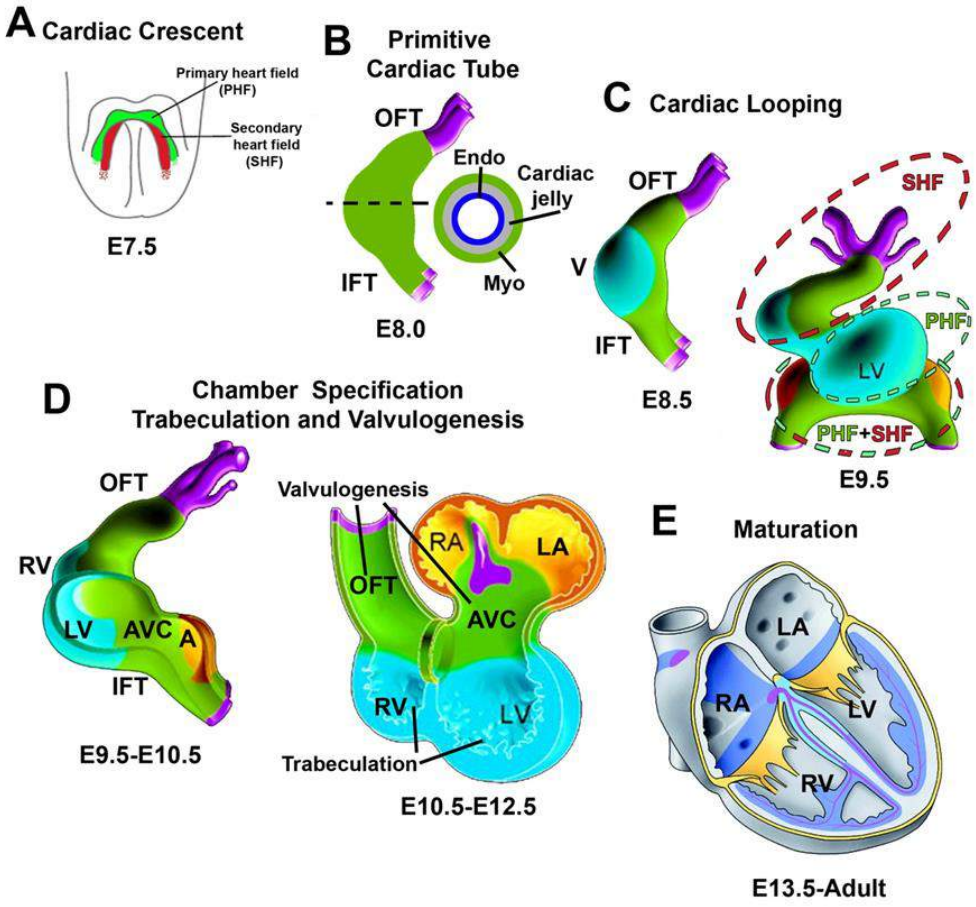

Figure 2. Schematic Representation of Cardiac Development.

(A) Ventral view of the cardiac crescent at E7.5. Cardiogenic progenitors form a crescent in the midline region of the embryo, in which it is possible to distinguish the primary heart field (PHF, light green) and the secondary heart field (SHF, red). (B) Primitive cardiac tube at E8.5, composed by an inner layer of endocardium (endo, dark blue) and an outer layer of myocardium (myo, dark green), separated by a type of ECM known as cardiac jelly (light blue). (C) Initiation or cardiac looping at E8.5. The heart tube evolves from a straight tube to a twisted one. The process is mediated by the ingression of SHF cardiac progenitors from both poles. (D) Chamber specification, trabeculation and valvulogenesis from E9.5 to E12.5. The process of valvulogenesis takes place in the inner curvature, whereas ventricular trabeculation occurs in the outer curvature. (E) Heart maturation from E13.5 onwards. Heart septation is completed. A: atrium; AVC: atrioventricular canal; Endo: endocardium; IFT: inflow tract; LA: left atria; LV: left ventricle; Myo: myocardium; OFT: outflow tract; PHF: primary heart field; RA: right atria; RV: right ventricle; SHD: secondary heart field; V: ventricular chamber. Taken without any changes from Del Monte-Nieto G. *et al.* (2011) [1].

Blastodermal cardiogenic precursors have been identified already in the rostral epiblast, at both sides of the primitive streak. After ingression through the primitive streak, cardiogenic precursors form two bilateral cardiogenic fields which rapidly migrate laterally and cranially in response to endodermal signals (E7.5) [4]. They end up merging in the cephalo-medial region of the splanchnic mesoderm, forming a continuous crescent-shaped cuboidal epithelium in which independent fields are no longer identifiable (**Figure 2A**) [4, 5]. This region has traditionally been referred to as the "cardiac crescent" and is formed by cardiogenic progenitors from the so-called Primary Heart Field (PHF) (**Figure 2A**) [4, 6]. The PHF will form the primary heart tube and contribute to the LV, AVC and parts of the atria [4, 6]. Importantly, there is a second population of cardiogenic precursors, known as the Second Heart Field (SHF), which lies medial and caudal to the cardiac crescent (**Figure 2A**) [4, 6]. This field will end up forming the RV, OFT, sinus venosus and parts of the atria [4, 6].

1.2.2. Formation of the Heart Tube (E7.5 – E8.0)

The heart primordium arises predominantly from the cardiac crescent within the splanchnic mesoderm [4, 5]. Cardiogenic precursors from the PHF progress to form a primordial plate at the cranial border of the embryonic disc [4, 6]. The splitting of the LPM into somatic and splanchnic mesoderm had formed the pericardial coelom, although at this stage the cardiac plate is still positioned inferior to the presumptive pericardial cavity. Cord-like masses of myocardial progenitors intermingled with a plexus of endothelial strands, located ventral to the pericardial coelom, start growing and elongating [4, 5]. They are known as angioblastic cords and end up canalizing to form the bilateral right and left endocardial tubes, aligned in a parallel fashion with each other in the middle region of the embryo. The dorsal aortae develop alongside the endocardial heart tubes and form a connection (the first aortic arch) with the tubes prior to their fusion [4, 5]. The massive growth of the cranial end of the neural tube when forming the brain, coupled with the invagination of the endoderm to generate the foregut, leads to the lateral folding of the embryo. This folding process allows the fusion of the endocardial heart tubes across the ventral midline, beginning cranially and extending caudally [4, 5]. The resulting cardiac tube has a rostral arterial pole (aortic sac) and a caudal venous pole (right and left sinus horns) (**Figure 2B**), and is placed between the newly formed foregut and the pericardial space which eventually ends up surrounding the whole heart tube.

At the same time the fusion of the endocardial tubes is happening, endothelial cells coming from both sides of the developing embryo start forming the lumen of the newly generated primordial

heart tube [4, 5]. These cells constitute the internal endocardial layer, which is enveloped by the primordial myocardial sleeve of the heart tube (**Figure 2B**). Nevertheless, the myocardium still does not completely surround the endothelial tube and retains continuity with the splanchnic mesoderm of the developing mediastinum through the dorsal mesocardium [4, 5]. Between the endocardial and the myocardial layers there is a space filled with a gelatinous ECM known as cardiac jelly (**Figure 2B**) [4, 5, 7].

At this point, cardiomyocyte progenitors differentiate into myocardial cells, allowing the heart tube to start beating. At first the contractions are irregular, but by E9.0 a regular heartbeat is established [4, 5]. The venous pole acts as the initial pacemaker, and the wave of muscle contraction propagates along the whole tubular heart [4, 5, 8].

1.2.3. Development and Looping of the Heart Tube (E8.0 – E9.5)

At this stage (E8.0) the heart is positioned in the center of the embryo and displays bilateral symmetry, taking the shape of an inverted Y. The two arms of the Y are positioned downwards and present continuity with the developing venous tributaries of the embryo, as well as with the yolk sac and placenta. Cells from the SHF, located posterior to the dorsal wall of the developing pericardial cavity, ingress into the cardiac region and contribute to the development of the cranial pole of the heart (**Figure 2C**) [4, 9, 10]. Those cells entering from the arterial pole give rise to the RV primordium and the outflow tract (OFT) (**Figure 2C**), which connects the RV with the arteries which arise from the aortic sac and extend into the pharyngeal arches [4, 9, 10]. On the other hand, those cells entering from the venous pole populate some regions of the atrium (**Figure 2C**) [4, 9, 10]. Therefore, by this time the heart tube contains all the components of the definitive cardiac chambers. At E9.0 the proepicardium develops at the sinus venosus region and releases cell clusters to the pericardial cavity that will attach the myocardial wall and spread cranially over the myocardium forming the epicardial layer [11-13].

SHF cell ingression from both poles results in the elongation of the primary heart tube (**Figure 2C**) [4, 5]. As a consequence of this growth, the mesocardium initially tethering the developing LV to the mediastinum is disrupted. Hence the larger part of the tube is liberated, which makes the tube itself bend to the right (**Figure 2C**) [4, 5]. This process, called cardiac looping, starts at around E8.5 and ends at E10.5 representing the first visual evidence of asymmetry in the developing embryo. During cardiac looping, the ventral wall of the former primitive heart tube becomes the outer curvature, and the dorsal wall becomes the inner curvature (**Figure 2C**) [4, 5].

1.2.4. Formation of the Cardiac Chambers (E9.5 – E10.5)

At the end of E9.5 the symmetrical arms of the primitive heart tube are incorporated caudally into the heart, thereby forming a prominent junctional component between the primary atrial component and the LV: the AVC (**Figure 2D**) [4, 5, 14]. The venous tributaries drain to either side of the newly formed atrium through the right and left sinus horns in a symmetrical fashion. In the last stage of cardiac looping (E9.5 – E10.5), the primitive heart tube within the pericardial cavity can already be divided in different areas corresponding to the OFT, the ventricular chambers, the AVC and the atrium (**Figure 2D**) [4, 5]. The heart receives blood from the systemic venous tributaries, which are embedded in the tissues of the posterior mediastinum and drain directly into the primary atrium. The blood flows traverse the entire ventricular loop until reaching the OFT, from where it is pumped out of the heart to the circulatory system.

At E9.5 ventricular trabeculation becomes histologically evident, although this process already started at E8.5. It occurs in the outer curvature chamber myocardium, which undergoes regional proliferation and differentiation to give rise to protrusions projected to the ventricular lumen, known as trabeculae (**Figure 2D**) [4, 15]. They will progress until forming a spongy-like structure, important for increasing the pumping efficiency of the heart during the first developmental stages. Trabeculation also takes place in the atrial chambers, but it happens later in development.

1.2.5. Heart Chambers Development (E10.5 – E13.0)

From E10.5, the myocardial cells from the outer curvature, induced by morphogens secreted from the forming epicardium, extensively proliferate thickening the ventricular wall and forming the compact myocardium. The atrium expands on both sides of the developing arterial pole, whereas the ventricular chambers grow in the ventricular loop along the outer curvature [5, 16, 17]. Ventricular trabeculae keep growing until E14.5 when they undergo a simplification process that contributes to the thickening of the compact layer in a process called compaction (**Figure 2D**). They will also contribute to the papillary muscles which support the tricuspid and mitral valves, part of the IVS, and the Purkinje fibers from the peripheral cardiac conduction system [4, 15].

In contrast, the inner curvature is composed of non-chamber tissue which forms the myocardium of the valves and the septum (**Figure 2D**). Valvulogenesis already started at E9.0 in the AVC region, where the myocardium secretes increased amount of ECM. The thickening of the cardiac

jelly results in the formation of the so-called endocardial cushions [18]. In addition, the endocardium lining the valvular primordium undergoes EMT and colonizes the endocardial cushions to end up forming the valvular mesenchyme [18, 19]. This tissue together with the endocardium lining the cardiac cushion and the addition of other cell types from extracardiac sources such as neural crest cells and epicardial derived cells (EPDCs), will form the four cardiac valves and also the IVS and IAS (**Figure 2D**) [20]. The IAS closes at E12.0 and the IVS at E13.0, moment in which the systemic and the pulmonary circulations are completely isolated in the developing embryo (**Figure 2E**) [2, 5, 17].

During these stages, the coronary vessels which irrigate the heart start forming. To understand its origin, we need to go back to E9.5-E10.0 when the epicardium starts forming along the myocardial surface. At the same time this process happens, an ECM known as subepicardium forms in between both tissue layers in the AV and interventricular grooves, both locations where the highest number of coronary vessels will form [21]. After subepicardium formation, epicardial cells from the AV groove, the ventricles and the OFT (but not from the atrium) undergo EMT and cellularize this newly formed ECM [21, 22]. These cells are known as EPDCs and have been identified as the progenitors for the muscular, fibroblastic and endothelial layers of the coronary vessel, also contributing to the AVC mesenchyme as mentioned before [21-23]. Finally, EPDCs migrate into the compact myocardium where the coronary vessels will develop by a combination of vasculogenesis (a primary plexus is initially formed with no connection with systemic circulation) and angiogenesis (the arterial coronary plexus connects with the body blood circuitry) [24].

During the last stages of fetal development, the whole heart undergoes growth and maturation (**Figure 2E**). The valves keep maturing and sculpting until giving rise to the adult valves just before birth (**Figure 2E**).

1.3. Gene Regulatory Networks and the Cardiac Kernel

Development of animal body plans occurs under a highly controlled genomic program, which proceeds by the progressive installation of transcriptional regulatory states in embryonic space and time. The underlying mechanism is the localized expression of regulatory genes encoding sequence-specific transcription factors (TFs) at specific times and places [25]. TFs bind target clusters of deoxyribonucleic acid (DNA) sequence elements, such as enhancers, silencers and insulators, known as cis-regulatory modules [25]. The activation of a particular cis-regulatory

module produces a specific pattern of gene expression in space and/or time, and the combinatorial activation of multiple modules can result in complex patterns of gene expression [25].

The regulatory inputs and functional outputs of developmental control genes constitute large network-like architectures known as gene regulatory networks (GRNs) [25, 26]. These networks are logic maps that consist on the functional linkages among regulatory genes, cis-regulatory DNA modules and genes that express remarkable components of signaling pathways [26]. GRNs structure is modular and hierarchical, and can be dissected in multigenic subcircuits of various forms with specific and distinct regulatory functions in the process of development [26].

Evolution of the mammalian heart from a simple contractile tube used in ancestral species for nutrient dispersal into a complex, multi-chambered organ as seen in mammals, relied in conserved GRNs. The cardiomyocyte GRN is controlled by lineage-restricted TFs, which interact to form a recursively wired sub-network termed the cardiac "kernel" [26]. Importantly, the kernel is inviolate in terms of the evolution of cardiac structures, as the removal of one component of the kernel leads to catastrophic effects on heart development [26]. Moreover, this fundamental genetic circuitry is relatively inflexible along evolution despite the evident morphological variation in the hearts of different phyla [26].

TFs part of the cardiac kernel are deeply conserved during evolution, display regional restricted patterns of expression in cardiac progenitor cells and differentiating lineages, and establish large and complex cross-regulatory networks [26, 27]. These cardiac TFs include GATA4/6, ISL1, MEF2C, TBX5, TBX20, SERUM RESPONSE FACTOR (SRF) and NKX2-5 [26, 27]. Importantly, their individual knockout (KO) phenotypes are catastrophic for early heart development, although none of them completely blocks heart formation [28-31]. Although all these individual KO phenotypes have in common defective tissue growth and patterning resulting in arrested cardiac development, each of the phenotypes show particular and distinct features [28-31]. This observation indicates that cardiac TFs carry out overlapping but also unique roles within the kernel. All together, they act as selector proteins which define cardiac-specific territories in the developing embryo and provide the combinatorial coding which guides the whole process of heart development [27]. Interestingly, certain combinations of cardiac TFs involving GATA4, TBX5 and MEF2C, plus additional micro-ribonucleic acids (micro-RNA) and/or small molecules modulating signaling and epigenetic states, are sufficient to reprogram non-cardiac embryonic and adult cells to cardiomyocytes [32, 33]. This is a clear evidence of the relevance of these TFs in defining cardiac fate.

1.4. NKX2-5

NKX2-5 is a well-studied TF which sits at the very top of the cardiac kernel and plays an early and critical role in development of the heart and heart-like organs of diverse species. Loss of NKX2-5 in mice results in embryonic lethality, whereas in humans *Nkx2-5* mutations are one of the most common causes of congenital heart disease (CHD).

1.4.1. *Nkx2-5* Ontology and Protein Structure

Nkx2-5, also referred to as *Cardiac specific homeobox gene* (*Csx*), belongs to the homeobox gene superfamily, a vast group of genes encoding for series of transcriptional regulatory proteins that act at critical points in development and ontogeny [34, 35]. The hallmark of these genes is the presence of the homeobox, which encodes for the homeodomain (HD) present in all these TFs (**Figure 3A**) [35, 36]. This HD is a sequence-specific DNA-binding motif of 60 amino acids, structurally conserved in all proteins from the family [35, 36]. Importantly, HD genes have been maintained throughout evolution as a highly conserved genetic unit. Functionally homologous homeobox genes with conserved structure, expression patterns and timing of gene activation have been described across species [37]. For instance, this is the case of the well-characterized *HOM-C* gene complex in *Drosophila* and the *Hox* gene clusters in mammals [38].

Nkx2-5 was first identified in screens for mouse homologs of the *tinman* gene from *Drosophila*. Both genes belong to the NK-2 class of HD genes, also first identified in *Drosophila*. NK-2 HDs are characterized by the presence of a tyrosine at position 54, which is not found at this position in other HDs [39]. This domain forms the conserved helix-loop-helix motif that mediates DNA association in all HDs, thereby making the third helix of the motif to lie in the major groove of the DNA helix [40]. Moreover, NK-2 HDs display highly similar DNA-binding specificities [39]. The NK-2 DNA binding site is known as NK element (NKE) and is found in many cardiac promoters [37]. Importantly, specifically in NKX2-5 the HD also functions as a protein-protein interface which mediates interactions with many other cofactors and TFs [37], some of them at a similar level in the cardiac regulatory hierarchy such as GATA4, TBX5, TBX20 and SRF.

The NK-2 family can be grouped into 3 classes based on the presence of two additional conserved domains [37]: the *tin*/*Nkx2-5*-domain (TN-domain) and the NK-2 Specific Domain (*NK2SD*). Class I NK-2 proteins such as NKX2-5 contain both domains (**Figure 3A**), class II proteins such as *tinman* contain only the TN-domain, and class III members have neither of these domains. The

evolutionary constraints preserving these two protein domains, both present in NKX2-5, suggest their critical role for the proper function of this TF.

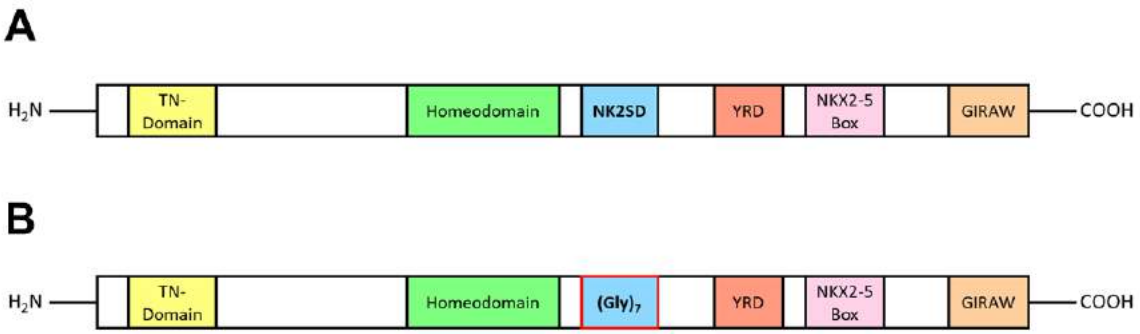

Figure 3. NKX2-5 Protein Structure. (A) Schematic representation of the NKX2-5 TF in which the main conserved protein domains are indicated. (B) Structure of the NKX2-5$^{\Delta NK2SD}$ protein, in which the NK2SD domain has been replaced by a Gly chain (highlighted in red). NK2SD: NK-2 Specific Domain; TN-Domain: tin/Nkx2-5-domain; YRD: Tyrosin-Rich Domain.

The TN-domain is highly conserved in the majority of NK-2 proteins (class I and class II). It is located in the amino-terminus (**Figure 3A**) and shares homology with the EH-1 repressor domain found in the *Drosophila* engrailed HD TF [41]. The TN-domain is not exclusive of the NK-2 protein family, but also present in many other TF families such as forkhead, zinc-finger and T-box [41]. In NK-2 proteins, this domain mediates interactions with members of the Groucho family of co-repressors [42, 43]. However, there is also data supporting a positive effect of the TN-domain on activating transcriptional processes [44]. Therefore, this domain functions in a modular and context-dependent manner, mediating interactions with co-activator and/or co-repressor proteins.

The *NK2SD* domain is exclusively specific of the class I NK-2 family of HD proteins [39]. It is found carboxyl-terminal to the HD (**Figure 3A**), separated by a short proline-rich linker polypeptide of 9-32 amino acids [37, 39, 45]. The hallmark of this domain is the hydrophobic core sequence (V/I-A-V-P-V-L-V), together with a proline-rich region and flanking basic amino acids [39, 46]. The role of the *NK2SD* domain is still not well characterized. It is known that is not required for sequence-specific DNA binding [39]. Some insights have been obtained from studies in other NK-2 family members. In *Nkx2-2*, the *NK2SD* domain has been reported to act as

an intramolecular transcriptional repressor which inhibits the C-terminal transactivation domain [46]. Studies on *vnd* gene revealed *NK2SD* favors the interaction between the TN-domain with Groucho co-repressors [47]. Finally, *Nkx3.2* executes a repressing effect on gene expression by binding phospho-Smad1 through the *NK2SD* domain, which in turn recruits histone deacetylase HDAC1 [48]. However, no data is available yet on the specific function of this domain in NKX2-5, and further research is required to elucidate the importance of *NK2SD* in this cardiac kernel TF.

Three additional domains are found in the NKX2-5 protein which share homology with regions present in other proteins subsets of the NK-2 family: GIRAW, *Nkx2-5* box and a tyrosine-rich domain (YRD) (**Figure 3A**). The function of these motifs is not well-known. The YRD domain is found C-terminal of the *NK2SD* domain (**Figure 3A**) in a vast number of NK-2 proteins [49]. Research has revealed that this domain is essential for NKX2-5 function during cardiogenesis and can act in some cases as a transcriptional activator domain [49]. GIRAW is the most carboxyl-terminal domain (**Figure 3A**), believed to be involved in protein-protein interactions, although there is still no data supporting this hypothesis [50]. The *Nkx2-5* box, situated in between YRD and GIRAW (**Figure 3A**), has completely unknown function [50].

1.4.2. *Nkx2-5* Gene Expression Pattern

Nkx2-5 is the only NK-2 gene which shows continuous expression throughout the whole process of heart development. In the mouse, *Nkx2-5* is expressed continually in the forming myocardium of the developing heart [51], already starting at E7.0 throughout the first and second heart fields located in the anterior splanchnic mesoderm of the epiblast [52]. However, *Nkx2-5* transcripts are missing in late embryonic stages in the sinoatrial node and the forming myocardium of the sinus horns [53], which will evolve to form the right and left caval veins and the sinus venarum. *Nkx2-5* remains abundantly expressed in adult hearts [51].

The expression of this TF is not exclusively restricted to the heart during embryonic development. *Nkx2-5* is also initially expressed in the pharyngeal endoderm overlying the lateral cardiac progenitor pools [51]. As development evolves and the foregut closes, *Nkx2-5* expression is limited to the pharyngeal floor, dorsal to the developing heart tube, until E9.5 [51]. Then the expression is gradually lost, and only remains maintained in the thyroid primordium, a derivative from the pharyngeal floor [51]. *Nkx2-5* is also expressed in tongue myocytes, mesenteric tissues, the splenic stroma and the distal region of the stomach [51].

1.4.3. The NKX2-5 Role in Heart Development - The *Nkx2-5* KO Mouse Model

Conventional and conditional *Nkx2-5* KOs have been generated in order to elucidate the function of this gene. The first approach was to disrupt the *Nkx2-5* locus by the introduction of a neomycin resistance cassette into the homeobox [28]. Other mouse transgenic lines following other KO strategies were later created to further confirm the *Nkx2-5* null phenotype, such as the entire replacement of the *Nkx2-5* gene by LacZ sequences [54] or the insertion of a GFP cassette after the first 35 amino acids of the protein [55].

Homozygous *Nkx2-5* null embryos in all mouse lines showed an uniform phenotype, characterized by early embryonic lethality at E9.5 due to hemodynamic insufficiency [28, 54, 55]. Unexpectedly, *Nkx2-5* was not essential for the initial specification of cardiomyocytes and the formation of the primitive and linear heart tube. These findings contrast with the phenotype observed in *Drosophila tinman* mutants, which completely lack any cardiac tissue [56, 57]. Nevertheless, cardiogenesis in the *Nkx2-5* null mouse embryos is blocked at the looping stage [28]. Mutant hearts showed a truncated and narrower OFT and a primitive and linear primary chamber which could not support chamber maturation [28, 54, 55]. The expansion and progression of the RV and LV is defective, indicating that dorsal-ventral patterning is impaired [28, 54, 55]. The cardiac myocardium derives from areas of the outer curvature of the primitive heart tube. Outer curvature markers which should be expressed in the LV myocardium, such as *Natriuretic peptide A* (*Nppa*) and *Myosin light chain 2v* (*Mlc2v*), are absent in *Nkx2-5* null hearts [28, 54, 55]. Therefore, *Nkx2-5* is necessary for the proper differentiation of the outer curvature into the working myocardium. Moreover, decreased expression levels of HAND1 were found in these mutants [58], a key cardiac TF which plays a critical role in controlling the balance between proliferation and differentiation of myocardial precursors. As expected due to the position of *Nkx2-5* on top of the cardiac kernel, other numerous markers and cardiac genes have also been described dysregulated in these hearts [28, 54, 55]. Overall, all these findings prove the critical role of *Nkx2-5* for the correct interpretation of early patterning information received by myocardial progenitors during cardiogenesis.

In *Nkx2-5* null embryos, the truncation of the OFT and the RV happens due to the severe compromise of the SHF [29]. The genetic pathways affected in the mutant hearts affect the cardiac specification and maintenance of the progenitor state in SHF cardiogenic precursors. Although at first SHF progenitors dramatically increased in number in the SHF due to the absence of *Nkx2-5*, they then collapsed due to problems in their proliferative capabilities. Genes

affected include *Tbx5*, *Pbx3*, the cytokine receptor platelet-derived growth factor receptor alpha (*Pdgfra*), the insulin-like growth factor binding protein (*Igfbp5*) and the cardiac inducing cytokines *Bmp2* and *Fgf10* [29, 37]. It is important to remark the crucial role of *Bmp2* in cardiogenesis. The BMP2/Smad1 signaling induces the expression of *Nkx2-5* and suppresses the proliferation of SHF progenitors [29]. In turn, *Nkx2-5* inhibits *Bmp2* expression and SMAD1 activation through a negative feedback loop, thereby regulating the temporal balance between proliferation, differentiation and specification of cardiogenic precursors [29]. Therefore, absence of *Nkx2-5* increases BMP2/Smad1 signaling which accounts for the decrease in the numbers of SHF progenitors.

Nkx2-5 displays other multiple important functions during the process of heart development. For instance, it is involved in forming and maintaining the boundaries between discrete compartments within the developing heart. This includes the specialization and formation of myocardium of the sinus horns and the sinoatrial node [53, 59, 60]. *Nkx2-5* represses pacemaker channel genes such as *Hcn4* and *Tbx3* in the atrium, thus delimiting the boundary between the sinoatrial node and the adjacent atrial myocardium [59]. However, *Nkx2-5* is also critical for the specification of myocardial tissue into conduction cells, including the sinoatrial node, the AV node, the Purkinje fibers and the His bundle, and the maintenance of this cardiac conduction system structures in postnatal stages [61, 62]. Finally, an early and transient role of *Nkx2-5* has been described in precursors of endocardial cells. *Nkx2-5* triggers the differentiation of these cells to endocardium, tissue in which the *Nkx2-5* expression is totally absent [52, 63].

1.5. Congenital Heart Disease

CHD is the most prevalent of all clinically relevant human birth defects, occurring in approximately 6 out of 1000 live births, and is a leading cause of infant mortality [64]. Treatment of CHD often involves highly invasive surgery in childhood, and represents a major economic burden to health resources. Indeed, much higher rates are scored when including mild clinically silent defects in children, such as persistent left superior vena cava, bicuspid aortic valve and atrial septum aneurism [65]. In recent years there has been an increase in the survival rates of patients suffering CHD, mainly due to improvements in prenatal diagnosis, advances in surgical procedures and aftercare in modern medicine. There are over 21 million adults worldwide presenting some form of congenital heart malformations based on recent data [66]. CHD survivors enjoy a relatively good quality of life and start new families. As a consequence, the proportion of severe cardiac dysfunctions is annually rising in modern society [67].

Perturbation of the morphogenetic programs controlling heart development results in heart malformations which can be life threatening and even cause abortion. Genetic mapping of familial CHD has shown a link between mutations in genes from the cardiac kernel and the disease state. Although mutations in multiple cardiac TFs including *Gata4*, *Tbx5* and *Tbx20* cause congenital heart defects, *Nkx2-5* is to date the most commonly mutated single gene in CHD [68, 69]. Heterozygous mutations, generally familial, have an incidence of ~4% of all CHD in patients and are related with severe morphological and functional cardiac impairment [70].

These research studies have identified more than 50 mutations in total within the *Nkx2-5* gene which are associated with a wide range of congenital heart abnormalities [71-74]. The most common type of DNA alterations in the *Nkx2-5* gene associated with CHD are missense mutations, the majority located in the HD. A large number of these mutations are associated with atrial septal defects, revealing the importance of *Nkx2-5* in cardiac septation during heart development [72, 75, 76]. Also many mutations correlate with progressive deterioration of conduction through the AV node (AV block), giving further evidence on how relevant is this TF for the formation of the embryonic cardiac conduction system [72, 74, 77]. *Nkx2-5* mutations are also found in patients showing ventricular septal defects, conotruncal malformations, Ebstein's anomaly, double-outlet RV, hypoplastic left heart, heterotaxia, dilated cardiomyopathy and tetralogy of Fallot [65, 70, 72]. This spectrum of cardiac defects reveals *Nkx2-5* displays important roles not only in cardiac septation and conduction physiology, but also in heart muscle and the development of the tricuspid valve. Structure-function analysis has been conducted in order to find out the molecular defects in the NKX2-5 protein underlying disease-causing mutations. The hallmark of all mutations located in the HD is the reduced ability of the NKX2-5 protein to bind DNA [78, 79]. Moreover, lack of binding to GATA4 and impaired dimerization capabilities were also reported to be related to several of these mutations [79].

Transgenic mouse models are useful tools in the field of CHD research. The *Nkx2-5* full KO mouse line is actually used as a model for the human condition, demonstrating that *Nkx2-5* haploinsufficiency leads to septal and mild conduction defects after birth [55]. Other mouse models based on diverse *Nkx2-5* gene alterations in the HD have been generated, which recapitulate multiple congenital defects observed in CHD human patients. For instance, a murine model based on a heterozygous point mutation in the NKX2-5 HD has been recently generated and characterized by Costa MW *et al* [80]. These mice closely reproduce the morphological and physiological clinical presentations observed in CHD patients, including adult-onset cardiac

dysfunction and atrial septal and conduction defects [80]. Progressive AV conduction defects and cardiac septal and valvular dysmorphogenesis had also been documented in other mouse models [81-83]. Nevertheless, there are still no transgenic mouse lines generated by mutations in other regions of the *Nkx2-5* gene rather than the homeobox.

It is of utmost importance to understand in detail cardiac developmental pathways, and how alterations in these combinatorial codes cause CHD at the genetic and mechanistic levels. In humans, new insights in this field would have an immediate benefit in prenatal screening of fetuses with risk of CHD, counseling of family members and long term follow up of affected children and adults. Pathway information would also have potential impact on translational research involving the conversion of embryonic stem cells (ESCs) and multipotent adult stem cells into cellular intermediates useful for tissue engineering, stem cell therapies for adult cardiac pathologies and creating models for drug screening.

This project aims to contribute to the field by investigating the role of the NK2SD domain within NKX2-5, one of the most important TFs of the cardiac kernel whose mutations have been directly linked to CHD. In order to address this issue, the Harvey lab generated a transgenic mouse line in which the *NK2SD* domain was removed and substituted by a glycine (Gly) chain in order to allow the proper folding of the protein, thereby disturbing as less as possible its 3D conformation (**Figure 3B**). This project aimed to characterize the embryonic phenotype of the homozygous mutant embryos lacking this domain in both alleles, study the morphological alterations of the mutant hearts by histological analysis and provide molecular insights on the downstream genes altered in these mutants. Our results showed embryonic lethality associated to the homozygous deletion of the *NK2SD* domain. More importantly, characterization of the mutant cardiac phenotype showed clear differences to the *Nkx2-5* full KO, with less severe cardiac defects mainly related to septal defects, increased ECM and downregulation of important cardiac genes specifically in the RV. The study allowed us to determine the validity of this transgenic line as a model for CHD opening the possibility for future studies to unravel the underlying genetic alterations present in this model.

2. Aims and Objectives

1.1. Aims

The main aim of this project is to characterize the morphological and molecular defects of the *Nkx2-5*$^{\Delta NK2SD}$ mouse line presenting a deletion of the NK2SD domain of the NKX2-5 TF. By doing so we expect to elucidate the importance of the NK2SD domain for the function of the NKX2-5 protein and the potential embryonic defects associated to it. Results will provide new insights on cardiac GRNs, heart development and CHD with potential applications in the clinical setting.

1.2. Research Objectives

The above aims will be accomplished by fulfilling the following research objectives:

- Proving the validity of the NK2SD mouse strain for our research purposes by confirming the expression of *Nkx2-5* at messenger RNA (mRNA) and protein levels, and the proper translocation of the TF to the nucleus.
- Identifying the embryonic lethality point(s) of the *Nkx2-5*$^{\Delta NK2SD/\Delta NK2SD}$ mutant mouse embryos.
- Analyzing the defects and abnormalities in the embryonic phenotype of the *Nkx2-5*$^{\Delta NK2SD/\Delta NK2SD}$ mutant mouse embryos compared to wild type (WT) embryos.
- Studying the morphological alterations in the *Nkx2-5*$^{\Delta NK2SD/\Delta NK2SD}$ mutant hearts by:
    a) Analyzing histological sections of *Nkx2-5*$^{\Delta NK2SD/\Delta NK2SD}$ hearts at the embryonic stage(s) close to lethality.
    b) Quantifying the differences in total heart size and areas of the different heart regions of *Nkx2-5*$^{\Delta NK2SD/\Delta NK2SD}$ hearts compared to WT hearts.
    c) Quantifying the area differences in the cardiac histological layers of *Nkx2-5*$^{\Delta NK2SD/\Delta NK2SD}$ hearts compared to WT hearts.
- Proving that the observed phenotype in *Nkx2-5*$^{\Delta NK2SD/\Delta NK2SD}$ is unique and different from the phenotype achieved in *Nkx2-5* full KO mouse models.
- Conducting a preliminary study on the molecular alterations underlying the *Nkx2-5*$^{\Delta NK2SD/\Delta NK2SD}$ mutant hearts phenotype by screening for differential gene expression compared to WT hearts.

3. Materials and Methods

3.1. Mouse Lines and Animal Work

This animal study was approved by the Garvan Institute of Medical Research/St Vincent's Animal Experimentation Ethics Committee (approval 16/03). Mice (*Mus musculus*) were kept and bred in the BioCORE facility at the Victor Chang Cardiac Research Institute, which provides appropriate housing standards and adheres to the policies of the National Health and Medical Research Council regarding the protection of animals used for experimental purposes. Mice handling, transport, husbandry and culling were conducted following Standard Operating Procedures approved by the BioCORE facility.

The *Nkx2-5*$^{\Delta NK2SD/+}$ mouse line was generated by the Harvey Lab in the Monash Animal Research Platform at Monash University (Melbourne, Australia) (**Figure 4A**). Briefly, a genomic fragment for the *Nkx2-5* gene, obtained from a mouse genomic library, was cloned in a pGEM 7Zf+ plasmid (**Figure 4B**). A pgk-Neo cassette flanked by LoxP sites was then incorporated inside the 3'UTR region and the NK2SD domain sequence was replaced by a Gly chain following a PCR strategy with specific primers (**Figure 4B**). The linearized targeting vector was electroporated in B4 ESCs from the C57Bl/6 strain (**Figure 4A**). After 7 days of selection with G418, 400 neomycin-resistant clones were picked and subsequently screened (**Figure 4A**). A first Southern Blot analysis was performed with 5' and 3' probes to confirm the presence of the 5' and 3' homology arms respectively. In addition, the presence of the mutant sequence was analyzed by PCR with specific primers. Positive clones were then reconfirmed by Southern analysis using again the 5' and 3' probes and a new internal probe annealing on the pgk-Neo cassette. Sequencing analysis was conducted in order to verify the presence and the integrity of both the region of the mutation and the LoxP sites. Confirmed targeted positive clones were injected into blastocysts in a foster mother in order to generate chimeric mice carrying the *Nkx2-5*$^{\Delta NK2SD-}$ allele (**Figure 4A**). *Nkx2-5*$^{\Delta NK2SD}$ chimeras were bred for germ line transmission (**Figure 4A**). Germ line progeny was identified from color coat and genotyping with specific primers (**Table 1**). The F1 generation was further confirmed by Southern Blot analysis with the 5' probe and sequencing of the mutant region using DNA extracted from the mouse tails (**Figure 4A**). The pgk-Neo cassette was eventually deleted by crossing F1 generation animal with ubiquitous CMV-Cre-deleting transgenic mice (C57Bl/6J background).

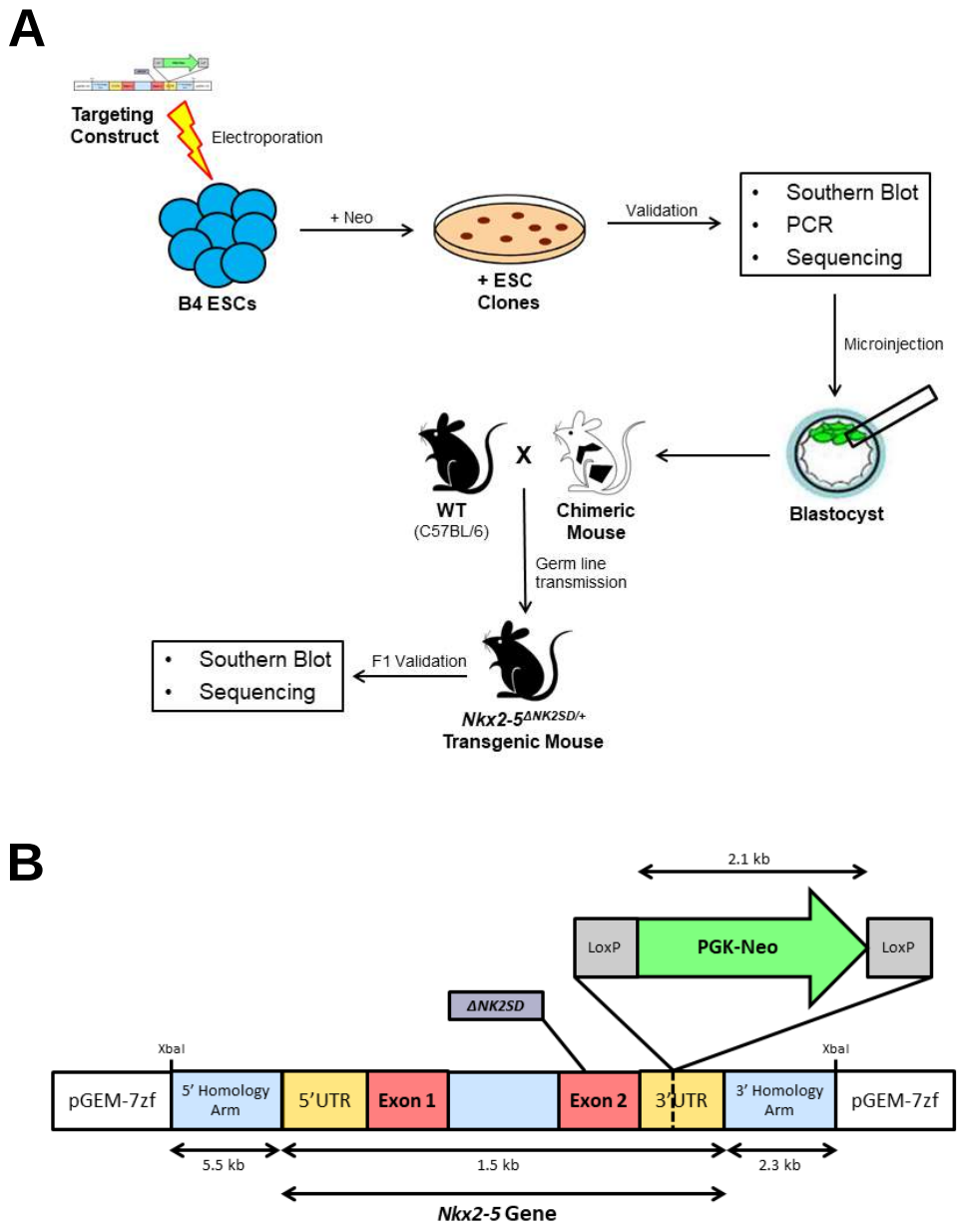

Figure 4. ***Nkx2-5$^{\Delta NK2SD}$*** **Mouse Line Generation.** (A) Schematic representation of the research strategy followed for producing the *Nkx2-5$^{\Delta NK2SD}$* transgenic mouse line using B4 ESCs. (B) Schematic representation of the *Nkx2-5$^{\Delta NK2SD}$* targeting construct. Neo: neomycin. ESCs: embryonic stem cells. UTR: untranslated region.

The *Nkx2-5*$^{GFP/+}$ mouse line was generated in the Harvey Lab at the VCCRI (Sydney, Australia) [55]. Briefly, a KO construct was generated by the insertion of sequences encoding for an enhanced variant of the jellyfish green fluorescent protein (GFP) into the *Nkx2-5* gene at a position corresponding to amino acid 35 of the protein. A pgk-Neo cassette flanked by LoxP sites was incorporated immediately 3' of the GFP insertion. This KO construct was transfected into W9.5 ES cells from the 129/SvJ strain. Targeted neomycin-resistant ES cell clones were used to generate mice carrying the *Nkx2-5*^{GFP} allele, which were bred onto C57Bl/6J for 2 to 6 generations. The pgk-Neo cassette was eventually removed by Cre recombinase-mediated deletion, achieved by crossing F1 generation animals with Cre-deleter transgenic mice (C57Bl/6J background), which express Cre recombinase in the germ line. Cre-deleted *Nkx2-5*^{GFP} mice were additionally bred onto C57Bl/6J background to segregate the transgene.

3.2. Embryo Harvesting

Timed matings between heterozygous *Nkx2-5*$^{\Delta NK2SD+}$ mutant males and females were set up to obtain *Nkx2-5*$^{\Delta NK2SD/\Delta NK2SD}$ KO embryos. Timed matings between heterozygous *Nkx2-5*$^{GFP/+}$ mutant females and males were set up to obtain *Nkx2-5*$^{GFP/GFP}$ full KO embryos. Pregnancy was determined by plug checks and weight follow-up. Embryonic stage was determined by counting days from the day a plug was identified, starting from 0.5 days. Pregnant females were culled by cervical dislocation and standard dissection techniques were performed to extract the uterus, which was then placed in ice-cold phosphate buffer saline (PBS) for embryo harvesting. Embryos were taken out from the decidua and the yolk sac using microdissection tweezers, and subsequently cleaned under the scope in PBS for embryos older than E10.5 or PBT (PBS containing 0.1% Tween-20) for embryos younger than E10.5 to avoid attachment of membranes to the plastic surface of the dissecting plate and fixation tube. An image of every embryo was taken and genotyping samples were collected: tail samples from E11.5 and E12.5 embryos, yolk sac samples from E8.5, E9.5 and E10.5 embryos or a piece of necrotic embryo tissue if available from resorptions. Finally, embryos were treated with KCl for diastolic cardiac arrest and fixed in 4% paraformaldehyde (PFA) overnight (ON) at 4°C.

3.3. Genotyping

For *Nkx2-5*$^{\Delta NK2SD}$ mice, DNA was purified from samples using the REDExtract-N-AMP^{TM} Tissue PCR kit (Sigma Aldrich). In the case of *Nkx2-5*^{GFP} mice, genomic DNA was extracted from embryos yolk sacs by treating samples with yolk-sac buffer (50 mM Tris pH 8.0, 1 mM EDTA,

0.5% Tween-20 in Milli-Q water) and 0.4 µg/µl proteinase K ON at 55°C, followed by vortexing, centrifuging at full speed for 5 min and 10 min heating at 95°C for proteinase K inactivation. Embryos were genotyped by Polymerase Chain Reaction (PCR) analysis using 50 ng of specific oligonucleotide primers (**Table 1**) and the MyTaq™ HS Red Mix (Bioline), following specific cycles programs for each mouse strain (**Table 2**) in an Applied Biosystems Veriti Thermal Cycler (Thermo Fisher Scientific).

Table 1. Primers sequences used for genotyping PCRs.

Primer	Sequence (5'–3')
Nkx2-5$^{\Delta NK2SD}$ WT Fw	CGTGAACTTTGGCGTCGGGG
Nkx2-5$^{\Delta NK2SD}$ KO Fw	AAAAGCGCCTCCCCTACCCG
Nkx2-5$^{\Delta NK2SD}$ WT/KO Rv	ATAAATACGGGTGGGTGGG
Nkx2-5^{GFP} WT Fw	CACTCTCTGCTACCCACCTG
Nkx2-5^{GFP} WT Rv	CGTAGGCTCCCGGGTAAAAT
Nkx2-5^{GFP} KO Fw	ACATGAAGCAGCACGACTTCTTCAAGTCCG
Nkx2-5^{GFP} KO Rv	TGTGGCGGATCTTGAAGTTCACCTTGATGCC

Table 2. Cycle programs used for genotyping PCRs.

***Nkx2-5*$^{\Delta NK2SD}$**			***Nkx2-5*^{GFP}**		
95ºC	3 min		95ºC	1 min	
95ºC	30 s	x35	95ºC	30 s	x34
56ºC	30 s		58ºC	30 s	
72ºC	45 s		72ºC	45 s	
72ºC	2 min		72ºC	10 min	

3.4. Paraffin-Embedding and Sectioning of Mouse Embryos

Embryo embedding was performed using standard protocols. Fixed embryos were first washed in PBS for 5 min and then dehydrated using ethanol (EtOH) serial concentrations (50%, 70%, 90% and 2x 100%) for 30 min each at room temperature (RT). Dehydrated embryos were cleared three times for 5 min with xylene at RT, followed by a 30 min incubation in 50:50 xylene/paraffin at 70°C and three 45 min incubations in 100% molted paraffin wax at 70°C. Embryos were adequately oriented in the paraffin blocks for transversal sections. Blocks were left for solidification on a cooler and eventually stored at 4°C.

Embryo sectioning was performed using the microtome (Leica). 10 μm serial transversal sections were obtained from the embryos, in which sections corresponding to the heart region was then identified and selected. The corresponding sections were mounted alternatively in order to obtain 3-5 slides per embryo (depending on the heart size) containing representative sections of the different heart regions. Sections were spread by using a water bath with MilliQ water at 43°C. Finally, slides were left to dry at 37°C ON and eventually stored at -80°C.

3.5. Morphological Analysis by Hematoxylin and Eosin (H&E) Staining

H&E stainings were performed following standard protocols. Briefly, dewaxing of paraffin-embedded tissue sections was performed by incubating slides for 15 min at 68°C for paraffin wax melting and then clearing three times for 10 min with xylene for paraffin wax removal. Tissue was progressively rehydrated by 5 min incubations in EtOH serial concentrations (2x 100% EtOH, 2x 90% EtOH, 70%, 50% and 30%) until reaching MilliQ water for 5 min. Sections were stained with Harris hematoxylin (Sigma Aldrich) for 9 min, washed with running tap water for 5 min, incubated for 10 sec in acid alcohol (0.5% HCl in 70% EtOH) for differentiation and washed again 3 times for 10 sec with distilled water. Tissue was then dehydrated until 70% EtOH by 2 min incubations in EtOH serial concentrations (30%, 50%, 70%), stained with eosin Y in alcoholic solution (Sigma Aldrich) for 9 min and eventually completely dehydrated by a 10 sec incubation in 90% EtOH followed by a 10 sec incubation in 100% EtOH. After a 3 min incubation in xylene, slides were mounted with DPX Neutral Mounting Medium (LabChem) and let to dry at RT.

3.6. H&E Image Analysis and Cardiac Morphology Quantifications

Digital images from H&E heart sections were generated using a Leica DM 5500B microscope equipped with a 5x (numerical aperture 0.15) and 10x (numerical aperture 0.30) objectives and an attached Leica DFC 425C camera controlled by the high-performance Leica LAS 4.4.0 software.

5x images from H&E heart sections were used to quantify the areas of the total heart and the different cardiac regions (RA, LA, RV, LV, IVS) in *Nkx2-5*$^{+/+}$ and *Nkx2-5*$^{\Delta NK2SD/\Delta NK2SD}$ embryos from stages E11.5 and E12.5. 10x images from H&E heart sections were used for quantifying the areas of the different cardiac histological layers (endocardium, trabecular myocardium, compact layer myocardium and ECM) in *Nkx2-5*$^{+/+}$ and *Nkx2-5*$^{\Delta NK2SD/\Delta NK2SD}$ embryos from stages E10.5,

E11.5 and E12.5. In this case, morphological tissue segmentation was applied to extract the different histological layers before the area quantification was performed.

Areas were obtained using the Amira® 5.5.0 software (FEI Visualization Services Group, USA) in 3 representative histological sections per embryo, and 1 (E11.5) or 2 (E9.5, E10.5, E12.5) embryos (*n*) per developmental stage analyzed. Total heart areas from *Nkx2-5*$^{\Delta NK2SD/\Delta NK2SD}$ embryos were normalized with the total heart area mean of *Nkx2-5*$^{+/+}$ embryos, in order to make them relative to the WT phenotype. Cardiac histological layers areas from a given section were normalized with the area of the most external monolayer of cardiomyocytes in order to make them relative to the LV chamber perimeter. Raw data was processed in Excel and eventually plotted as mean + standard error of mean (SEM) using GraphPad Prism 5 (Graphpad Software).

3.7. Immunofluorescence

Dewaxing and rehydration of paraffin-embedded tissue sections was performed as described in the H&E Staining section. After two washes in PBS for 5 min, samples requiring antigen retrieval processing were boiled in 10 mM sodium citrate pH 6.0 for 10 min in the microwave, left 20 min at RT for temperature stabilization and then washed twice for 5 min with MilliQ water and once for 5 min with PBS. Slides were then incubated in 1% H_2O_2 in 100% MetOH for quenching endogenous peroxidase activity. Then, slides were washed two times for 5 min in PBS followed by tissue permeabilization with 0.3% Triton-X100 in PBS two times for 10 min and blocking of antibodies unspecific binding with Blocking Solution[*1] (BS[*1]: 3% bovine serum albumin (BSA) (Sigma Aldrich), 20 mM $MgCl_2$, 0.3% Tween-20 (Sigma Aldrich), 5% fetal calf serum (Sigma Aldrich) in PBS) for 1 h at RT in humidified chamber. Primary antibody incubation was performed ON at 4ºC with primary antibodies diluted in BS[*1] in a humidified chamber. Slides were then washed twice in PBS for 5 min, twice in 0.3% Triton-X100 in PBS for 5 min and subsequently incubated for 1 h at RT with biotinylated secondary antibodies diluted in 5% BSA in PBS in humidified chamber. Then, samples were washed twice in PBS washes for 5 min and twice 0.3% Triton-X100 in PBS washes for 5 min. In order to amplify the antibody signal, sections were incubated with the avidin-biotin-horseradish peroxidase (HRP) complex (ABC) reagent (Vector Laboratories) for 1 h at RT in humidified chamber, washed again twice in PBS-T for 5 min and incubated with Tyramide Signal Amplification (TSA) working solution (TSA™-Plus Cyanine 5 System, Perkin Elmer) for 3.5 min at RT. Sections were subsequently washed twice in 0.3% Triton-X100 in PBS for 5 min and incubated ON at 4ºC with 1:500 anti-alpha smooth muscle actin (SMA)/FITC antibody (mouse, Sigma Aldrich) and 1:1000 DAPI (Sigma

Aldrich). After two final washes in 0.3% Triton-X100 in PBS for 5 min each, slides were mounted with Fluoromount-G® (SouthernBiotech) and let to dry in the dark.

The following primary antibodies were used: anti-NKX2-5 (goat, Santa Cruz Biotechnology) diluted 1:100, anti-NOTCH1 Intracellular Domain (N1ICD) (rabbit, Cell Signaling Technology) diluted 1:100. The following biotinylated secondary antibodies were used: anti-goat (Vector Laboratories) diluted 1:100, anti-rabbit (Vector Laboratories) diluted 1:100.

3.8. RNA In Situ Hybridization

Dewaxing and rehydration of paraffin-embedded tissue sections was performed as described in the H&E Staining section, in this case under RNase-free conditions. After a 5 min wash in PBS, sections were post-fixed in 4% PFA for 20 min at RT and subsequently washed twice in PBS for 5 min. Tissue was first permeabilized by enzymatic digestion with proteinase K (10 μg/ml) (Roche) in PBS for 10 min at 37ºC. After a 5 min wash in PBS, sections were again post-fixed in 4% PFA for 5 min at RT and washed twice in PBS for 5 min. Tissue underwent a second permeabilization step with HCl 0.07 N shaking for 15 min at RT for protein denaturation, was then washed twice in PBS for 5 min and acetylated with 0.25% acetic anhydride (Sigma Aldrich) in 100 mM triethanolamine pH 8 buffer (Sigma Aldrich) shaking for 10 min at RT for reducing non-specific binding of negatively charged riboprobes to the positively charged tissue and glass slide. After washing slides in PBS for 5 min and then in Milli-Q water for 5 min, blocking non-specific binding of riboprobes was reinforced by treating sections with prehybridization buffer for 2 h at 70ºC in humidified chamber. Prehybridization buffer composition: 50% formamide (Sigma Aldrich), 5x saline-sodium citrate (SSC) buffer pH 5.5, 1x Dehardt's (1% w/v BSA (Sigma Aldrich), 1% w/v Ficoll (Sigma Aldrich), 1% w/v polyvinylpyrrolidone (Sigma Aldrich)), 0.1% Tween-20 (Sigma Aldrich), 0.1% CHAPS detergent (3-[(3-cholamidopropyl)dimethylammonio]-1-propanesulfonate) (Sigma Aldrich), 50 μg/ml transfer RNA (Roche) in Milli-Q water. Chamber buffer composition: 50% formamide (Sigma Aldrich), 5x SSC buffer pH 5.5 in Milli-Q water. Tissue was then hybridized with ~100 ng/section of digoxigenin (DIG)-labeled riboprobes in 300 μl hybridization buffer ON at 70ºC in humidified chamber with chamber buffer. On the following day, sections were washed twice with posthybridization buffer I (50% formamide, 5x SSC buffer pH 5.5, 1% Sodium Dodecyl Sulfate (SDS) in Milli-Q water) for 30 min at 65ºC, twice with posthybridization buffer II (50% formamide, 2x SSC buffer pH 5.5, 0.2% SDS in Milli-Q water) for 30 min at 65ºC, and three times with Maleic Acid Buffer Tween (MABT: 100 mM maleic acid (Sigma Aldrich), 250 mM NaCl (Merck), 0.25% Tween-20 (Sigma Aldrich) in Milli-Q

water, pH 7.5 adjusted with solid NaOH (Merck)) for 5 min. Unspecific binding of anti-DIG antibody was prevented by incubating slides with Blocking Solution^{*2} (BS^{*2}: 20% sheep serum (Sigma Aldrich), 1% blocking reagent (Roche) in MABT) for 2 h at RT in humidified chamber with distilled water. Antibody detection of DIG-labeled riboprobes was performed by incubating sections with alkaline phosphatase (AP) conjugated anti-DIG antibody (Roche) diluted 1:1000 in BS^{*2} ON at 4ºC in humidified chamber with distilled water. The next day, slides were washed at RT with MABT twice for 10 min followed by three times for 1 h. Tissue was cleared with AP buffer (100 mM NaCl, 50 mM $MgCl_2$, 100 mM Tris-HCl pH 9.5, 0.1% Tween-20 (Sigma Aldrich), 2 mM tetramisole hydrochloride (Sigma Aldrich) in Milli-Q water) three times for 10 min at RT to condition for AP enzymatic reaction. Color development was achieved by incubating sections with BM Purple AP substrate (Roche) in humidified chamber with distilled water for a variable time at 37ºC, RT or 4ºC depending on the riboprobe. After developing, slides were washed twice in Milli-Q water for 5 min, post-fixed in 4% PFA for 20 min at RT and washed again twice with Milli-Q water for 5 min. Finally, sections were dehydrated by 1.5 min incubations in EtOH serial concentrations (30%, 50%, 70%, 90%, 2x 100%), cleared in xylene for 2 min, mounted with DPX Neutral Mounting Medium (LabChem) and let to dry at RT.

3.9. Statistical Analysis

Statistical analysis was conducted using GraphPad Prism 5 (Graphpad Software). In the embryonic lethality table, statistical significance between the percentage of homozygous mutant embryos in a given embryonic stage and the immediately preceding one was analyzed by one-tailed *t*-test. Statistical significance in all area quantifications obtained with Amira® 5.5.0 software (FEI Visualization Services Group, USA) was analyzed by one-tailed *t*-test. *P*-values < 0.05 were considered statistically significant ($*p < 0.05$, $**p < 0.01$, $***p < 0.001$). Normality was confirmed with the Shapiro-Wilk test.

Special considerations are required for conducting statistical analysis in the cardiac areas quantifications, especially in E11.5 hearts since $n=1$ provides a poor statistical power, not enough to conduct a significance test. At a given embryonic stage, we calculated the standard deviation for the areas obtained from sections of the same embryo, and in parallel we also calculated the standard deviation for the areas from sections of different embryos with the same phenotype. Statistical analysis revealed no significant differences between the two calculated standard deviations at any of the analyzed embryonic stages neither in the WT nor in the mutant phenotype. Based on this information, we considered the areas from each section as independent

data in order to conduct the *t*-test statistical test and obtain some information from the area quantification at these stages. Although the obtained results are obviously not conclusive, they uncover a trend in the data of the differences which might be underlying the WT and the *Nkx2-5*$^{\Delta NK2SD/\Delta NK2SD}$ mutant phenotypes at these embryonic stages. These results will be further confirmed in the future by completing the quantifications required to have *n*=3 per embryonic stage and, thus, a strong statistical power.

4. Results

4.1. Embryonic Lethality of Nkx2-5$^{\Delta NK2SD/\Delta NK2SD}$ Mice

Once generated, the *Nkx2-5$^{\Delta NK2SD}$* mouse line was maintained in heterozygosity. Monitoring of the *Nkx2-5$^{\Delta NK2SD/+}$* animals showed no obvious defects affecting their life expand or fertility. Therefore, in order to study the effects of the homozygous deletion of the NK2SD domain in the NKX2-5 TF, *Nkx2-5$^{\Delta NK2SD/+}$* animals were intercrossed to generate *Nkx2-5$^{\Delta NK2SD/\Delta NK2SD}$* homozygotes.

First we analyzed the proportion of homozygous animals present at birth. Genotyping of newborn mice from 12 litters revealed that litters were formed only by WT (42%) and heterozygous (58%) pups (**Table 3**). The absence of viable *Nkx2-5$^{\Delta NK2SD/\Delta NK2SD}$* mutants at birth suggested that homozygosis for the NK2SD deletion in the NKX2-5 TF results in embryonic lethality. To assess the timing and the cause of embryonic death, timed mattings between heterozygous mice were performed. Embryos were harvested at different stages starting from the ones closer to birth, continuing progressively at earlier stages until homozygous animals were found and finishing when the proportion of homozygous embryos followed Mendelian ratios. Genotyping of decidual swellings corresponding to death embryos was not possible in some cases due to the absence of embryonic tissue. Hence resorptions have been excluded from the genotyping calculations (**Table 3**).

The % of WT (+/+) and heterozygous (+/-) embryos stayed relatively constant and close to the expected Mendelian ratios (25% and 50% respectively) across the embryonic stages analyzed in this study (**Table 3**). The percentage of homozygous (-/-) mutant embryos remained close to the predicted Mendelian proportion (25%) from E8.5 to E10.5 (~20%), but it was halved at E11.5 (~10%) and eventually no homozygous embryos were obtained from E13.5 onwards (**Table 3**). Importantly, both drops in the percentage of homozygotes at E11.5 and E13.5 were statistically significant (**Table 3**). Regarding resorptions, the percentage stayed constant at around ~6% from E8.5 to E10.5. However, at E11.5 it dramatically increased until ~22%, kept rising at E12.5 (~28%) and E13.5 (~34%), and eventually dropped to ~23% at E14.5, most likely due to total resorption of death embryos (**Table 3**). Therefore, the increase in the percentage of resorptions at E11.5 matched the first drop in the percentage of homozygous embryos. Moreover, the maximum observed percentage of resorptions was reached at E13.5, first embryonic stage in which there

were no *Nkx2-5*$^{\Delta NK2SD/\Delta NK2SD}$ homozygotes alive anymore. Therefore, these results indicate the presence of two embryonic lethality points for *Nkx2-5*$^{\Delta NK2SD/\Delta NK2SD}$ mutant embryos: the first one at E10.5 and the second one at E12.5.

Age	N° Litters	Total N° Embryos	N° Embryos (%)			N° RS (%)	*p*-value
			+/+	-/+	-/-		
E8.5	8	61	16 (25,64)	27 (43,80)	14 (23,81)	4 (6,75)	NA
E9.5	10	83	22 (26,33)	37 (43,24)	19 (23,82)	5 (6,61)	ns
E10.5	11	88	16 (17,80)	51 (58,06)	16 (18,33)	5 (5,81)	ns
E11.5	13	103	24 (23,66)	47 (45,25)	9 (9.60)*	23 (21,48)	$p = 0.042$
E12.5	11	94	16 (16,58)	41 (43,48)	11 (11,97)	26 (27,97)	ns
E13.5	7	52	11 (20,53)	23 (45,88)	0 (0.00)**	18 (33,59)	$p = 0.001$
E14.5	6	43	10 (24,35)	23 (52,78)	0 (0,00)	10 (22,87)	ns
Newborn	12	70	29 (42,07)	41 (57,93)	0,00	NA	ns

Table 3. Determination of embryonic lethality in *Nkx2-5*$^{\Delta NK2SD/\Delta NK2SD}$ embryos.
Table showing the number of litters, number of embryos and the percentage (%) of each genotype per stage analyzed. Genotypes of resorbed embryos were not available. Embryos and newborn pups were genotyped by PCR analysis with yolk sac or tip tail DNA as described in *Materials and Methods*. *T*-test was used to analyze whether the difference between the percentage of homozygous mutant embryos in a given embryonic stage and the immediately preceding embryonic stage is statistically significant (*$p < 0.05$, **$p < 0.01$, ns: non-significant). -/+: *Nkx2-5*$^{\Delta NK2SD/+}$; -/-: *Nkx2-5*$^{\Delta NK2SD/\Delta NK2SD}$; RS: resorptions; NA: not applicable.

Embryonic Lethality Comparison between *Nkx2-5*$^{\Delta NK2SD/\Delta NK2SD}$ and *Nkx2-5*$^{GFP/GFP}$ Mice

One of the objectives of this research project was to determine the phenotypic differences between the newly generated *Nkx2-5*$^{\Delta NK2SD/\Delta NK2SD}$ homozygous mutant embryos and the previously described *Nkx2-5*$^{GFP/GFP}$ mutant embryos [28, 55]. As explained in *Materials and Methods*, the *Nkx2-5*$^{GFP/GFP}$ animals represent a full KO mouse model for *Nkx2*-5 generated by inserting a GFP cassette in the position corresponding to amino acid 35 of the NKX2-5 protein.

The *Nkx2-5*$^{GFP/GFP}$ mutant study defined the embryonic lethality of these embryos around E9.5 (24ps) [28, 55]. In contrast, our study revealed that *Nkx2-5*$^{\Delta NK2SD/\Delta NK2SD}$ mouse embryos present two lethality points at E10.5 and E12.5 as described above (**Table 3**). Therefore, both mouse lines

show different embryonic lethality, suggesting a less severe phenotype for the *Nkx2-5*$^{\Delta NK2SD/\Delta NK2SD}$ embryos compared to *Nkx2-5*$^{GFP/GFP}$ embryos.

4.2. Analysis of the Embryonic Phenotype of Nkx2-5$^{\Delta NK2SD/+}$ *Mice*

Morphological analysis of *Nkx2-5*$^{\Delta NK2SD/+}$ compared to WT showed no obvious differences in the embryonic phenotype at any of the embryonic stages analyzed in the study (**Figure 5A, B, D, E, H, I; Figure 7A, B, D, E**). This, together with the fact that *Nkx2-5*$^{\Delta NK2SD/+}$ offspring is viable, fertile and does not show any obvious symptoms of disease after birth, we decided to exclude these animals from further analysis and focus the project on *Nkx2-5*$^{\Delta NK2SD/\Delta NK2SD}$ mutant mouse embryos.

4.3. Analysis of the Embryonic Phenotype of Nkx2-5$^{\Delta NK2SD/\Delta NK2SD}$ *Mice*

4.3.1. Analysis of the Mutant Embryonic Phenotype in Early Embryonic Stages

The analysis of the morphological phenotype in the *Nkx2-5*$^{\Delta NK2SD/\Delta NK2SD}$ mutant embryos at E8.5 revealed no obvious differences compared to the *Nkx2-5*$^{+/+}$ WT embryos (**Figure 5A-C**). In contrast, similar analysis at E9.5 and E10.5 determined the presence of two clearly different mutant phenotypes (**Figure 5D-K**). Therefore, in order to better analyze the phenotype and prevent heterogeneity in the results, mutant embryos were classified in two independent groups: embryos with a mild phenotype (**Figure 5F, J**), and embryos with a severe phenotype (**Figure 5G, K**). Mutant embryos included in the mild phenotype group showed no obvious differences neither in their general appearance nor specifically in their hearts shape, size and position compared to WT embryos (**Figure 5F, J**). In contrast, mutant hearts from embryos included in the severe phenotype group showed an upward angle of the AVC and the LV relative to the body of the embryo compared to WT (**Figure 5G, K**). The overall appearance of these mutant hearts was more linear compared to normal hearts (**Figure 5D, H**), indicating possible defects in the process of cardiac looping ongoing at this stage. Nevertheless, chamber morphogenesis appeared relatively normal with atrial and ventricular regions well delineated similar to WT hearts, and a AV groove was present although less evident than in WT hearts (**Figure 5D, G, H, K**). In addition to the previously described defects, severe mutant hearts at E10.5 showed arrested growth and their developmental stage was comparable to E9.5 hearts (**Figure 5D, H, K**). Moreover, these embryos were paler and showed signs of necrosis (**Figure 5H, K**), indicating their proximity to death.

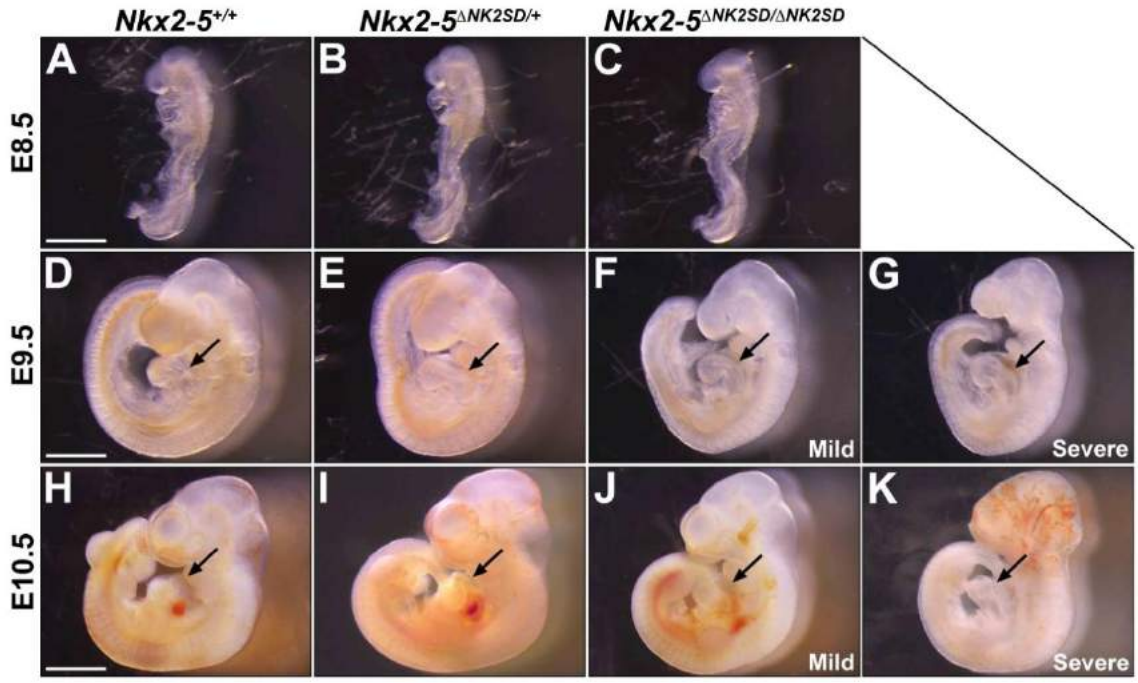

Figure 5. Embryonic Phenotype Timecourse at Early Embryonic Stages.
(A-K) Images of *Nkx2-5*$^{+/+}$ (A, D, H), *Nkx2-5*$^{\Delta NK2SD/+}$ (B, E, I) and *Nkx2-5*$^{\Delta NK2SD/\Delta NK2SD}$ embryos (C, F, G, J, K) at E8.5 (10ps, A-C), E9.5 (25ps, D-G) and E10.5 (35ps, H-K). Images of *Nkx2-5*$^{\Delta NK2SD/\Delta NK2SD}$ mutant embryos with a mild (F, J) and a severe (G, K) phenotype are shown at E9.5 (F, G) and E10.5 (J, K). Images were taken under the scope right after harvesting the embryos out of the decidua. Black arrows point to the embryonic heart. Scale bar (A-C): 350 μm; Scale Bar (D-G): 700 μm; Scale Bar (H-K): 960 μm.

Embryonic Phenotype Comparison between *Nkx2-5*$^{\Delta NK2SD/\Delta NK2SD}$ and *Nkx2-5*$^{GFP/GFP}$ Mice

Once we defined the macroscopic cardiac defects of the *Nkx2-5*$^{\Delta NK2SD/\Delta NK2SD}$ mutants, these embryos were compared with *Nkx2-5*$^{GFP/GFP}$ embryos. The cardiac looping defect described for the *Nkx2-5*$^{\Delta NK2SD/\Delta NK2SD}$ mutant hearts from the severe group was more evident in *Nkx2-5*$^{GFP/GFP}$ embryos (**Figure 6B, E**). However, in contrast to the relatively normal curvature present in the *Nkx2-5*$^{\Delta NK2SD/\Delta NK2SD}$ mutant hearts (**Figure 6B**), the *Nkx2-5*$^{GFP/GFP}$ embryos showed essentially linear hearts (**Figure 6E**). These results confirm a less severe cardiac looping phenotype in *Nkx2-5*$^{\Delta NK2SD/\Delta NK2SD}$ mutant embryos compared to *Nkx2-5*$^{GFP/GFP}$ mutant embryos, in which severe cardiac looping defects have been well characterized [28].

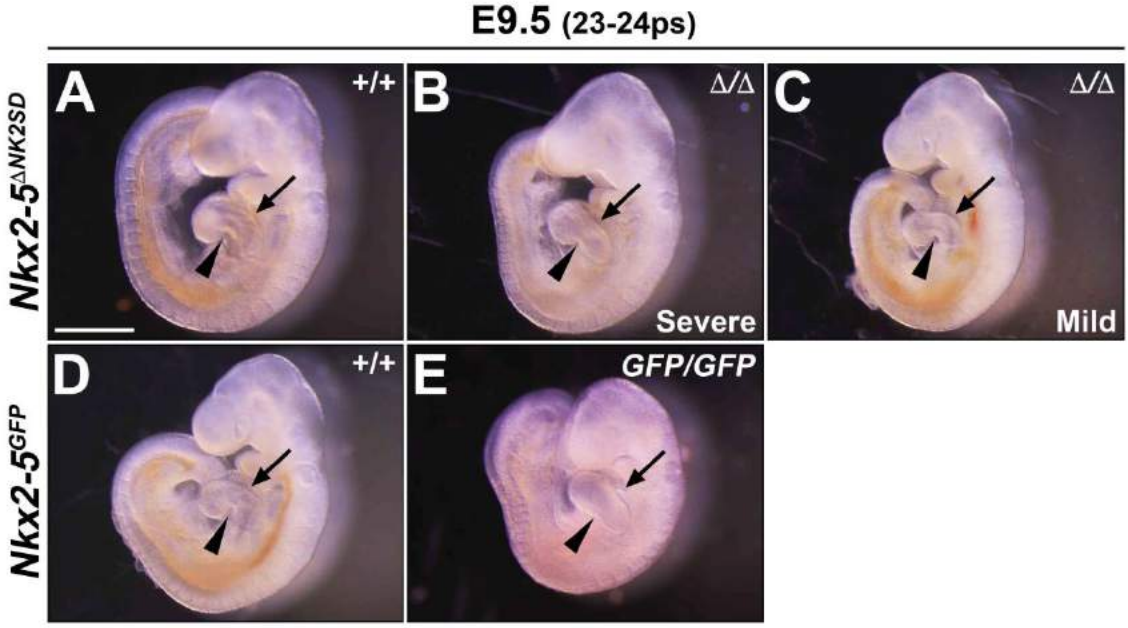

Figure 6. Macroscopic Embryonic Phenotype Comparison between *Nkx2-5$^{\Delta NK2SD/\Delta NK2SD}$* and *Nkx2-5$^{GFP/GFP}$* Mutant Homozygotes at E9.5.

(A-C) Images of E9.5 *Nkx2-5$^{+/+}$* (23ps, A), severe *Nkx2-5$^{\Delta NK2SD/\Delta NK2SD}$* (24ps, B) and mild *Nkx2-5$^{\Delta NK2SD/\Delta NK2SD}$* (24ps, C) embryos. (D, E) Images of E9.5 *Nkx2-5$^{+/+}$* (24ps, D) and *Nkx2-5$^{GFP/GFP}$* (23ps, E) embryos. Images were taken under the scope right after removing the embryos out of the decidua. Black arrows point to the pericardium, remarking the presence of pericardial edema only in the *Nkx2-5$^{GFP/GFP}$* embryo. Black arrowheads point to the AV demarcation. Δ/Δ: *ΔNK2SD/ΔNK2SD*. Scale Bar (A-E): 700 μm.

However, there are some important differences between the macroscopic phenotype observed in the mutant hearts from both mouse lines. *Nkx2-5$^{GFP/GFP}$* hearts presented a completely absence of AV groove, lack of elongation of the AVC and ventricular ballooning defects (**Figure 6D, E**). In contrast, severe *Nkx2-5$^{\Delta NK2SD/\Delta NK2SD}$* hearts showed a much more evident AV groove, proper elongation of the AVC and no deficits in the process of ventricular ballooning (**Figure 6A, B**). Moreover, *Nkx2-5$^{GFP/GFP}$* mutant embryos developed pericardial edema (**Figure 6E**), also seen in embryos that die from cardiac defects as a result of other mutations [84, 85], and showed growth and developmental retardation compared to their WT littermates with similar pairs of somites (**Figure 6D, E**). These features were not observed in *Nkx2-5$^{\Delta NK2SD/\Delta NK2SD}$* mutant mouse embryos, which did not develop pericardial edema at this early stages and presented same size and developmental stage as their WT littermates (**Figure 6A-C**). Overall, the embryonic phenotype of

Nkx2-5$^{GFP/GFP}$ mutant mouse embryos is more severe and dramatic, whereas the one observed in severe *Nkx2-5*$^{\Delta NK2SD/\Delta NK2SD}$ mutant mouse embryos is milder and closer to the WT phenotype.

4.3.2. Analysis of the Mutant Embryonic Phenotype in Late Embryonic Stages

Similar morphological analysis of *Nkx2-5*$^{\Delta NK2SD/\Delta NK2SD}$ mutants at late embryonic stages showed no major macroscopic morphological defects between normal and mutant embryos (**Figure 7A-F**). The heart at these stages is already encapsulated in the body of the embryo and thus difficult to observe. However, mutant embryos at E11.5 and E12.5 showed bleedings in the cephalic region, between the limb buds and the head (**Figure 7C, F**). These bleedings were only present in ~56% of the analyzed E11.5 homozygous mutant embryos, whereas they were larger and more obvious in all E12.5 homozygous embryos (**Figure 7F**).

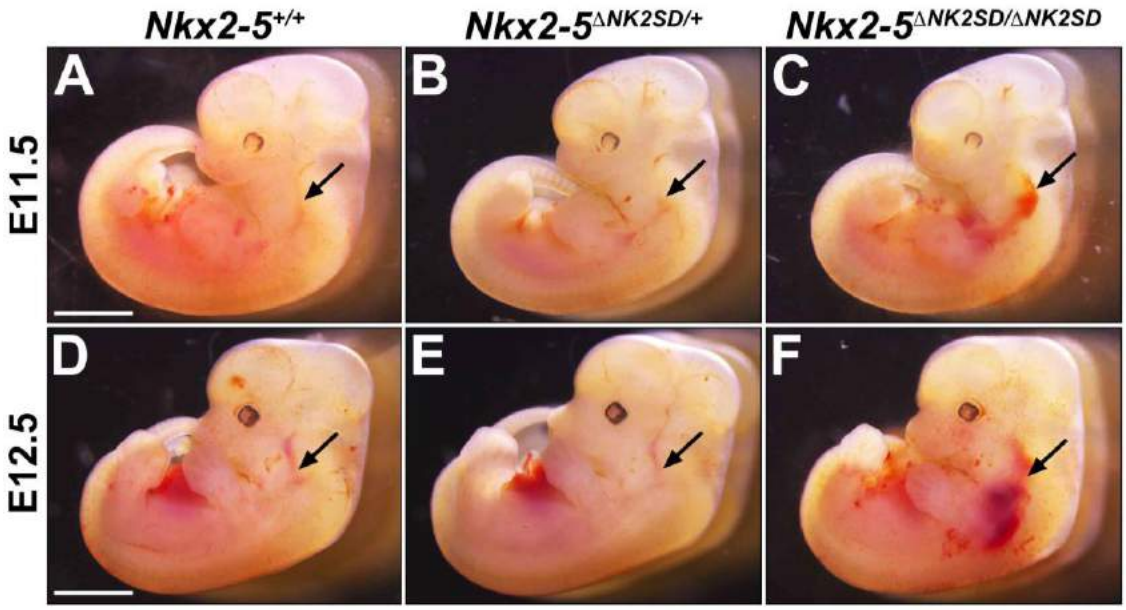

Figure 7. Embryonic Phenotype Timecourse at Late Embryonic Stages.
(A-F) Images of *Nkx2-5*$^{+/+}$ (A, D), *Nkx2-5*$^{\Delta NK2SD/+}$ (B, E) and *Nkx2-5*$^{\Delta NK2SD/\Delta NK2SD}$ (C, F) embryos at E11.5 (A-C) and E12.5 (D-F). Images were taken under the scope right after harvesting the embryos out of the decidua. Black arrows point to the anterior cardinal vein region where bleedings are present in *Nkx2-5*$^{\Delta NK2SD/\Delta NK2SD}$ embryos. Scale bar (A-C): 1.4 mm; Scale Bar (D-F): 1.8 mm.

4.4. Histological Analysis of Cardiovascular Phenotype in Nkx2-5$^{\Delta NK2SD/\Delta NK2SD}$ Mice

After analyzing the embryonic phenotype and macroscopic heart abnormalities in *Nkx2-5$^{\Delta NK2SD/\Delta NK2SD}$* mutant embryos, we continued our study by analyzing the underlying cardiac morphological defects on histological sections of WT and mutant hearts at the different embryonic stages stained with H&E.

4.4.1. Histological Analysis of Mutant Cardiac Phenotype at E8.5

The histological analysis by H&E stainings on sections of *Nkx2-5$^{\Delta NK2SD/\Delta NK2SD}$* mutant hearts at E8.5 revealed no major differences compared to *Nkx2-5$^{+/+}$* WT hearts. The structure of the normal heart tube at this stage shows that the process of cardiac looping has already started (**Figure 8A-C**'). All heart structures are clearly identified including OFT (**Figure 8A**), AVC and developing ventricular and atrium chambers (**Figure 8B**) and the sinus venosus region (**Figure 8C**). At this stage, the heart wall is formed by the myocardial and endocardial cellular layers separated by a thick ECM layer called cardiac jelly (**Figure 8B**).

In homozygous mutant embryos, the structure of the heart tube and the cellular integrity of the heart wall were essentially normal (**Figure 8A'-C'**). The looping of the heart tube was obvious and the morphology of OFT (**Figure 8A'**), the ventricular and atrial chambers (**Figure 8B'**) and the sinus venosus (**Figure 8C'**) seemed close to the WT phenotype (**Figure 8A-C**). The cellular composition of the heart wall was normal (**Figure 8B'**) and there were no relevant differences in the amount of cardiac jelly separating the myocardial and the endocardial layers compared to WT hearts (**Figure 8B, B'**). These data indicate that the deletion of the NK2SD domain in the NKX2-5 protein does not compromise the first stages of heart development including the formation of the primitive heart tube and the beginning of the cardiac looping process.

4.4.2. Histological Analysis of Mutant Cardiac Phenotype at E9.5

The histological analysis on H&E sections of *Nkx2-5$^{\Delta NK2SD/\Delta NK2SD}$* mutant hearts at E9.5 revealed no major morphological differences compared to *Nkx2-5$^{+/+}$* WT hearts. At this stage, the WT heart was in the final steps of looping. The developing ventricular and atrial chambers were clearly visible at this stage (**Figure 9A, C, E, F**) and chamber ballooning can be appreciated (**Figure 9A, E, F**). There were still no evidences of atrial and ventricular septation, and both the atrial chamber and the ventricular chamber kept an open conformation (**Figure 9A, C, E, F**). The AVC region in between the LV and the atrium had elongated and narrowed, and the endocardial

cushion which will give rise to the AVC valves had already formed (**Figure 9A, C, D**). As described before at E8.5, two different cellular layers can be distinguished in the WT heart: myocardium and endocardium (**Figure 9A, C, E, F**). At this stage, in the ventricular region the process of differentiation of the myocardial wall into compact and trabecular myocardium was already undergoing (**Figure 9E, F**). The trabecular myocardium will generate a sponge-like network of cardiomyocytes infiltrated by endocardium to form what is known as intertrabecular sinusoids. At this stage, a relatively thick heterogeneous layer of cardiac jelly separated the myocardial tissue from the endocardium (**Figure 9F**). However, the thickness of this ECM had already started to reduce as the trabecular myocardium grows towards the ventricular lumen (**Figure 9F**).

The morphology of the heart tube and the cellular integrity of the heart wall were essentially normal in mutant embryos, both mild and severe. The looping of the heart tube appeared relatively normal in the two phenotypes (**Figure 9A', A''**). In both severe and mild phenotype, the morphology and cellular composition of OFT (**Figure 9B', B''**), ventricles (**Figure 9A', A'', E'-F''**) and atrium (**Figure 9A', A'', C', C''**) looked normal, and the endocardial cushion had properly formed in between the LV and the atrial chamber (**Figure 9A', A'', D', D''**). However, decellularization and reduced extension of the AVC groove in the severe mutants was evident (**Figure A'', C'', D''**), confirming the observations performed in wholemount. Regarding the structure of the heart wall, the morphology of the cardiac histological layers were close to the WT phenotype, with ventricular trabeculation and intertrabecular sinusoids evident in both KO phenotypes (**Figure 9E'-F''**). Histological quantifications of the LV region measuring the areas of trabecular myocardium, compact layer and endocardium revealed no differences in these tissues between WT and mutant hearts (**Figure 9G**). However, there was a statistical significant increase (one-tailed *t*-test; $t(9) = 6.6$, *p*-value < 0.0001) in the amount of cardiac jelly separating the endocardium and the myocardium in the mutant hearts compared to WT (**Figure 9G**).

The normal structure of the heart wall, together with the relatively normal looping and chamber specification found in both groups of *Nkx2-5*$^{\Delta NK2SD/\Delta NK2SD}$ mutants, suggest that at E9.5 no mayor morphological defects are present. However, the defects observed in the AVC area only in the severe mutants supports our approach to separate these two mutant groups for further analysis. Moreover, both groups of mutants showed an increase in ECM content in the chambers that, although not associated to any important defect at this stage, anticipates the possible onset of defects in later stages.

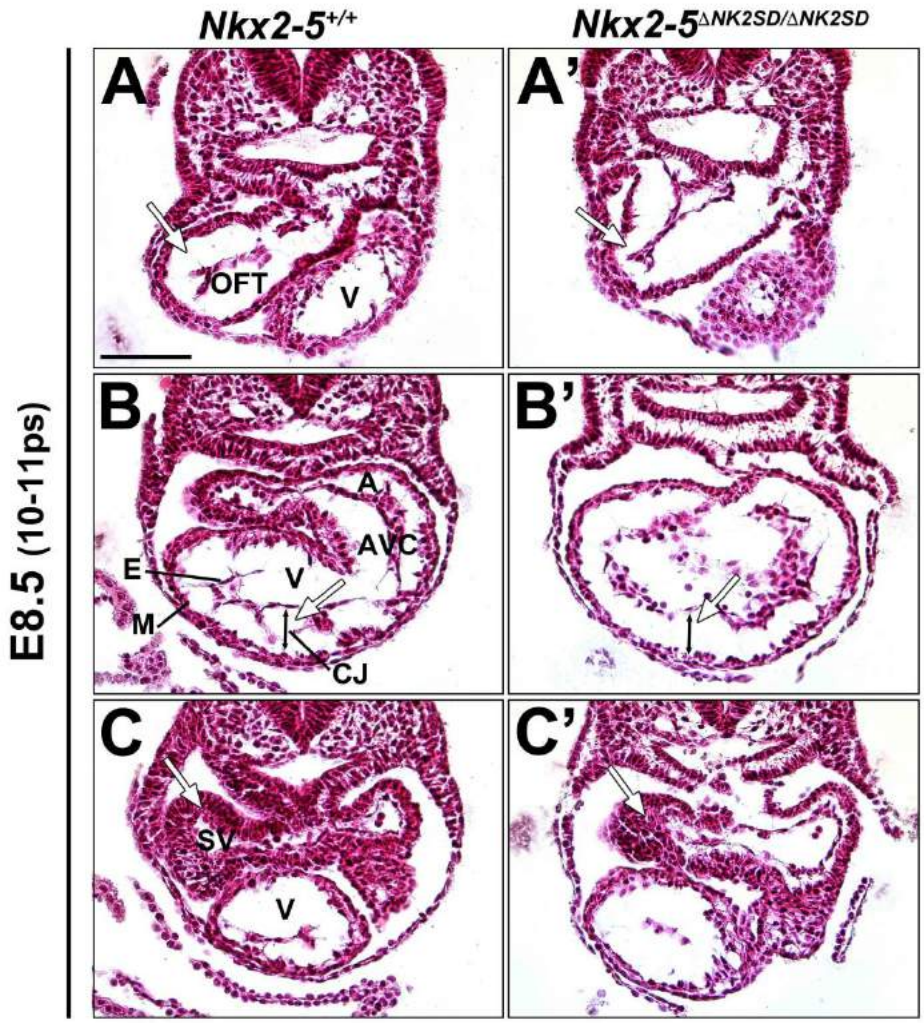

Figure 8. Histological Analysis by H&E staining of *Nkx2-5*$^{\Delta NK2SD/\Delta NK2SD}$ Mutant Hearts at E8.5.

H&E histological heart sections corresponding to E8.5 *Nkx2-5*$^{+/+}$ (10ps, A-C) and *Nkx2-5*$^{\Delta NK2SD/\Delta NK2SD}$ (11ps, A'-C') embryos. (A-A') Histological sections showing the OFT region of the primitive heart tube. (B-B') Histological sections showing the ventricular, atrial and AVC regions of the primitive heart tube. Double-headed black arrows highlight the thickness of the cardiac jelly, which is relatively similar in both WT and mutant hearts. (C-C') Histological sections showing the sinus venosus region of the primitive heart tube. A: atrium; AVC: atrioventricular canal; CJ: cardiac jelly; E: endocardium; V: ventricular chamber; M: myocardium; OFT: outflow tract; SV: sinus venosus. Scale Bar (A-C'): 80 μm.

Mutant Cardiac Phenotype Comparison between *Nkx2-5*$^{\Delta NK2SD/\Delta NK2SD}$ and *Nkx2-5*$^{GFP/GFP}$ Mice

Once we defined the histological cardiac defects of the *Nkx2-5*$^{\Delta NK2SD/\Delta NK2SD}$ mutant hearts at E9.5, these hearts were compared with *Nkx2-5*$^{GFP/GFP}$ hearts. The structure of the primordial *Nkx2-5*$^{GFP/GFP}$ heart tube was completely abnormal, largely linear in shape and without any evidence of looping or chamber morphogenesis (**Figure 9A'''**). In a general view of the heart tube, it was not possible to discern the boundaries of the cardiac chambers including both atrial and ventricular chambers (**Figure A''', D''', E'''**), or to appreciate any elongation or narrowing in between them that could suggest the presence of the AV groove (**Figure 9A''', C'''**). In addition, no endocardial cushions were formed (**Figure 9A''', D'''**). In addition, the OFT was shorter and narrower in these mutant hearts (**Figure 9B'''**). Therefore, the whole heart including atrium and ventricles formed an open and continuous monochamber (**Figure 9A''', D''', E'''**).

The heart wall displayed a normal cellular composition, but there were important defects affecting the main histological layers. The general overview of the ventricular chamber showed a stage of development more similar to the normal pretrabecular ventricle with no clear evidence of trabecular-like structures (**Figure 9E''', F'''**). There was no evidence of interaction between the endocardium and the myocardial wall, resulting on defects in the formation of the trabeculae carnae (**Figure 9E''', F'''**). Indeed, the trabecular myocardium in these mutant hearts did not form myocardial protrusions accompanied by the development of the characteristic intertrabecular endocardial sinusoids. In contrast, a continuous monolayer of cardiomyocytes had lost adhesion to the compact layer and appeared separated from it by cardiac jelly (**Figure 9F'''**). Furthermore, the cardiac jelly separating the endocardium and the myocardium appeared thicker similar to the pretrabecular stage (**Figure 9F'''**). Morphological area quantifications further supported this observation, showing a statistical significant increase (one-tailed *t*-test; $t(9) = 6.4$, *p*-value < 0.0001) in the amount of ECM compared to WT hearts. This ECM defects are similar to the ones described above for *Nkx2-5*$^{\Delta NK2SD/\Delta NK2SD}$ mutants (**Figure 9G**). Nevertheless, no differences in area quantifications of trabecular myocardium, compact layer and endocardium were observed in these hearts compared to the WT or *Nkx2-5*$^{\Delta NK2SD/\Delta NK2SD}$ mutant hearts (**Figure 9G**).

Therefore, with the exception of the increase in ECM, none of the previously described cardiac defects were observed in any of the *Nkx2-5*$^{\Delta NK2SD/\Delta NK2SD}$ mutant groups (**Figure 9A'-F', A''-F''**). In summary, these results further confirm that the cardiac phenotype observed in *Nkx2-*

$5^{\Delta NK2SD/\Delta NK2SD}$ mutant embryos is different and less severe than the one observed in *Nkx2-5*$^{GFP/GFP}$ mutants.

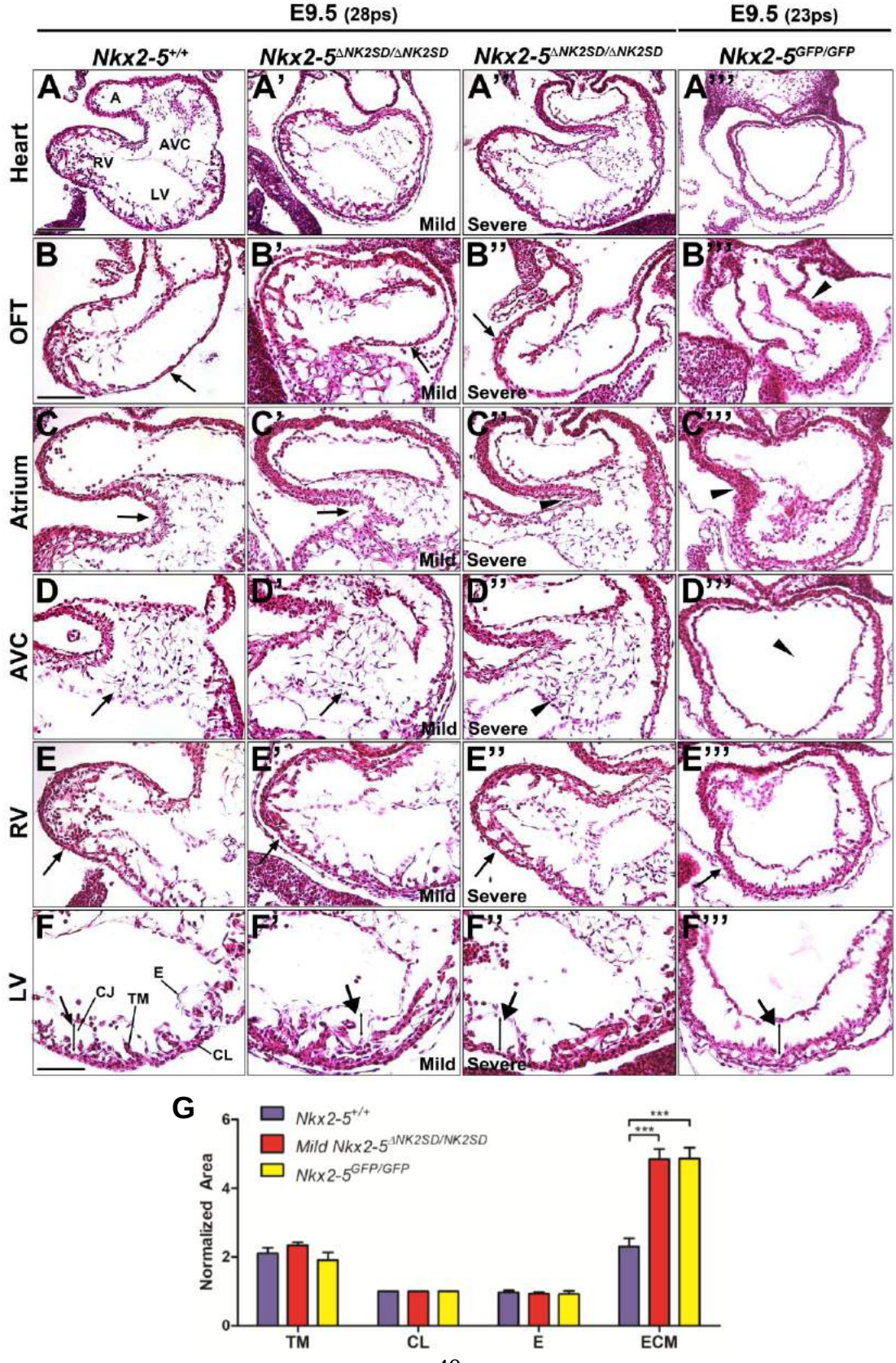

Figure 9. Histological Analysis of *Nkx2-5*$^{\Delta NK2SD/\Delta NK2SD}$ Mutant Hearts at E9.5 and Comparison with the *Nkx2-5*$^{GFP/GFP}$ Mutant Cardiac Phenotype.

(A-F’’’) H&E histological heart sections of *Nkx2-5*$^{+/+}$ (A-F), mild *Nkx2-5*$^{\Delta NK2SD/\Delta NK2SD}$ (A’-F’), severe *Nkx2-5*$^{\Delta NK2SD/\Delta NK2SD}$ (A’’-F’’) and *Nkx2-5*$^{GFP/GFP}$ (A’’’-F’’’) hearts at E9.5. (A-A’’’) Histological sections showing a general view of the heart tube in low magnification (10x). (B-F’’’) Histological sections showing the OFT (B-B’’’), atrium (C-C’’’), AVC (D-D’’’), RV (E-E’’’) and LV (F-F’’’) regions in high magnification (20x). Note that the overall size of the *Nkx2-5*$^{GFP/GFP}$ heart is smaller than the *Nkx2-5*$^{+/+}$ and both *Nkx2-5*$^{\Delta NK2SD/\Delta NK2SD}$ hearts, reason why an image of the whole ventricular chamber is shown in E’’’. Black arrows indicate: (B-B’’) Normal morphology and size of the OFT; (C, C’) Normal extension of the AVC groove; (D, D’) Presence of endocardial cushions in the AVC region; (E-E’’’) RV region; (F) Normal cardiac jelly. Black arrowheads indicate: (B’’) Short and narrow OFT; (C’’, C’’’) Lack of elongation of the AVC groove; (D’’) Reduced cellularization of the endocardial cushions in the AVC region; (D’’’) Complete absence of endocardial cushions in the AVC region. Thick black arrows in (F’-F’’’) indicate increased amount of cardiac jelly. Double-headed black arrows in (F-F’’’) indicate the cardiac jelly thickness. (G) Morphological quantifications showing the normalized areas of the trabecular myocardium, compact layer, endocardium and ECM in the LV, quantified on H&E histological sections of *Nkx2-5*$^{+/+}$ (*n*=2, 3 sections/embryo), mild *Nkx2-5*$^{\Delta NK2SD/\Delta NK2SD}$ (*n*=2, 3 sections/embryo) and *Nkx2-5*$^{GFP/GFP}$ (*n*=2, 3 sections/embryo) hearts. Asterisks indicate conventional statistical significance (***$p < 0.001$; one-tailed *t*-test). AVC: atrioventricular canal; A: atrium; CJ: cardiac jelly; CL: compact layer; E: endocardium; LV: left ventricle; RV: right ventricle; TM: trabecular myocardium. Scale Bar (A-A’’’): 110 μm; Scale Bar (B-E’’’): 80 μm; Scale Bar (F-F’’’): 70 μm.

4.4.3. Histological Analysis of Mutant Cardiac Phenotype at E10.5

The histological analysis on H&E sections of mild and severe *Nkx2-5*$^{\Delta NK2SD/\Delta NK2SD}$ mutant hearts at E10.5 revealed remarkable differences compared to *Nkx2-5*$^{+/+}$ WT hearts. At this developmental stage, WT hearts had already finished looping, with chambers positioned in their final location (**Figure 10A**). The process of ventricular ballooning was advanced (**Figure 10A, E, F**) and the first evidences of interventricular septation had appeared (**Figure 10A, E**). The atrium had expanded, and a primordium of IAS had budded in the demarcation between both atrial chambers (**Figure 10C**). The endocardial cushions of the AVC and OFT regions, formed at E9.5, have thickened and were cellularized with cells resulting from endocardial EMT (**Figure 10A, B,**

D). At this stage, the ventricular chambers showed a complex network of sponge-like trabeculae carnae filling up the ventricular lumen (**Figure 10E, F**), whereas the atrial chambers remained as smooth myocardial walls (**Figure 10C**). The ventricular chamber endocardium showed a heterogeneous pattern with respect to their distance to the myocardium. The endocardium in the regions near to the compact layer was closely in contact with the myocardium, whereas the endocardium surrounding the luminal areas of the trabecular myocardium was separated from the myocardium by a thick cardiac jelly (**Figure 10F**). In contrast, the entire endocardium of the atrium was in close contact with the myocardium besides the endocardium surrounding the IAS primordia (**Figure 10C**).

The mild *Nkx2-5*$^{\Delta NK2SD/\Delta NK2SD}$ phenotype showed no defects in cardiac looping (**Figure 10A'**). However, the heart appeared significantly smaller with cardiac chambers clearly reduced in size, suggesting a delay in the chamber ballooning processes (**Figure 10A', C', E', F'**). No defects in the cellularization of OFT or AVC regions were observed in the mild mutant heart (**Figure 10B', D'**). Detailed analysis of the ventricular chambers showed a clear reduction of the amount of trabecular myocardium in both ventricles (**Figure 10E', F'**). Furthermore, the distance between the endocardium and the myocardium in the trabecular region was clearly increased compared to WT chambers, suggesting thicker cardiac jelly (**Figure 10F'**). But the most striking phenotype observed in the mild mutants was the lack of neither IVS (**Figure 10A', E'**) nor IAS (**Figure 10C'**) primordiums compared to WT hearts (**Figure 10A, C, E**).

Similar analysis performed in the severe *Nkx2-5*$^{\Delta NK2SD/\Delta NK2SD}$ mutants confirmed the observations described in the macroscopic description and showed a necrotic appearance with inflammatory cells filling the lumen and cardiac jelly (**Figure 10B'', D''-F''**). Furthermore, the myocardium showed signs of decomposition and rupture (**Figure 10A''-F''**). Therefore, these embryos were excluded from further analysis.

In order to further confirm the histological observations described above for the *Nkx2-5*$^{\Delta NK2SD/\Delta NK2SD}$ mild mutants, area quantification of the different cardiac histological layers in the LV was performed. The analysis confirmed a statistical significant decrease (one-tailed *t*-test; $t(8) = 6.7$, *p*-value < 0.0001) in the amount of trabecular myocardium (**Figure 10G**), as described above for both RV and LV (**Figure 10E', F'**). No significant differences were observed in the compact myocardium or endocardium composition of the mutant LV compared to WT (**Figure 10G**). Importantly, a statistical significant increase (one-tailed *t*-test; $t(9) = 3.1$, *p*-value = 0.006)

in the amount of ECM was also observed at this embryonic stage compared to the WT phenotype (**Figure 10G**).

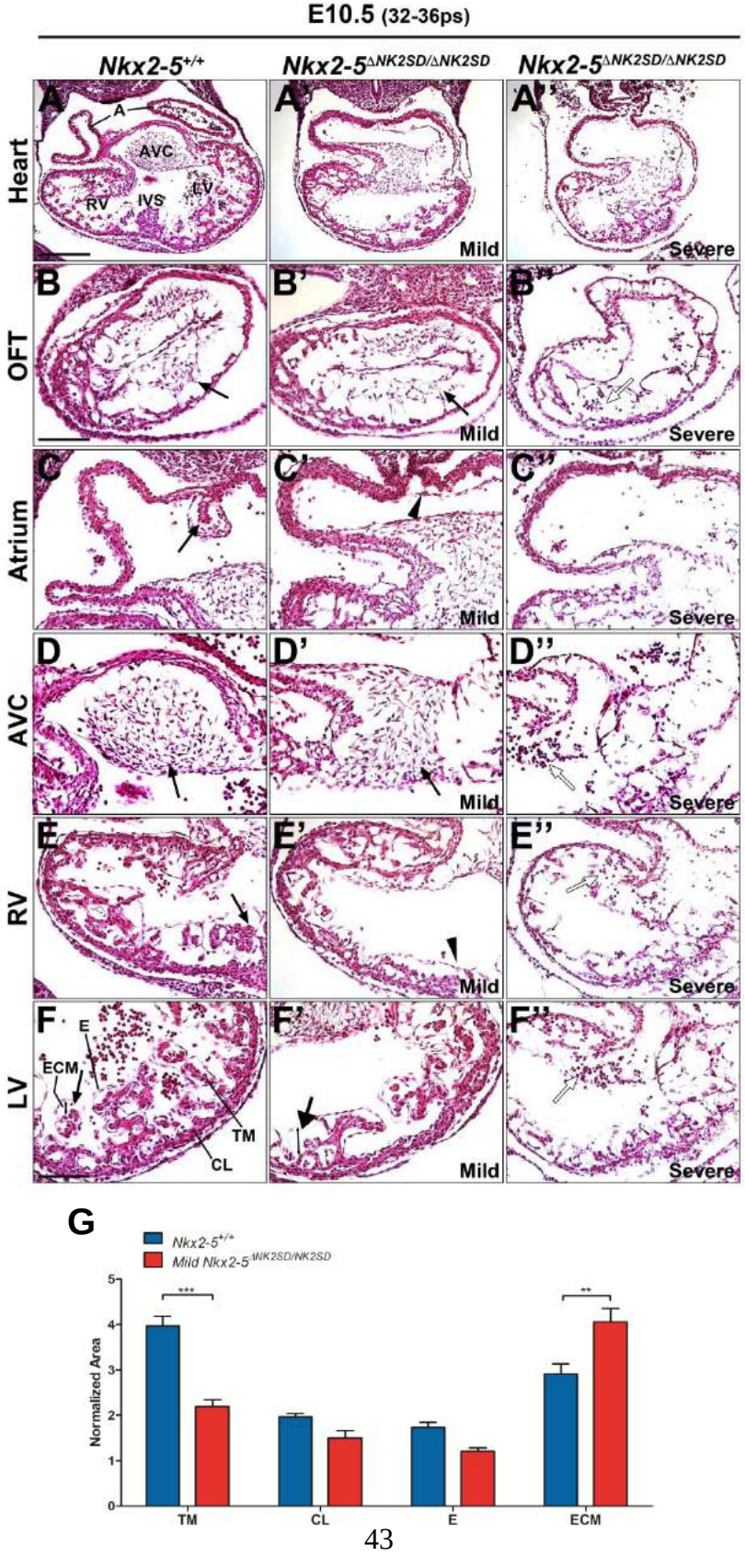

Figure 10. Histological Analysis of *Nkx2-5*$^{\Delta NK2SD/\Delta NK2SD}$ Mutant Hearts at E10.5.
(A-F'') H&E histological sections at the level of the heart region of E10.5 *Nkx2-5*$^{+/+}$ (A-F), mild *Nkx2-5*$^{\Delta NK2SD/\Delta NK2SD}$ (A'-F') and severe *Nkx2-5*$^{\Delta NK2SD/\Delta NK2SD}$ embryos (A''-F''). (A-A'') Low magnification (10x) images of histological sections showing the entire heart in a 4 chamber view. (B-F''). High magnification (20x) images showing histological sections at the OFT (B-B''), atrium (C-C''), AVC (D-D''), RV (E-E'') and LV (F-F'') regions. Black arrows indicate: (B, B') Normal OFT; (C) Presence of IAS primordium; (D, D') Normal AVC; (E) Presence of IVS primordium; (F) Normal ECM. Black arrowheads indicate: (C') Lack of IAS primordium; (E') Lack of IVS primordium. Thick black arrow in (F') indicates increased amount of cardiac jelly. Double-headed black arrows in (F, F') indicate the cardiac jelly thickness. White arrows in (B'', D''-F'') point immune cells infiltrations in necrotic tissue. (G) Morphological quantifications showing the normalized areas of the trabecular myocardium, compact layer, endocardium and ECM in the LV, quantified on H&E histological sections of *Nkx2-5*$^{+/+}$ (*n*=2, 3 sections/embryo) and mild *Nkx2-5*$^{\Delta NK2SD/\Delta NK2SD}$ (*n*=2, 3 sections/embryo) hearts. Asterisks indicate conventional statistical significance (***$p < 0.001$; **$p < 0.01$, one-tailed *t*-test). AVC: atrioventricular canal; A: atrium; CJ: cardiac jelly; CL: compact layer; E: endocardium; IVS: interventricular septum; LV: left ventricle; RV: right ventricle; TM: trabecular myocardium. Scale Bar (A-A''): 230 μm; Scale Bar (B-E''): 110 μm; Scale Bar (F-F''): 100 μm.

4.4.4. Histological Analysis of Mutant Cardiac Phenotype at E11.5

The histological analysis on H&E sections of *Nkx2-5*$^{\Delta NK2SD/\Delta NK2SD}$ mutant hearts at E11.5 showed important differences compared to *Nkx2-5*$^{+/+}$ WT hearts. At this developmental stage, WT hearts showed more mature chambers (**Figure 11A-D**). The ventricular ballooning process was advanced and both ventricles displayed a large lumen (**Figure 16A, C, D**), bigger in the LV as required for systemic circulation. The AVC is now located in the center of the heart and separates the atrium from both ventricles (**Figure 11A-C**). Furthermore, the process of septation of both atrium and ventricles was undergoing, with IAS present in between the RA and the LA (**Figure 11A, B**), and IVS in between the RV and the LV (**Figure 11A, C**). However, neither of them were completely formed, showing communication between both atria and both ventricles respectively. The ventricular trabeculation gained in area and complexity (**Figure 11C, D**). As it happened in the regions where the endocardium contacts the compact layer, at this stage the

cardiac jelly has also been reduced to a thin layer of ECM in between the intertrabecular endocardial sinusoids and the trabecular myocardium (**Figure 11D**).

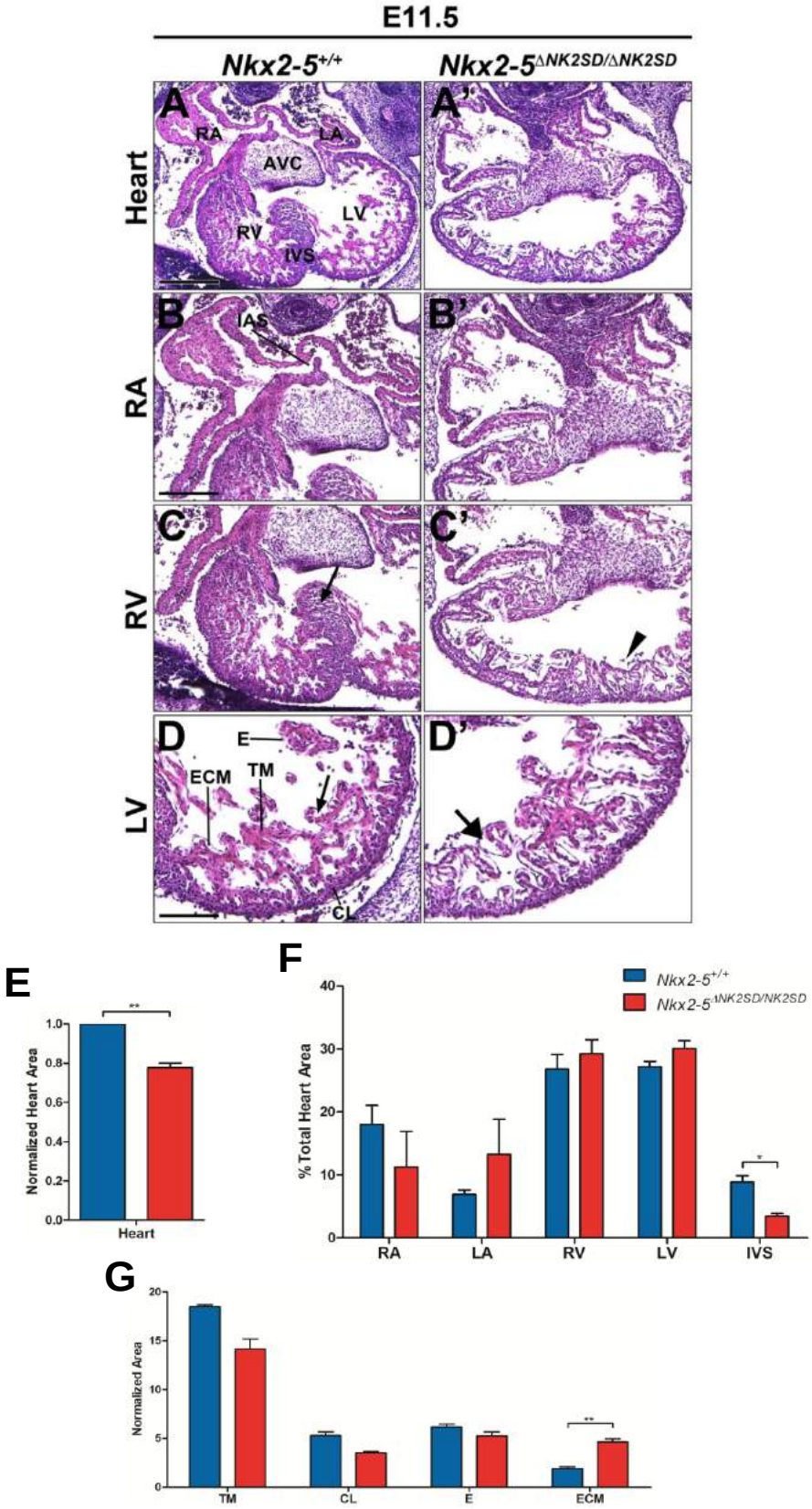

Figure 11. Histological Analysis of *Nkx2-5*$^{\Delta NK2SD/\Delta NK2SD}$ Mutant Hearts at E11.5.

(A-D') H&E histological analysis on heart sections of *Nkx2-5*$^{+/+}$ (A-D) and *Nkx2-5*$^{\Delta NK2SD/\Delta NK2SD}$ (A'-D') embryos. (A-A') Sections showing a general overview of the whole heart in low magnification (5x). RV, LV, RA, LA and AVC can be distinguished in both WT and mutant hearts. (B-B') Sections showing the RA region in high magnification (10x). (C-C') Sections showing the RV region in high magnification (10x). Black arrow indicates the presence of IVS. Black arrowhead indicates the absence of IVS. (D-D') Sections showing the LV region in high magnification (10x). Black arrow indicates normal amount of ECM. Thick black arrow indicates increased ECM. (E) Morphological quantifications showing normalized total cardiac areas, quantified on H&E histological sections of *Nkx2-5*$^{+/+}$ (*n*=1, 3 sections/embryo) and *Nkx2-5*$^{\Delta NK2SD/\Delta NK2SD}$ (*n*=1, 3 sections/embryo) hearts. (F) Morphological quantifications showing in percentage (%) the areas of the 4 cardiac chambers (RA, LA, RV, LV) and the IVS, quantified on H&E histological sections of *Nkx2-5*$^{+/+}$ (*n*=1, 3 sections/embryo) and *Nkx2-5*$^{\Delta NK2SD/\Delta NK2SD}$ (*n*=1, 3 sections/embryo) hearts. (G) Morphological quantifications showing the normalized areas of the trabecular myocardium, compact layer, endocardium and ECM in the LV, quantified on H&E histological sections of *Nkx2-5*$^{+/+}$ (*n*=1, 3 sections/embryo) and *Nkx2-5*$^{\Delta NK2SD/\Delta NK2SD}$ (*n*=1, 3 sections/embryo) hearts. Asterisks indicate conventional statistical significance (*$p < 0.05$, **$p < 0.01$; one-tailed *t*-test). Statistical analysis was performed on the basis explained in *Materials and Methods*. AVC: atrioventricular canal; LA: left atria; RA: right atria; CL: compact layer; E: endocardium; ECM: extracellular matrix; IAS: interatrial septum; IVS: interventricular septum; LV: left ventricle; RV: right ventricle; TM: trabecular myocardium. Scale Bar (A-A'): 290 μm; Scale Bar (B-C'): 220 μm; Scale Bar (D-D'): 140 μm.

At E11.5, the *Nkx2-5*$^{\Delta NK2SD/\Delta NK2SD}$ mutant hearts were ~20% smaller in size compared to WT hearts (**Figure 11A'**). This observation was confirmed by quantification of the total heart area (one-tailed *t*-test; t(3) = 7.5, *p*-value = 0.003) in the analyzed sections (**Figure 11E**). The mutant heart showed the normal four-chambered conformation, with clear RA, LA, RV and LV chambers (**Figure 11A'-D'**). Area quantification of the different heart regions showed no clear differences in the size of the atrial and ventricular chambers compared to WT (**Figure 11F**). The AVC displayed a normal location and conformation (**Figure 11A'-C'**).

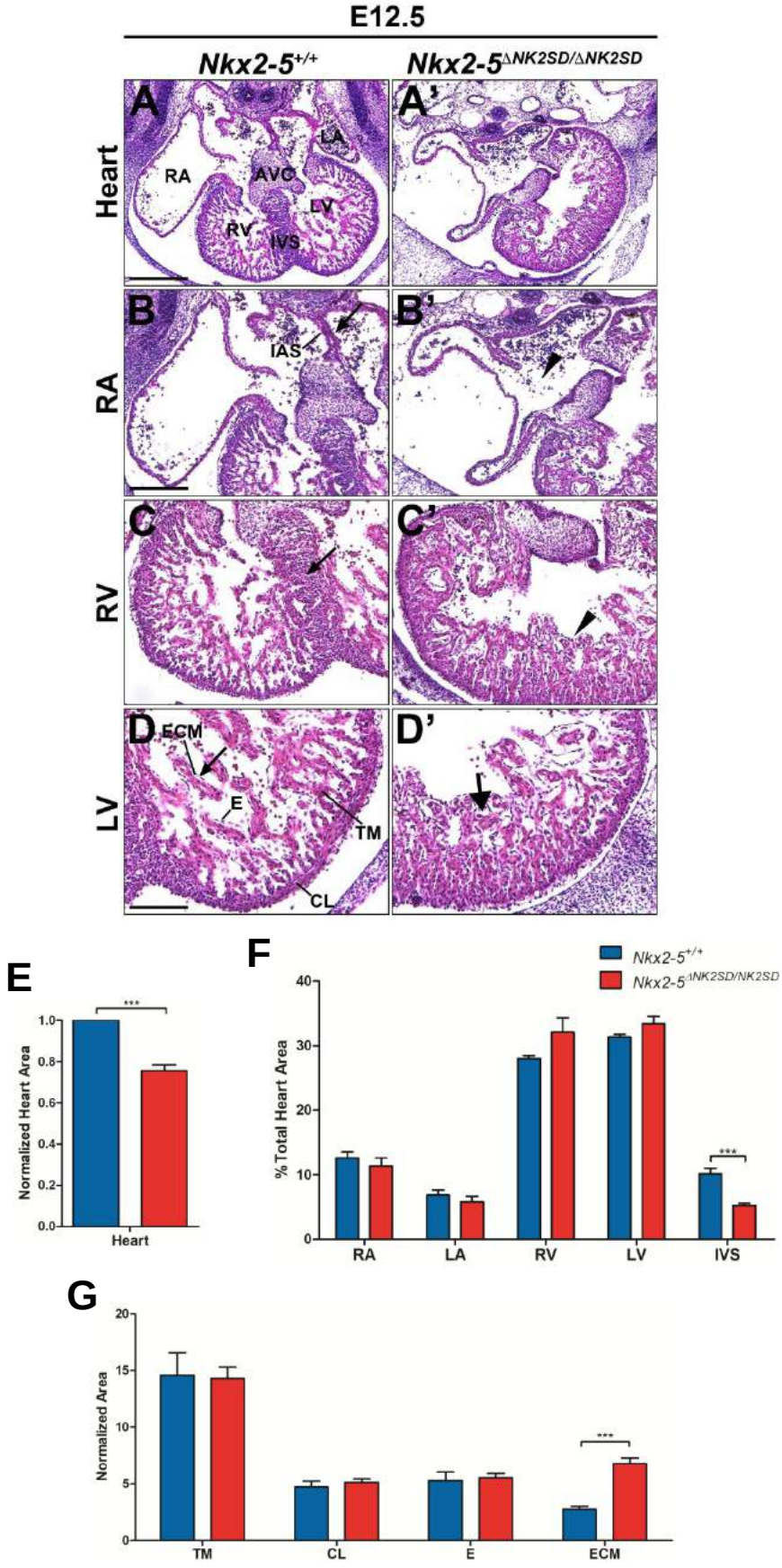
E12.5
Nkx2-5+/+
Nkx2-5ΔNK2SD/ΔNK2SD
Heart
RA
LV
RV
A
A'
RA
AVC
LA
RV
IVS
B
B'
IAS
C
C'
D
D'
ECM
E
TM
CL
E
Normalized Heart Area
1.0
0.8
0.6
0.4
0.2
0.0
***
Heart
F
Nkx2-5+/+
Nkx2-5ΔNK2SD/NK2SD
% Total Heart Area
40
30
20
10
0
***
RA
LA
RV
LV
IVS
G
Normalized Area
20
15
10
5
0
***
TM
CL
E
ECM

Figure 12. Histological Analysis of *Nkx2-5*$^{\Delta NK2SD/\Delta NK2SD}$ Mutant Hearts at E12.5.

(A-D') H&E histological staining on heart sections of *Nkx2-5*$^{+/+}$ (A-D) and *Nkx2-5*$^{\Delta NK2SD/\Delta NK2SD}$ (A'-D') embryos. (A-A') Sections showing a general overview of the whole heart in low magnification (5x). The RV, LV, RA, LA and AVC can be distinguished in both WT and mutant hearts. (B-B') Sections showing the RA region in high magnification (10x). Black arrow indicates the presence of IAS. Black arrowhead indicates the lack of IAS. (C-C') Sections showing the RV region in high magnification (10x). Black arrow indicates the presence of IVS. Black arrowhead indicates the absence of IVS. (D-D') Sections showing the LV region of the heart in high magnification (10x). Black arrow indicates normal amount of ECM. Thick black arrow indicates increases amount of ECM. (E) Morphological quantifications showing normalized total cardiac areas, quantified on H&E histological sections of *Nkx2-5*$^{+/+}$ (*n*=3, 3 sections/embryo) and *Nkx2-5*$^{\Delta NK2SD/\Delta NK2SD}$ (*n*=2, 3 sections/embryo) hearts. (F) Morphological quantifications showing in percentage (%) the areas of the 4 cardiac chambers (RA, LA, RV, LV) and the IVS, quantified on H&E histological sections of *Nkx2-5*$^{+/+}$ (*n*=3, 3 sections/embryo) and *Nkx2-5*$^{\Delta NK2SD/\Delta NK2SD}$ (*n*=3, 3 sections/embryo) hearts. (G) Morphological quantifications showing the normalized areas of the trabecular myocardium, compact layer, endocardium and ECM in the LV, quantified on H&E histological sections of *Nkx2-5*$^{+/+}$ (*n*=3, 3 sections/embryo) and *Nkx2-5*$^{\Delta NK2SD/\Delta NK2SD}$ (*n*=2, 3 sections/embryo) hearts. Asterisks indicate conventional statistical significance (***$p < 0.001$; one-tailed *t*-test). AVC: atrioventricular canal; CL: compact layer; E: endocardium; ECM: extracellular matrix; IAS: interatrial septum; IVS: interventricular septum; LA: left atria; LV: left ventricle; RA: right atria; RV: right ventricle; TM: trabecular myocardium. Scale Bar (A-A'): 390 μm; Scale Bar (B-C'): 190 μm; Scale Bar (D-D'): 130 μm.

However, there was a total absence of IVS in mutant hearts (**Figure 11A'-C'**), observation also confirmed by quantification (one-tailed *t*-test; t(2) = 4.8, *p*-value = 0.02) (**Figure 11F**). Although there was also no evidence of atrial septation (**Figure 11A'-B'**), it is difficult to make any definitive conclusions due to the orientation of the heart in the sections. Trabeculation seemed more convoluted than in WT chambers (**Figure 11C'-D'**), although LV tissue area quantification showed a reduction in the trabecular myocardium area in *Nkx2-5*$^{\Delta NK2SD/\Delta NK2SD}$ hearts compared to WT (**Figure 11G**). No differences were observed in the areas corresponding to the endocardium and the compact layer between WT and mutant hearts (**Figure 11G**). However, as observed in previous embryonic stages, area quantifications showed an increase of ECM area (one-tailed *t*-

test; t(3) = 7.5, *p*-value = 0.002) in the mutant hearts (**Figure 11G**). These results confirm the IVS deficit, and the defects in trabecular myocardium and ECM in the ventricular chambers already observed at E10.5.

4.4.5. Histological Analysis of Mutant Cardiac Phenotype at E12.5

The histological analysis on H&E sections of *Nkx2-5*$^{\Delta NK2SD/\Delta NK2SD}$ mutant hearts at E12.5 showed important differences compared to *Nkx2-5*$^{+/+}$ WT hearts, in the same line as what was described at E11.5. The WT heart at this stage displayed a similar general morphology than E11.5 hearts with further development of the cardiac chambers and valves (**Figure 12A**). Both the IAS and the IVS had finally sealed, dividing the heart in two regions (right heart and left heart) in solitary confinement (**Figure 12A-C**). The trabecular myocardium was well developed in both ventricles (**Figure 12C-D**). There was further reduction of ECM in between the endocardium and the myocardium (**Figure 12D**), what means the endocardial cells are in closer contact with trabecular cardiomyocytes. However, there was still some ECM spread around the areas in between the trabecular myocardium and the endocardium (**Figure 12D**).

Nkx2-5$^{\Delta NK2SD/\Delta NK2SD}$ hearts were ~25% smaller in size compared to the WT heart (**Figure 12A**), as confirmed by quantification of the total heart area in the sections analyzed (one-tailed *t*-test; t(7) = 7.8, *p*-value < 0.0001) (**Figure 12E**). Quantification of the areas of the different heart regions showed no size differences in the four cardiac chambers (**Figure 12F**). *Nkx2-5*$^{\Delta NK2SD/\Delta NK2SD}$ hearts were characterized at this stage by a total lack of septation in both the atrium and the ventricular chamber, resulting in non-septated atrial and ventricular chambers (**Figure 12A', B', C'**). Indeed, IVS absence was further confirmed by quantification (one-tailed *t*-test; t(10) = 5.4, *p*-value = 0.0001) (**Figure 12F**). Ventricular trabeculation in mutant hearts appeared more convoluted compared to WT (**Figure 12C', D'**), although area quantifications of LV trabecular myocardium did not show significant area differences between mutant and WT trabecular myocardium (**Figure 12G**). There were also no differences by area quantification in endocardium or compact layer areas between WT and mutant hearts (**Figure 12G**). Nevertheless, at this stage there was a significant increase (one-tailed *t*-test; t(7) = 7.3, *p*-value < 0.0001) in the ECM area in mutant hearts by histological quantification, consistent with the findings in previous embryonic stages (**Figure 12G**). Hence data at E12.5 further confirms *Nkx2-5*$^{\Delta NK2SD/\Delta NK2SD}$ hearts are characterized by septal defects accompanied by ventricular abnormalities in the trabecular myocardium and the ECM.

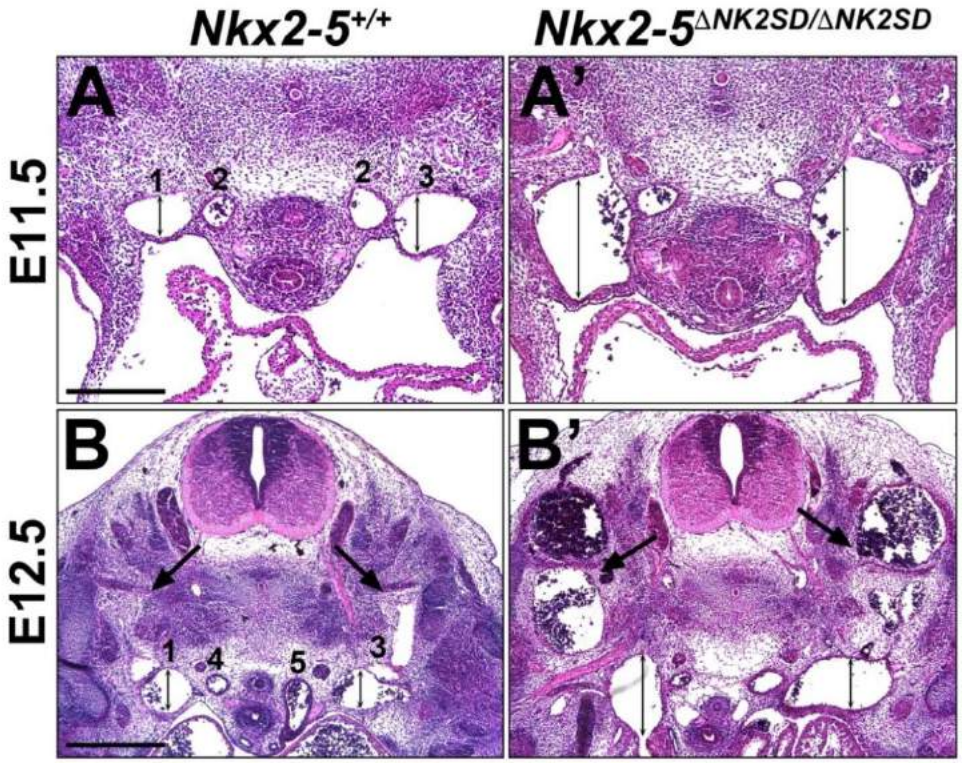

Figure 13. Histological Analysis of the Vasculature in *Nkx2-5*$^{\Delta NK2SD/\Delta NK2SD}$ Mutant Embryos at E12.5.

(A-B') H&E histological sections corresponding to *Nkx2-5*$^{+/+}$ (A, B) and *Nkx2-5*$^{\Delta NK2SD/\Delta NK2SD}$ (A', B') embryos. Images show a general overview in low magnification (5x) of the main vessels located around the heart region at E11.5 (A, A') and E12.5 (B, B'). Black double-headed arrows indicate the diameter of the right and left anterior cardinal veins right after leaving the heart. Black arrows in (B, B') highlight the massive enlargement of the right and left anterior cardinal veins in the posterior region of the body in *Nkx2-5*$^{\Delta NK2SD/\Delta NK2SD}$ embryos at E12.5. 1: anterior cardinal vein; 2: dorsal aorta; 3: left anterior cardinal vein; 4: right common carotid artery; 5: left descending aorta. Scale bar (A, A'): 290 μm; Scale Bar (B, B'): 390 μm.

4.4.6. Histological Analysis of the Vascular Phenotype in *Nkx2-5*$^{\Delta NK2SD/\Delta NK2SD}$ Mice at Late Embryonic Stages

After completing the morphological characterization of the homozygous mutant heart regions across the different embryonic stages, we continued with the analysis of the vasculature on the *Nkx2-5*$^{\Delta NK2SD/\Delta NK2SD}$ embryos, aiming to elucidate the causes of the bleedings observed at E11.5

and E12.5 (**Figure 7**). Whereas at early embryonic stages there were no major differences between the WT and the mutant phenotypes (data not shown), the histological analysis of the mayor vessels ingressing and coming out from the heart revealed interesting findings at late embryonic stage, which provide another important feature of the *Nkx2-5*$^{\Delta NK2SD/\Delta NK2SD}$ mutant phenotype. At both stages, a massive increase in the size of the right and left anterior cardinal veins could be observed (**Figure 13A', B'**). This abnormality was especially dramatic at E12.5, in which these veins were occupying the majority of the embryonic body in that region (**Figure 13B'**). No abnormalities were detected in the rest of the vessels which appeared on the sections including the dorsal aorta at E11.5, and the left descending aorta and the right common carotid artery at E12.5 (**Figure 13A-B'**). Therefore, the deletion of NK2SD from the NKX2-5 TF not only has an effect on cardiac development but also in the vasculature.

4.5. Analysis of the Expression of Nkx2-5 and its Translocation to the Nucleus in Nkx2-5$^{\Delta NK2SD/\Delta NK2SD}$ *Hearts*

There is always a level of uncertainty in every experiment and research strategy, even though it has been planned and conducted carefully. The generation of a novel mouse transgenic line involves multiple complex steps which could have potentially ignored secondary effects in the altered gene or even in the whole genome. One of the research objectives of this project was to confirm that *Nkx2-5* was normally expressed in the *Nkx2-5*$^{\Delta NK2SD/\Delta NK2SD}$ mutant embryos and more importantly, whether the protein translocates to the nucleus. The cardiac and vascular defects described so far could be also explained, at least partly, by the lack of expression of *Nkx2-5* as its downregulation or lack nuclear translocation has been related with some of these defects [28, 55]. Therefore, to be able to determine whether or not the mutant phenotype described above is only due to the lack of NK2SD specific function in the NKX2-5 TF and not due to other causes, it is of utmost importance to analyze the expression profile of the gene along the analyzed embryonic stages.

4.5.1. Expression of *Nkx2-5* at mRNA Level

The expression of *Nkx2-5* was first studied at mRNA level by *in situ* hybridization with a specific probe (see *Materials and Methods*). Histological tissue sections from WT and *Nkx2-5*$^{\Delta NK2SD/\Delta NK2SD}$ hearts at E9.5, E10.5, E11.5 and E12.5 were studied. The results showed that *Nkx2-5* expression was uniformly located in the myocardium of WT hearts (**Figure 14A-D**). No changes in expression pattern were observed in *Nkx2-5*$^{\Delta NK2SD/\Delta NK2SD}$ hearts, confirming the presence of *Nkx2-*

5 mRNA in the mutant hearts across all the embryonic stages analyzed. However, the staining was less intense in mutant hearts compared to WT hearts at E9.5 (**Figure 14A, A'**), E11.5 (**Figure 14C, C'**) and E12.5 (**Figure 14D, D'**), indicating that *Nkx2-5* expression might be slightly downregulated in the mutant hearts. Further studies by real time quantitative PCR (RT-qPCR) are required to confirm this finding. Therefore, these results suggest that the deletion of the NK2SD domain in the NKX2-5 TF does not affect the expression pattern of the gene but could affect the transcriptional levels of expression of the gene.

4.5.2. Expression of *Nkx2-5* at Protein Level and Translocation to the Nucleus

Next, *Nkx2-5* expression was analyzed at protein level by immunofluorescence (see *Materials and Methods*). Histological sections from *Nkx2-5*$^{\Delta NK2SD/\Delta NK2SD}$ hearts at E8.5, E9.5, E10.5, E11.5 and E12.5 were analyzed by immunofluorescence with NKX2-5 antibody and co-stained for SMA as a myocardial marker and DAPI as a nuclear counterstain (**Figure 15**). Confocal images showed the expected nuclear localization of NKX2-5 in WT cardiomyocytes (**Figure 15A-E**). Importantly, clear NKX2-5 nuclear staining was also detected in *Nkx2-5*$^{\Delta NK2SD/\Delta NK2SD}$ hearts at all the stages analyzed (**Figure 15A'-E', B''**). Furthermore, no expression pattern changes were observed in mutant hearts either with a mild or a severe phenotype at E9.5 (**Figure 15B', B''**). Intensity differences in respect to the WT phenotype were noticed in the mutant hearts at E9.5 (more intense in the mild phenotype (**Figure 15B'**) and less intense in the severe phenotype (**Figure 15B''**)), E10.5 (less intense, **Figure 15C'**) and E11.5 (more intense, **Figure 15D'**). However, the lack of consistency in the intensity level of the staining across stages might be due to variability in the experimental procedure, including differences in the fixation and embedding processes, rather than to an underlying molecular cause related to the NK2SD deletion. This hypothesis is further supported by the similar NKX2-5 levels observed in WT and mutant hearts at E12.5 (**Figure 15E, E'**). Co-localization of the NKX2-5 staining with the SMA mask proved the myocardial specific expression of the TF in the myocardium. Moreover, the specific nuclear pattern of the NKX2-5 signal confirmed that the lack of NK2SD domain in the NKX2-5 protein does not prevent the proper translocation of the protein to the nucleus.

Altogether, our data confirmed the proper expression of *Nkx2-5* at mRNA and protein levels, and its translocation to the nucleus in the absence of the NK2SD domain, confirming the validity of this mouse line for our research purposes.

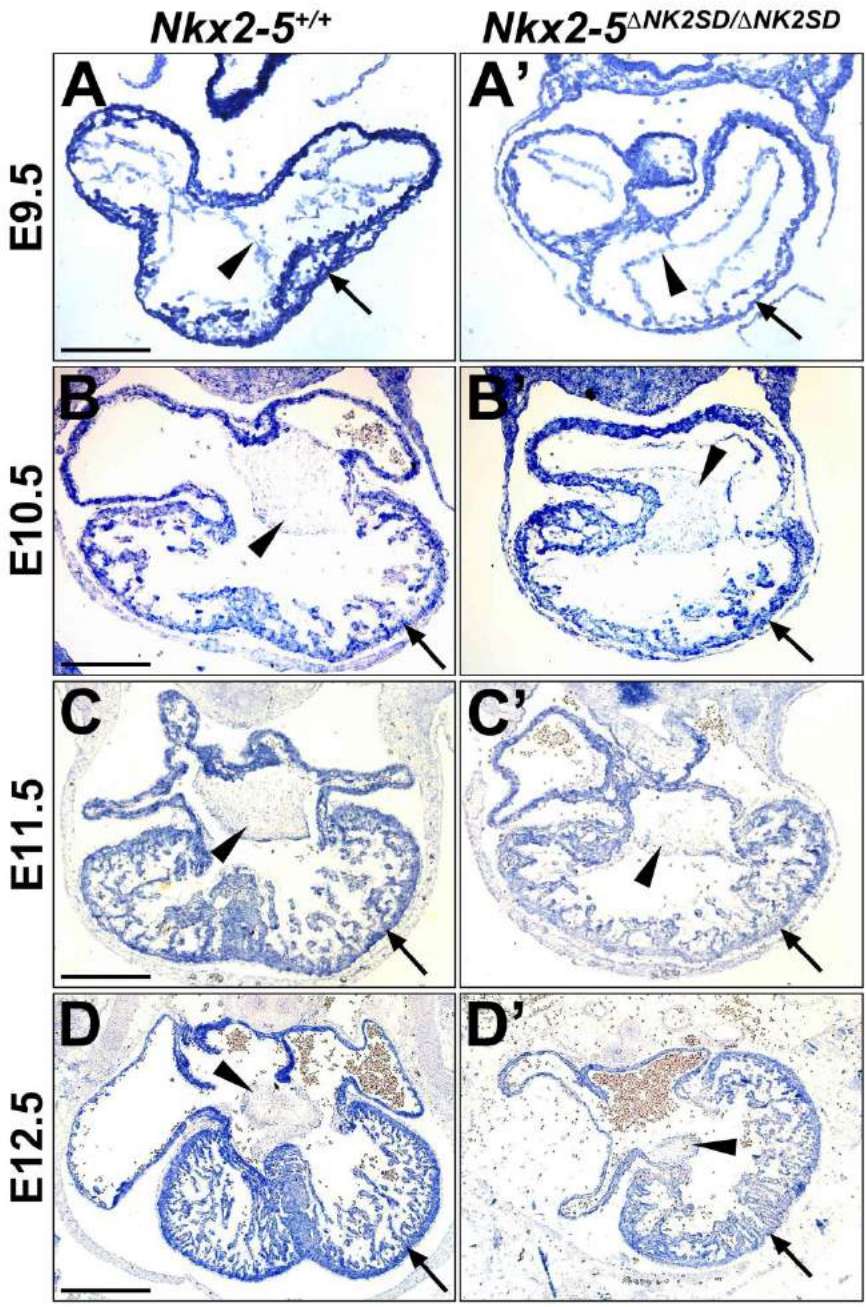

Figure 14. Gene Expression Analysis of *Nkx2-5* at mRNA Level in *Nkx2-5*$^{\Delta NK2SD/\Delta NK2SD}$ Mutant Hearts along Embryonic Development.

In situ hybridization on histological sections from *Nkx2-5*$^{+/+}$ and *Nkx2-5*$^{\Delta NK2SD/\Delta NK2SD}$ hearts hybridized with *Nkx2-5* probe. The following embryonic stages were analyzed: (A, A') E9.5 (28ps, *n*=2); (B, B') E10.5 (35ps, *n*=2); (C, C') E11.5 (*n*=3); (D, D') E12.5 (*n*=3). Black arrows highlight the positive myocardial staining. Black arrowheads indicate background staining. Scale bar (A, A'): 110 μm; Scale Bar (B, B'): 230 μm; Scale Bar (C, C'): 290 μm; Scale Bar (D, D'): 390 μm.

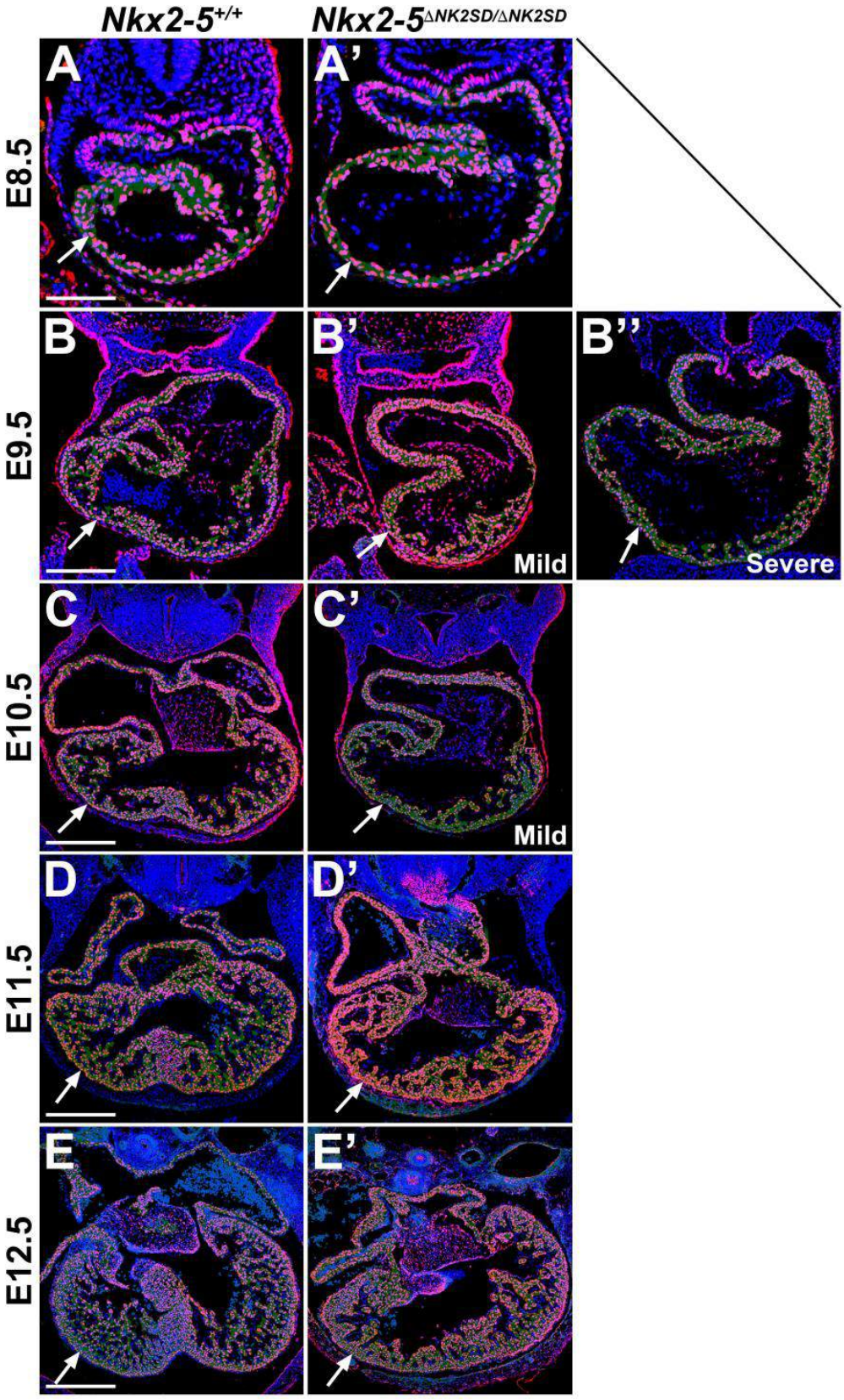
Nkx2-5+/+
Nkx2-5ΔNK2SD/ΔNK2SD
A
A'
E8.5
B
B'
B''
E9.5
Mild
Severe
C
C'
E10.5
Mild
D
D'
E11.5
E
E'
E12.5

Figure 15. Analysis of the *Nkx2-5* Expression at Protein Level in *Nkx2-5*$^{\Delta NK2SD/\Delta NK2SD}$ Mutant Hearts along Embryonic Development.

(A-E') Immunofluorescent staining on histological sections of *Nkx2-5*$^{+/+}$ (A-E) and *Nkx2-5*$^{\Delta NK2SD/\Delta NK2SD}$ (A'-E', B'') hearts stained for NKX2-5 (red), SMA (green mask) for myocardium labeling and DAPI (blue) for nuclear labeling. Embryonic stages analyzed: (A-A') E8.5 (11ps, *n*=2); (B-B') E9.5 (28ps, *n*=3); (C-C') E10.5 (35ps, *n*=2); (D-D') E11.5 (*n*=3); (E-E') E12.5 (*n*=3). Images of *Nkx2-5*$^{\Delta NK2SD/\Delta NK2SD}$ mutant hearts with a mild (B') and a severe (B'') phenotype are shown at E9.5. White arrows point positive nuclear NKX2-5 staining in myocardial tissue. Scale bar (A, A'): 80 μm; Scale Bar (B, B'): 110 μm; Scale Bar (C, C'): 230 μm; Scale Bar (D, D'): 290 μm; Scale Bar (E, E'): 390 μm.

NKX2-5 Protein Expression Comparison between *Nkx2-5*$^{\Delta NK2SD/\Delta NK2SD}$ and *Nkx2-5*$^{GFP/GFP}$ Hearts

We also compared the expression of the NKX2-5 protein in *Nkx2-5*$^{\Delta NK2SD/\Delta NK2SD}$ hearts and *Nkx2-5*$^{GFP/GFP}$. As explained in *Materials and Methods*, this mouse line was generated by the insertion of a GFP cassette in the position corresponding to amino acid 35 of the protein. Therefore, a fusion protein is expressed in the cardiomyocytes of these mutant hearts, formed by the first 35 amino acids of NKX2-5 and the GFP peptide. The antibody used for these immunostainings binds the N-terminal domain of the NKX2-5 TF. Therefore, we expected a positive staining in the *Nkx2-5*$^{GFP/GFP}$ hearts revealing the localization of this fusion protein. Indeed, our data showed positive staining in the *Nkx2-5*$^{GFP/GFP}$ hearts, although the pattern in this case was not nuclear but cytosolic (**Figure 16B'**). As predicted, the fusion protein is not active and cannot be translocated to the nucleus. This staining clearly contrasts with the pattern observed in the *Nkx2-5*$^{\Delta NK2SD/\Delta NK2SD}$ hearts, in which a clear nuclear localization of the protein is observed (**Figure 16A', A''**) as in WT hearts (**Figure 16A, B**). Therefore, these results further confirm the proper expression and integrity of the NKX2-5 protein in the *Nkx2-5*$^{\Delta NK2SD/\Delta NK2SD}$ hearts at E9.5.

4.6. Analysis of the Molecular Defects Underlying the Mutant Cardiac Phenotype Observed in Nkx2-5$^{\Delta NK2SD/\Delta NK2SD}$ *Hearts*

Finally, the last objective of this research project was to provide preliminary insights on the potential molecular alterations induced by NK2SD domain deletion, responsible for the cardiovascular defects described above. For that purpose, we conducted a preliminary molecular

screening by *in situ* hybridization and immunofluorescence on E12.5 mutant hearts, searching for changes in the expression of relevant genes in the cardiac kernel and involved in normal heart development and physiology.

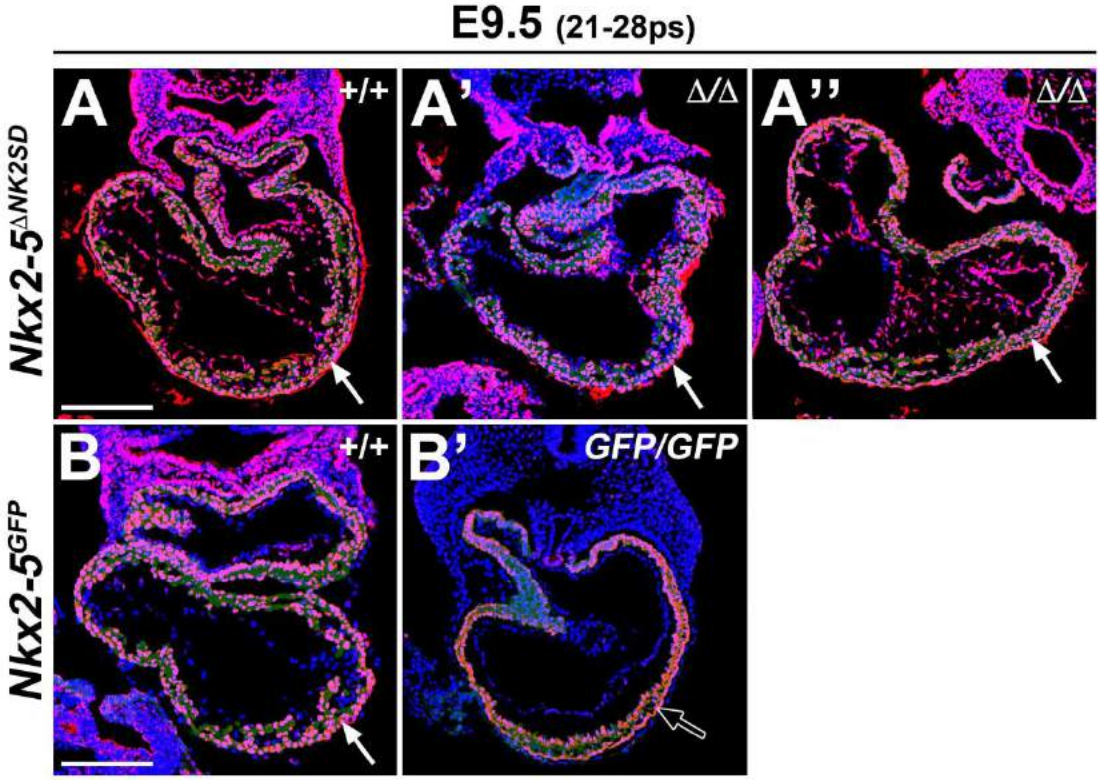

Figure 16. NKX2-5 Protein Expression Comparison between *Nkx2-5*$^{\Delta NK2SD/\Delta NK2SD}$ and *Nkx2-5*$^{GFP/GFP}$ Mutant Hearts at E9.5.

(A-B') Immunofluorescent staining on histological sections of E9.5 *Nkx2-5*$^{+/+}$ (28ps, A; 21ps, B), mild *Nkx2-5*$^{\Delta NK2SD/\Delta NK2SD}$ (28ps, *n*=3, A'), severe *Nkx2-5*$^{\Delta NK2SD/\Delta NK2SD}$ (28ps, *n*=3, A'') and *Nkx2-5*$^{GFP/GFP}$ (28ps, *n*=3, B') hearts, stained for NKX2-5 (red), SMA (green mask) for myocardium labeling and DAPI (blue) for nuclear labeling. +/+: *Nkx2-5*$^{+/+}$; Δ/Δ: *Nkx2-5*$^{\Delta NK2SD/\Delta NK2SD}$; *GFP/GFP*: *Nkx2-5*$^{GFP/GFP}$. Scale bar (A-A''): 110 μm; Scale Bar (B, B'): 90 μm.

4.6.1. Expression Analysis of Compact Layer Markers

We first checked the mRNA levels of *Hairy/Enhancer-of-Split Related Protein 2* (*Hey2*), a TF which plays a crucial role in cardiovascular development [86-88] and whose expression is restricted to the compact layer of the developing ventricular chamber in WT E12.5 hearts (**Figure**

17A, C, D). Similar to the WT expression pattern (**Figure 17B**), *Nkx2-5*$^{\Delta NK2SD/\Delta NK2SD}$ hearts did not express this gene in the atrium (**Figure 17B'**). In the ventricular chambers, reduced expression of *Hey2* was found on the RV compared to WT chambers (**Figure 17C, C'**). In contrast, *Hey2* was expressed in the compact layer of the LV (**Figure 17D'**) at similar levels than found in WT chambers (**Figure 17D**). Interestingly, the strong *Hey2* expression found in the IVS of WT hearts was completely downregulated in the mutants (**Figure 17D, D'**). These results suggest that the NK2SD deletion prevents the normal expression of *Hey2* especially in the IVS and the RV.

4.6.2. Expression Analysis of Atrial and Trabecular Myocardial Marker

Next, the transcriptional expression of genes with restricted expression in the trabecular myocardium but also expressed in the atrial myocardium were analyzed: *Natriuretic peptide A* (*Nppa*), *Gap junction protein alpha 5* (*Gja5*) and *Mesoderm specific transcript* (*Mest*).

Nppa gene encodes for the ATRIAL NATRIURETIC FACTOR (ANF), which controls the extracellular fluid volume and electrolyte homeostasis [89, 90]. *Nppa* has been described as a direct target gene of *Nkx2-5* [54, 91]. At E12.5, *Nppa* WT expression is mainly located in the trabecular myocardium of both ventricles, but also in the atrial chambers (**Figure 17E, F, G, H**). Importantly, there is no *Nppa* expression in the IVS (**Figure 17E, G**). *Nppa* expression analysis in *Nkx2-5*$^{\Delta NK2SD/\Delta NK2SD}$ hearts revealed no important differences in the expression levels of this gene neither in the atrium (**Figure 17E', F'**) nor in the ventricular chambers (**Figure 17E', G', H'**). However, ectopic expression of *Nppa* was detected in the region corresponding to the presumptive IVS of mutant hearts (**Figure 17G'**).

Gja5 is a member of the connexin gene family which encodes for a protein component of the GAP junctions called CONNEXIN40 (CX40). Hence this gene is required for proper contraction of the cardiac muscle tissue [92, 93]. Similar to the *Nppa* expression pattern, *Gja5* is expressed in the chamber myocardium, particularly in the RV and LV trabecular myocardium (**Figure 17I, K, L**) and in the atrial myocardium (**Figure 17I, J**), and excluded from the IVS (**Figure 17L**). *Gja5* expression analysis in *Nkx2-5*$^{\Delta NK2SD/\Delta NK2SD}$ hearts showed a normal expression profile in the LV (**Figure 17I', L'**) and LA (**Figure 17I', J'**). However, total expression downregulation was observed in the RV (**Figure 17I', K'**) and the RA (**Figure 17I', J'**), suggesting an important role of *Nkx2-5* in the control of *Gja5* expression in the right side of the heart.

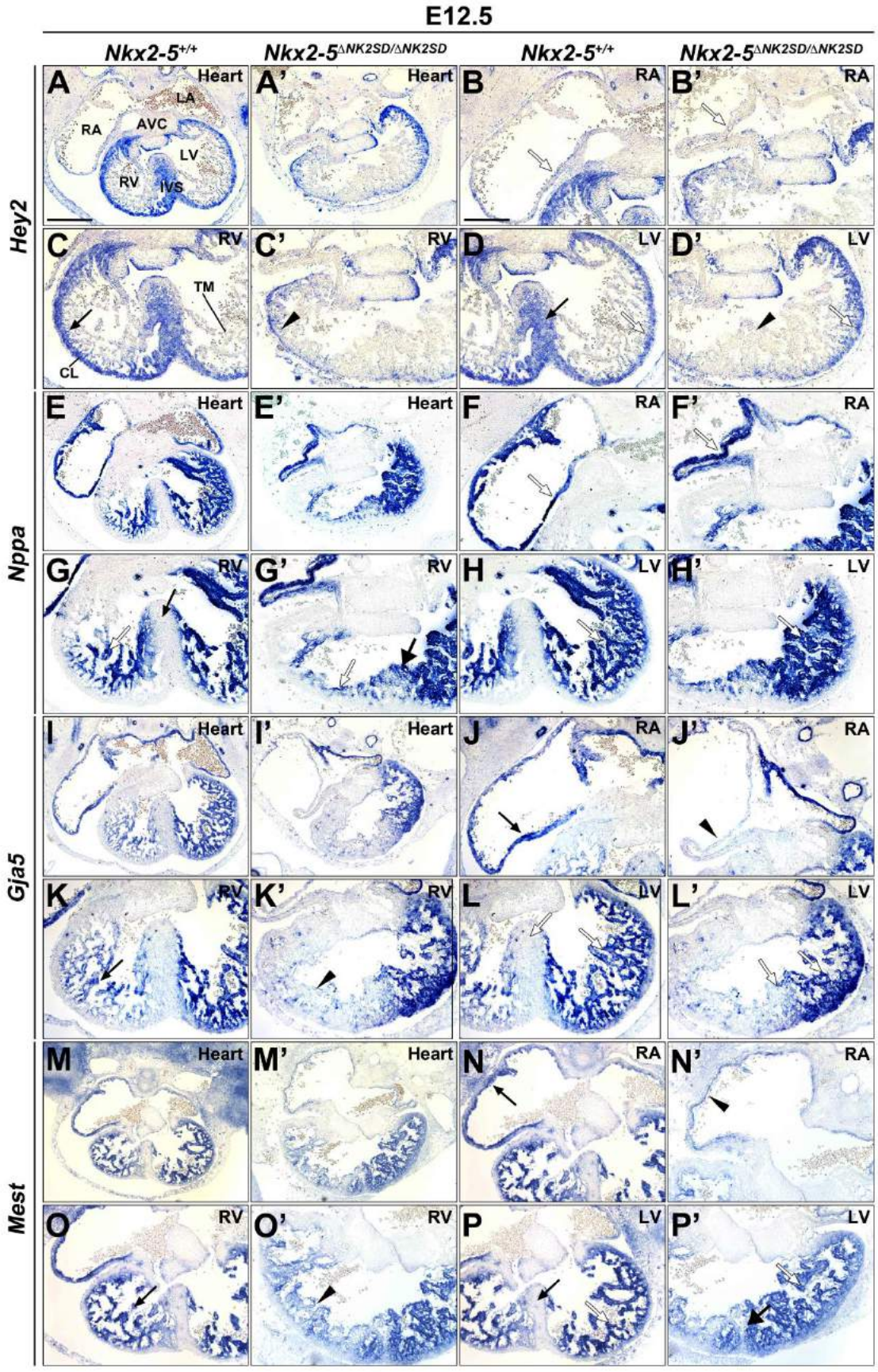
E12.5
Nkx2-5+/+
Nkx2-5ΔNK2SD/ΔNK2SD
Nkx2-5+/+
Nkx2-5ΔNK2SD/ΔNK2SD
Hey2
Nppa
Gja5
Mest
A
Heart
LA
RA
AVC
LV
RV
IVS
A'
Heart
B
RA
B'
RA
C
RV
TM
CL
C'
RV
D
LV
D'
LV
E
Heart
E'
Heart
F
RA
F'
RA
G
RV
G'
RV
H
LV
H'
LV
I
Heart
I'
Heart
J
RA
J'
RA
K
RV
K'
RV
L
LV
L'
LV
M
Heart
M'
Heart
N
RA
N'
RA
O
RV
O'
RV
P
LV
P'
LV

Figure 17. Molecular Analysis by *In Situ* of Compact and Trabecular Myocardium Markers in *Nkx2-5*$^{\Delta NK2SD/\Delta NK2SD}$ Mutant Hearts at E12.5.

(A-P') Histological sections of *Nkx2-5*$^{+/+}$ (A-P) and *Nkx2-5*$^{\Delta NK2SD/\Delta NK2SD}$ (A'-P') hearts at E12.5 hybridized with specific probes for: *Hey2* (A-D', *n* = 1), *Nppa* (E-H', *n* = 1), *Gja5* (I-L', *n* = 1) and *Mest* (M-P', *n* = 1). (A-A', E-E', I-I', M-M') Low magnification (5x) images showing a general overview of the whole heart. (B-B', F-F', J-J', N-N') High magnification (10x) images showing the RA region. (C-C', G-G', K-K', O-O') High magnification (10x) images showing the RV region. (D-D', H-H', L-L', P-P') High magnification (10x) images showing the LV region. Arrows have been used to highlight the similarities and differences in the staining between *Nkx2-5*$^{+/+}$ and *Nkx2-5*$^{\Delta NK2SD/\Delta NK2SD}$ hearts basing on the following code: white arrows in both WT and mutant hearts indicate no differences in the staining at the pointed region; normal black arrow in the WT heart and black arrowhead in the mutant heart indicates reduced expression of the analyzed gene in the pointed region; normal black arrow in the WT heart and thicker black arrow in the mutant heart indicates ectopic expression of the analyzed gene in the pointed region. AVC: atrioventricular canal; LA: left atria; RA: right atria; IVS: interventricular septum; LV: left ventricle; RV: right ventricle. Scale bar (A-A', E-E', I-I', M-M'): 390 μm; Scale Bar (B-D', F-H', J-L', N-P'): 190 μm.

Mest encodes for MESODERM-SPECIFIC TRANSCRIPTION HOMOLOG PROTEIN (MEST), which is involved in the differentiation of the trabecular myocardium from the compact layer during heart development [94]. In WT hearts at E12.5, *Mest* is expressed at high level in the trabeculae carnae (**Figure 17M, O, P**), but also in the ventricular compact layer (**Figure 17M, O, P**) and the atrial chambers (**Figure 17M, N**). Importantly, there is no *Mest* expression in the IVS (**Figure 17M, P**). *Mest* expression analysis in *Nkx2-5*$^{\Delta NK2SD/\Delta NK2SD}$ hearts showed normal expression in the LV (**Figure 17M', P'**). In contrast, *Mest* expression was downregulated in the RV (**Figure 17M', O'**) and the atrium (**Figure 17M', N'**), and displayed ectopic expression in the region of the presumptive IVS (**Figure 17M', P'**). These results suggest that *Nkx2-5* may be involved in the regulation of *Mest* expression in the atrial and RV regions and its repression in the IVS region.

In summary, the preliminary molecular analysis performed in *Nkx2-5*$^{\Delta NK2SD/\Delta NK2SD}$ mutants compared to WT identified changes in the expression patterns of chamber genes in the IVS providing the first evidence of the molecular defects behind the lack of IVS found in these mutant

hearts. Furthermore, the downregulation of these genes specifically in the right side of the heart predicts an important role of NKX2-5 in the control of RV development at later stages.

4.6.3. Expression Analysis of Endocardial Markers

Finally, the expression of N1ICD was analyzed by immunostaining in E11.5 and E12.5 *Nkx2-5*$^{\Delta NK2SD/\Delta NK2SD}$ mutant hearts compared to WT. The Notch signaling pathway has been described to play a crucial role in cardiovascular development. Moreover, there is a research line in the Harvey lab focused on studying how Notch1 controls the ECM dynamics during embryonic cardiogenesis. The normal expression pattern of this protein is exclusively in the endocardium of the developing hearts (**Figure 18A, B**). The immunostaining results showed that the N1ICD expression levels and pattern in the mutant hearts was unchanged at both embryonic stages analyzed (**Figure 18A', B'**). Therefore, our results suggest that Notch signaling pathway may not be responsible for the ECM and trabecular myocardium defects observed in the *Nkx2-5*$^{\Delta NK2SD/\Delta NK2SD}$ mutant hearts.

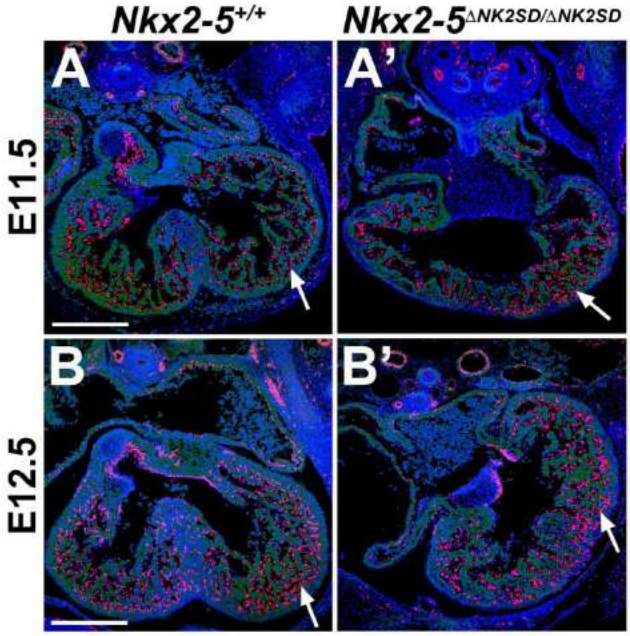

Figure 18. Immunofluorescence Analysis of the Active Form of Notch1 Receptor (N1ICD) in *Nkx2-5*$^{\Delta NK2SD/\Delta NK2SD}$ Mutant Hearts at E11.5 and E12.5.

(A-B') Confocal images of histological sections at the level of the heart region of *Nkx2-5*$^{+/+}$ (A, B) and *Nkx2-5*$^{\Delta NK2SD/\Delta NK2SD}$ (A', B') embryos at E11.5 (A, A'; *n*=1) and E12.5 (B, B'; *n*=1), stained for N1ICD (red), SMA (green mask) for myocardium labeling and DAPI (blue) for nuclear counterstaining. White arrows point N1ICD positive endocardial staining. Scale bar (A, A'): 290 µm; Scale Bar (B, B'): 390 µm.

5. Discussion

Nkx2-5 is a master gene on the very top of the cardiac kernel, expressed from early stages in development and a central regulator of key processes during cardiogenesis. Numerous studies in the last years using the powerful tools of genetics have provided new information about the binding partners of this TF, its target genes and novel functions in heart development and morphogenesis. Numerous mouse models based on *Nkx2-5* alterations have been generated, which faithfully reproduce congenital heart defects observed in humans and are currently used in CHD research. To date, all the studies have been mainly focused on studying the effects of genetic alteration in the HD, which is actually the most important domain of all genes in the homeobox superfamily. However, little is known about the importance and function of other NKX2-5 domains conserved in certain subsets of NK-2 proteins. This is the case of NK2SD, a domain exclusively present in the class I NK-2 group of TFs, from which the available information so far is very limited and scarce. The present study aimed to provide new insights on the importance of the NK2SD within the NKX2-5 TF and to unravel the possible function during heart development. The Harvey Lab generated a transgenic mouse line in which NK2SD was replaced by a Gly chain to preserve the 3D folding of the protein. After the corresponding validation of the line by extensive analysis by Southern Blot, PCR and sequencing, we performed the characterization of the newly generated cardiac mutant phenotype.

5.1. NK2SD deletion is embryonic lethal at two embryonic time points

As expected from the standard *Nkx2-5* KO line, heterozygous animals for the NK2SD mutation were viable and fertile and were born at normal Mendelian ratios. However, no *Nkx2-5*$^{\Delta NK2SD/\Delta NK2SD}$ mutant homozygotes were found at birth suggesting embryonic lethality. Genotyping analysis confirmed this hypothesis, proving the absence of homozygous mutant embryos from E13.5 onwards. Interestingly, the proportion of mutants did not recover Mendelian ratios at E12.5 or E11.5 and only E9.5 and E10.5 and earlier stages followed Mendelian ratios. At E11.5 the percentage of mutants experimented a first statistical significant drop. This reduction continued progressively from E11.5 to E13.5 and no mutant embryos were found in later stages. These results suggested the presence of two lethality points in the *Nkx2-5*$^{\Delta NK2SD/\Delta NK2SD}$ mutant embryos: one at E10.5 and the second one at E12.5. Therefore, the lack of the NK2SD domain in the NKX2-5 TF results in a dramatic outcome highlighting the importance of the domain for the normal NKX2-5 function during embryonic development. All deleterious genetic mutations

induce different mechanisms to compensate the lack of function of the defective proteins. Therefore, we hypothesize that the two lethality points identified for the *Nkx2-5*$^{\Delta NK2SD/\Delta NK2SD}$ mutants might be caused by variability in the compensatory mechanisms activated in the developing embryos as a consequence of the altered *Nkx2-5* function, resulting in early lethality in some embryos at E10.5 whereas the rest die at E12.5.

5.2. Two mutant embryonic phenotypes are clearly distinguishable in Nkx2-5$^{\Delta NK2SD/\Delta NK2SD}$ *embryos in early embryonic stages*

Once determined the embryonic lethality of the *Nkx2-5*$^{\Delta NK2SD/\Delta NK2SD}$ homozygous mouse embryos, we then proceeded to characterize the mutant embryonic phenotype. Although no obvious differences were observed at E8.5, the first defects were detected at E9.5 and E10.5 but only in some *Nkx2-5*$^{\Delta NK2SD/\Delta NK2SD}$ embryos. According to these phenotypic differences among mutants at the same embryonic stage, we classified them in two separate groups: embryos with a mild phenotype and embryos with a severe phenotype. Embryos from the mild group showed a similar embryonic appearance as WT embryos, and no obvious macroscopic differences were detected.

In contrast, embryos from the severe group, showed abnormalities which included an upward angle of the AVC and the LV relative the body of the embryo and a more linear heart tube shape. These changes in the orientation of the primitive heart tube within the pericardial cavity suggest defects in the process of cardiac looping undergoing at these stages. At E10.5, the severe mutant hearts were clearly delayed, appearing with a morphology closer to E9.5, suggesting arrested development at E9.5 embryonic stage. Indeed, these observations were confirmed by the necrotic signs found in the cardiac chambers at E10.5 confirming the compromised viability of the severe homozygotes. The clear differences in viability between the 2 mutant groups analyzed allowed us to determine that the mutant embryos included in the severe group correspond to the embryos responsible for the first drop in the proportion of *Nkx2-5*$^{\Delta NK2SD/\Delta NK2SD}$ mutant embryos found in litters. Similarly, the mutant embryos included in the mild group correspond to the embryos that survive the first lethality point and die at E12.5.

5.3. Severe Nkx2-5$^{\Delta NK2SD/\Delta NK2SD}$ *mutant cardiac phenotype is characterized by lack of AV demarcation, cardiac development arrest and increased ECM in early embryonic stages*

Nkx2-5$^{\Delta NK2SD/\Delta NK2SD}$ mutant hearts with a severe phenotype in early embryonic stages (E9.5 – E10.5) presented reduced elongation of the AVC groove and increased ECM. Implications of the

alterations in the amount of ECM in *Nkx2-5*$^{\Delta NK2SD/\Delta NK2SD}$ mutant hearts will be further discussed in the next section. Regarding the defects in the AVC region, previous research had already reported a link between *Nkx2-5* and the formation of the AVC during heart development. Indeed, in *Nkx2-5*$^{GFP/GFP}$ mutant mice, there is a total absence of AVC and the corresponding endocardial cushions [28]. Multiple studies on CHD patients showed the association between mutations in *Nkx2-5* and congenital defects on AV valves formation, especially on the tricuspid valve [72], structures that evolve from the AVC tissue in late cardiac development. Our results are in the same line, indicating a NK2SD-dependent role of NKX2-5 in AVC development and, likely, in valvulogenesis. Although the pathways involved in the *Nkx2-5* regulation of the AVC formation are still unknown, they have been well characterized for *Gata4* [95], one of the main binding partners of NKX2-5 and key member of the cardiac kernel. The NK2SD domain could be mediating the interaction between these two TF, which might be necessary for the activation of AVC specific genetic pathways.

Importantly, we believe that the morphological cardiac defects observed in severe *Nkx2-5*$^{\Delta NK2SD/\Delta NK2SD}$ mutant hearts are not catastrophic enough to be the reason promoting the embryonic death as early as at E10.5. Therefore, we hypothesize that the cause of death could be in defects on proper myocardium contraction associated to defective formation of sarcomeres in the CM or defects in cellular components involved in promoting the electrical coupling of the CM causing a conduction system failure. *Nkx2-5* plays a key role in the specification of myocardial tissue in conduction cells of the sinoatrial node, the AV node, the Purkinje fibers and the His bundle [55, 80, 96, 97]. Further investigation on these mutant embryos, focused on the study the heart beat and myocardial contraction together with the analysis of the components of the sarcomeres and cardiac protein channels will be conducted to confirm our hypothesis.

5.4. Mild Nkx2-5$^{\Delta NK2SD/\Delta NK2SD}$ *mutant cardiac phenotype is characterized by reduced cardiac size, lack of septation and increased ECM in late embryonic stages*

As discussed before, our data suggest that *Nkx2-5*$^{\Delta NK2SD/\Delta NK2SD}$ mutant embryos with a mild phenotype at early embryonic stages (E9.5 – E10.5) are the embryos most likely surviving until the second lethality point at E12.5. The hearts from these embryos at E11.5 and E12.5 presented several defects, including reduced heart size, complete absence of IAS and IVS, and increased ECM and trabecular complexity.

Defects in ECM thickness in the LV chambers from E9.5 until lethality has been a constant in our results from *Nkx2-5*$^{\Delta NK2SD/\Delta NK2SD}$ mutant hearts supported by area quantification analysis. Furthermore, thicker ECM was also present in *Nkx2-5*$^{GFP/GFP}$ mutant hearts. This is the first time these defect has been documented even though this mouse model has been available since 2000. *Nkx2-5* has been described to regulate ECM in blood vessels by activating the expression of collagen type I in vascular smooth muscle cells [98]. However, this report is the only study currently available in the literature on the possible role of *Nkx2-5* in ECM regulation. Nothing is known about how *Nkx2-5* could potentially control ECM formation and/or degradation in the heart. Indeed, the role of ECM during early ventricular chamber development is mostly unknown, as the field is mainly focused in the study of the myocardium and in less extent in the endocardium. The Harvey lab has been extensively conducting cutting-edge research on this topic in the last years. On this study, my supervisor Dr. Gonzalo del Monte Nieto has redefined cardiac ventricular development and in particular the process of trabeculation integrating endocardium, myocardium and ECM in a new paradigm-shifting model currently in revision in *Nature*. We believe ECM will become a hot topic in the cardiovascular field in the years to come and further investigation in our *Nkx2-5*$^{\Delta NK2SD}$ mouse line could be not only helpful but essential.

The *Nkx2-5* role in heart size during development has been previously documented. Gain-of-function studies in *Xenopus* and zebrafish embryos have shown hyperplastic hearts in the presence of high levels of *Nkx2-5* due to increased myocardial cell number [99, 100]. However, no data is available on how alterations in *Nkx2-5* affects heart size during mouse heart development. This project provides novel information which correlates with what has already been described in amphibians and fish models, suggesting that *Nkx2-5* may be required for proper heart growth during murine development. Moreover, *Nkx2-5* has been extensively described to be necessary for cardiomyocyte proliferation and growth. It is well-known that *Nkx2-5* suppresses BMP2/Smad1 signaling, which has a negative effect on the proliferative capabilities of cardiogenic precursors [29]. Therefore, based on our data, we can hypothesize that the NK2SD domain deletion might affect the ability of NKX2-5 to perform this inhibitory function on the BMP2/Smad1 signaling pathway. Indeed, the direct interaction between Smad1 and the NK2SD domain has been described in *Nkx3.2*, another member of the class I NK-2 family [48]. In addition, a genetic link between *Nkx2-5* and the Wnt signaling pathway, a key regulator of myocardial growth, has been recently reported . *Nkx2-5* upregulates the expression of *R-spondin3* during cardiogenesis, a potent Wnt agonist which enhances the proliferative capabilities of cardiogenic precursors [101]. We hypothesize that these defects in this pathway may be a

possible explanation for the *Nkx2-5*$^{\Delta NK2SD/NK2SD}$ phenotype we have described. Finally, NKX2-5 also binds and regulates the expression of multiple TFs and signaling molecules which are also involved in controlling myocardial growth and proliferation including GATA4, HOPX and BMP10 [102-104]. Therefore, NK2SD could also be involved in NKX2-5-dependent cardiac growth by mediating the binding capabilities of NKX2-5 to other TFs, which in turn could also be affecting the efficiency of NKX2-5 to bind its regulatory DNA sequences.

Finally, it is well-known *Nkx2-5* plays a key role on cardiac septation. Mutations in *Nkx2-5* have been clearly linked with atrial and ventricular defects in CHD patients [72, 75]. Moreover, murine models generated by *Nkx2-5* targeted mutation nicely reproduce the same atrial and ventricular septal defects observed in humans [80, 81]. However, there is a lack of knowledge on the genetic pathways downstream *Nkx2-5* related to heart septation. Due to the early expression of *Nkx2-5* in heart development and its position on top of the cardiac kernel, it is likely to be one of the master genes involved in activating the genetic pathways which guide the whole process of cardiac septation. Mutations in other master TFs which also sit on top of the cardiac kernel, such as *Gata4* and *Tbx5*, have also been linked to septal defects [105], confirming that NKX2-5 is not the only master TF required for proper developing of the IAS and the IVS. Due to the nature of the NK2SD domain, we believe its deletion is affecting the ability of NKX2-5 to bind protein partners also involved in the activation of the septal cardiac kernel subnetwork.

5.5. Nkx2-5$^{\Delta NK2SD/\Delta NK2SD}$ *mutant embryos present dramatic vascular defects affecting the cardinal veins*

The encapsulation of the heart in the body of the embryo from E11.5 onwards prevented us from detecting any obvious macroscopic morphological cardiac defect in the *Nkx2-5*$^{\Delta NK2SD/\Delta NK2SD}$ mutant embryos. However, these embryos showed large bleedings in the cephalic region between the limb buds and the head, especially evident at E12.5 suggesting the presence of vascular defects in the late *Nkx2-5*$^{\Delta NK2SD/\Delta NK2SD}$ mutants. Therefore, the cause of death for these mutants might not be only heart related but associated to defects in the vascular system as well. These findings unraveled a possible NK2SD-dependent role of NKX2-5 in vascular development.

Histological analysis on the major vessels ingressing and coming out from the heart revealed a dramatic increase in the size of both right and left cardinal veins in the *Nkx2-5*$^{\Delta NK2SD/\Delta NK2SD}$ mutant embryos at late embryonic stages. These findings clearly explain the bleedings detected in the cephalic region of the embryos at E11.5 and E12.5. Although the involvement of *Nkx2-5* in

vascular development is a mainly unexplored field, some links have recently appeared. For instance, it has been described NKX2-5 binds the promoter and directly regulates the expression of *Etv2*, a key gene involved in late vascular development [63]. Further research will be needed to explore the involvement of *Nkx2-5* in controlling genetic programs from vascular development, and confirm the observed defects in the *Nkx2-5*$^{\Delta NK2SD/\Delta NK2SD}$ mutant phenotype are due to the NK2SD deletion. Alternatively, the vascular defects observed could be also explained as a secondary effect originated from the cardiac phenotype. Therefore, it will be necessary to investigate whether the cause of death for *Nkx2-5*$^{\Delta NK2SD/\Delta NK2SD}$ mutant embryos at E12.5 is the cardiac or the vascular defects.

5.6. NK2SD replacement by a Gly chain does not affect the expression pattern of Nkx2-5 and the integrity of the protein

As mentioned before, it was of utmost importance to confirm the expression of *Nkx2-5* and the proper translocation of the mutant protein to the nucleus in the *Nkx2-5*$^{\Delta NK2SD/\Delta NK2SD}$ hearts in order to be able to relate the previously described cardiac defects to the absence of the NK2SD domain function and not to the lack of activity of the entire protein due to aberrant cellular localization or lack of expression. *In situ* hybridization data showed a homogenous pattern of *Nkx2-5* expression in the mutant hearts from E9.5 to E12.5. Nevertheless, less staining was detected at E9.5, E11.5 and E12.5, suggesting downregulation of *Nkx2-5* due to NK2SD deletion. Interestingly, NKX2-5 binds its own promoter and is believed to auto-regulate its own expression [106]. Therefore, the reduced expression of *Nkx2-5* in the *Nkx2-5*$^{\Delta NK2SD/\Delta NK2SD}$ mutant heart could be a consequence of impaired or reduced ability of NKX2-5 to activate its own promoter, and thus enhance its own transcriptional expression. This would imply the NK2SD domain is necessary for the proper establishment of the NKX2-5 regulatory positive feedback loop and this way keep *Nkx2-5* transcriptional levels in the physiological range during heart development. Nevertheless, further research is required to confirm this hypothesis including RT-qPCR analysis of *Nkx2-5* expression, DNA adenine methyltransferase identification (DamID) or chromatin immunoprecipitation assays (ChIP).

Immunofluorescence experiments revealed no major differences in *Nkx2-5* expression at the protein level in mutant hearts from E8.5 to E12.5. Similar to the WT situation, NKX2-5 staining was nuclear and exclusively in the myocardial tissue. Slight differences in the staining at some stages could lead to think NK2SD deletion might be affecting the translation of the Nkx2-5 mRNA. Nevertheless and as mentioned before, further analysis are required to determine if the

intensity differences observed between WT and mutant hearts, not consistent in the different stages analyzed are real changes in the relative expression of *Nkx2-5* or related to differences in the processing of the embryonic samples. Protein quantification by WB is required to answer this question. Therefore, our data proved the proper NKX2-5 protein expression and cellular localization suggesting that the NK2SD domain replacement for the chain of Gly allows normal translocation to the nucleus as it occurs with the WT NKX2-5.

5.7. Nkx2-5$^{\Delta NK2SD/\Delta NK2SD}$ embryos phenotype does not recapitulate the severe mutant phenotype of Nkx2-5$^{GFP/GFP}$ embryos

One of the main aims of this project was to determine if the role of the NK2SD domain was as critical for the proper NKX2-5 function that could result in a mutant phenotype comparable to the *Nkx2-5* full KO phenotype. In order to discard this possibility, we systematically compared all the results we obtained from the morphological characterization of the early *Nkx2-5*$^{\Delta NK2SD/\Delta NK2SD}$ hearts with *Nkx2-5*$^{GFP/GFP}$ hearts, searching for phenotypic differences. The first differences between both mouse models were detected in the embryonic lethality timing. As explained above, there are two embryonic lethality points in *Nkx2-5*$^{\Delta NK2SD/\Delta NK2SD}$ mutant mice at E10.5 and E12.5, which contrasts with the earlier lethality of *Nkx2-5*$^{GFP/GFP}$ mutant mice at E9.5. These results already suggested different and milder cardiac defects in *Nkx2-5*$^{\Delta NK2SD/\Delta NK2SD}$ embryos, which are viable for a longer period of time.

Embryonic phenotype comparison revealed essentially linear primitive heart tubes in *Nkx2-5*$^{\Delta NK2SD/\Delta NK2SD}$ mutant embryos showing a severe phenotype at E9.5. That phenotype is in the same line but less severe that the phenotype observed in *Nkx2-5*$^{GFP/GFP}$ embryos. This similarity supports the hypothesis that the phenotype may be caused by cardiac looping defects underlying the NK2SD deletion, defects well-characterized in the full KO mouse model [28]. However, important differences could be detected between both mutant phenotypes. *Nkx2-5*$^{GFP/GFP}$ embryos showed growth and developmental retardation, and their hearts exhibited clearly reduced AV groove, shorter AVC, deficits in the process of ventricular ballooning and pericardial edema. Importantly, none of these abnormalities were detected in the *Nkx2-5*$^{\Delta NK2SD/\Delta NK2SD}$ mutant homozygotes, what further supports the hypothesis of milder defects in the *Nkx2-5*$^{\Delta NK2SD/\Delta NK2SD}$ hearts even in its more severe form.

Finally, the histological analysis on H&E sections further confirmed the differences between the *Nkx2-5*$^{\Delta NK2SD/\Delta NK2SD}$ and *Nkx2-5*$^{GFP/GFP}$ mutant phenotypes. *Nkx2-5*$^{GFP/GFP}$ mutant hearts were

characterized by largely linear contours, no evidence of cardiac looping, chamber morphogenesis, elongation or narrowing of the AV region and lack of endocardial cushions. The whole atrium and ventricles formed an open monochamber, and the OFT was shorter and narrower. The heart wall was characterized by complete absence of trabeculation and increase amount of cardiac jelly compared to the WT. *Nkx2-5*$^{\Delta NK2SD/\Delta NK2SD}$ mutant hearts showed an extensively different phenotype: cardiac looping and chamber morphogenesis were present, the OFT was similar to the WT and the heart wall was normal, with the first signs of trabeculation although an increase in the amount of cardiac jelly was noticed. The only defect in common with the *Nkx2-5*$^{GFP/GFP}$ observed although in less severity in the *Nkx2-5*$^{\Delta NK2SD/\Delta NK2SD}$ severe mutants was the AV region formation that although it had proper endocardial cushions, presented elongation defects.

All these results together prove that the deletion of the NK2SD domain in the NKX2-5 protein promotes less catastrophic morphological defects in early cardiogenesis than the total lack of this TF. Thus we can conclude that the NK2SD domain is not critical for the role NKX2-5 plays during the early morphogenetic events during early heart development (E7.0 – E9.5).

5.8. Nkx2-5$^{\Delta NK2SD/\Delta NK2SD}$ *mutant hearts present aberrant expression patterns of key cardiac genes required for proper heart development and physiology*

Molecular analysis of gene expression in *Nkx2-5*$^{\Delta NK2SD/\Delta NK2SD}$ mutant hearts at E12.5 compared to the WT by *in situ* hybridization showed changes in the expression pattern and levels of four key cardiac genes involved in early chamber development: *Hey2*, *Nppa*, *Gja5* and *Mest*.

First main differences were observed in the IVS region of the mutant hearts. *Hey2*, a marker of the myocardial compact layer and the IVS, was downregulated in the presumptive IVS region in the *Nkx2-5*$^{\Delta NK2SD/\Delta NK2SD}$ mutant hearts. On the other hand, *Nppa* and *Mest*, normally expressed in the trabecular myocardium but not in the IVS, showed ectopic expression in the IVS region of the mutant hearts. Overall, the tissue in the region of the presumptive IVS in the *Nkx2-5*$^{\Delta NK2SD/\Delta NK2SD}$ hearts displays aberrant gene expression of trabecular myocardial genes and lack of expression of IVS markers, indicating aberrant differentiation of the IVS. Therefore, these results offer a molecular explanation for the histological morphological observations described above. The aberrant expression of these gene in the IVs most likely represents the lack of activation of the gen regulatory networks that prevents the IVS from differentiating into chamber myocardium (positive for *Nppa* and *Mest*) and therefore the morphology of the IVS myocardium of *Nkx2-*

5$^{\Delta NK2SD/\Delta NK2SD}$ mutant hearts clearly resembles the rest of the myocardium found in the nearby ventricular chambers.

It is also interesting to note that *Hey2*, *Gja5* and *Mest* were clearly downregulated specifically in the right side of the *Nkx2-5*$^{\Delta NK2SD/\Delta NK2SD}$ mutant hearts. *Hey2* is a key TF controlling several processes during heart development such as chamber maturation and AVC formation and development [107, 108]. Its total absence in the RV could explain to some extent the reduced size of the mutant hearts and the problems in the formation of the AVC endocardial cushions. *Gja5* encodes for CX40, a protein which forms part of the GAP junctions and thus is key for the proper contraction of the muscle tissue [92, 93]. Its downregulation in the right heart could be the evidence of a problem in the propagation of the electrical impulse necessary for heart contraction, which could result in an impaired or aberrant heartbeat. This supports our hypothesis of conduction defects as the cause of death of severe mutant embryos at E10.5, although expression analysis of these markers at early stages is necessary to make a final conclusion. Finally, *Mest* is involved in the regulation of trabecular myocardium differentiation from the compact layer during heart development [94]. Indeed, *Mest* KO mutant embryos show an increase in trabecular myocardium thickness [94]. Downregulation of *Mest* in the RV correlates with our results from the morphological analysis in which we observed increased convolution of the trabecular myocardium in the mutant RV. However, *Mest* expression was normal in the LV of these hearts, chamber in which increased convolution was also observed.

Overall, the defective expression of several genes in the right heart of the mutant embryos indicates that the NK2SD domain within the Nkx2-5 TF may be important for the control of the genes involved in the proper development of the right chambers. Interestingly, a role for *Nkx2-5* in the establishment of the right and left asymmetry of the heart has not been described before. Further research will be conducted studying the expression of other genes with restricted expression in different sides of the heart such as HAND2, only expressed in the RV [109, 110].

As mentioned before, the Harvey Lab is focused on the study of the importance of ECM dynamics in the process of heart development. Their recent results, included in the study currently in revision in *Nature*, showed that the Notch1 signaling pathway is critical in the regulation of ECM degradation critical for the proper morphogenesis of the ventricular chambers. Indeed, Notch1 is expressed in the endocardium and enhances ECM degradation. As previously discussed, our results from the morphological quantifications showed increased ECM in all the *Nkx2-5*$^{\Delta NK2SD/NK2SD}$ mutant hearts across the analyzed embryonic stages. With the aim to try to find

an explanation for these ECM defects, we checked for the expression of N1ICD by immunofluorescent staining at E11.5 and E12.5. Results showed no changes in the levels of N1ICD in the mutant hearts compared to the WT phenotype suggesting that the increase in ECM observed in these mutants is not associated to lack of activity of the Notch1 pathway and remove the possibility of Notch1 activity regulation by *Nkx2-5*.

Future Perspectives

As future plans, in the short term we plan to finish the morphological characterization analysis of the mutant hearts from E8.5 to E12.5. This will include completing the areas quantifications of the heart regions at E11.5 and E12.5, and the cardiac histological layers from E9.5 to E12.5. In addition, 3D reconstructions of the *Nkx2-5*$^{\Delta NK2SD/\Delta NK2SD}$ hearts that were started during the current study will be completed in order to further confirm the described mutant phenotype and maybe help to elucidate further abnormalities unnoticed in the 2D analysis. Whole mount immunostaining for alpha-smooth muscle actin (SMA), an early myocardial marker was performed in WT, *Nkx2-5*$^{\Delta NK2SD/\Delta NK2SD}$ with mild and severe phenotypes, and *Nkx2-5*$^{GFP/GFP}$ embryos at E9.5 or WT and *Nkx2-5*$^{\Delta NK2SD/\Delta NK2SD}$ mutants at E11.5 and E12.5 followed by confocal imaging hearts for E9.5 embryos, or optical projection tomography (OPT) for E11.5 and E12.5 hearts. Images were processed using the Amira® 6 software (FEI Visualization Services Group, USA) to segment the myocardial layer and generate the 3D reconstructions of the embryonic hearts. Indeed, these techniques have been carried out and optimized during this project and some preliminary data was obtained. However, due to the time constraints results were not ready to be presented in this thesis.

As mentioned before, aiming to further investigate the possible NK2SD-dependent auto-regulatory feedback loop, we would like to conduct quantitative assays to confirm the reduced expression of *Nkx2-5* in *Nkx2-5*$^{\Delta NK2SD/\Delta NK2SD}$ hearts, such as RT-qPCR and Western-Blot. Moreover, the binding affinity of NKX2-5$^{\Delta NK2SD}$ for its own promoter will be studied by DamID and ChIP sequencing assays.

We also plan to deepen in the molecular analysis which was already initiated in this project and whose resulting preliminary results are already very informative. The best approach considered is performing RNA sequencing (RNAseq) analysis on RNA samples at E11.5 and E9.5, embryonic stages in which the defects in the mutant hearts are already present but embryos are still not close enough to lethality to show secondary network decompensations. The resulting upregulated

and/or downregulated genes highlighted from the comparison with the RNAseq WT data will be further confirmed by RT-qPCR, *in situ* hybridization and immunofluorescent stainings.

In order to find out how the deletion of NK2SD affects the binding capabilities of NKX2-5 to other TFs and transcriptional cofactors, it would be interesting to perform immunoprecipitation assays with protein extracts from the mutant hearts. This could provide relevant and novel information about NKX2-5 binding partners and the complex pathways of the cardiac kernel network.

6. Conclusions

The present project has reached the following conclusions:

- NK2SD deletion is embryonic lethal at two embryonic time points (E10.5 and E12.5), suggesting the importance of the domain for normal NKX2-5 function.
- NK2SD deletion results in two clearly differentiated embryonic phenotypes: a mild one and a severe one.
- NK2SD deletion in severe mutants leads to AVC defects and increased cardiac ECM in early embryonic stages, similar but less severe than the standard *Nkx2-5* KO.
- NK2SD deletion in mild mutants leads to reduced heart size, septal defects, increased cardiac ECM and vascular abnormalities in late embryonic stages.
- NK2SD deletion results in aberrant gene expression patterns of key cardiac genes involved in chamber development, with the main defects localized in the IVS and the right side of the heart.
- The phenotype described for the *Nkx2-5*$^{\Delta NK2SD}$ homozygous embryos represents a less severe phenotype compared to the *Nkx2-5* full KO mutants, which allows the embryos to reach later stages of development and recapitulates some of the heart defects previously described in CHD associated to *Nkx2-5* heterozygous mutations in humans.
- The newly generated *Nkx2-5*$^{\Delta NK2SD}$ mouse line has been characterized as a valid murine CHD model which will be used for future investigation in the field.

References

1. Monte-Nieto, G.d., *Expression and functional analysis of Notch signalling during cardiac development with special focus on the epicardium and coronary vasculature.* 2011.
2. Anderson, R.H. and A.E. Becker, *Cardiac anatomy: Integrated text and colour atlas.* 1980: London: Churchill Livingstone, 1980.
3. Krishnan, A., et al., *A detailed comparison of mouse and human cardiac development.* Pediatric research, 2014. **76**(6): p. 500.
4. Moorman, A.F. and V.M. Christoffels, *Cardiac chamber formation: development, genes, and evolution.* Physiological reviews, 2003. **83**(4): p. 1223-1267.
5. Moorman, A., et al., *DEVELOPMENT OF THE HEART: (1) FORMATION OF THE CARDIAC CHAMBERS AND ARTERIAL TRUNKS.* Heart, 2003. **89**(7): p. 806-814.
6. Buckingham, M., S. Meilhac, and S. Zaffran, *Building the mammalian heart from two sources of myocardial cells.* Nature reviews. Genetics, 2005. **6**(11): p. 826.
7. Wessels, A. and R. Markwald, *Cardiac morphogenesis and dysmorphogenesis I. Normal development.* Developmental Biology Protocols: Volume II, 2000: p. 239-259.
8. Kaufman, M.H. and V. Navaratnam, *Early differentiation of the heart in mouse embryos.* Journal of anatomy, 1981. **133**(Pt 2): p. 235.
9. María, V., *Primitive Cardiac Segment, Normal Heart, and Congenital Heart Diseases*, in *Living Morphogenesis of the Heart*. 1998, Springer. p. 219-228.
10. Van Den Berg, G. and A.F. Moorman, *Concepts of cardiac development in retrospect.* Pediatric cardiology, 2009. **30**(5): p. 580-587.
11. Viragh, S. and C.E. Challice, *The origin of the epicardium and the embryonic myocardial circulation in the mouse.* The Anatomical Record, 1981. **201**(1): p. 157-168.
12. Komiyama, M., K. Ito, and Y. Shimada, *Origin and development of the epicardium in the mouse embryo.* Anatomy and embryology, 1987. **176**(2): p. 183-189.
13. Männer, J., et al., *The origin, formation and developmental significance of the epicardium: a review.* Cells Tissues Organs, 2001. **169**(2): p. 89-103.

14. Fananapazir, K. and M. Kaufman, *Observations on the development of the aortico-pulmonary spiral septum in the mouse.* Journal of anatomy, 1988. **158**: p. 157.

15. Sedmera, D., et al., *Developmental patterning of the myocardium.* The Anatomical Record, 2000. **258**(4): p. 319-337.

16. Savolainen, S.M., J.F. Foley, and S.A. Elmore, *Histology atlas of the developing mouse heart with emphasis on E11. 5 to E18. 5.* Toxicologic pathology, 2009. **37**(4): p. 395-414.

17. Anderson, R.H., N.A. Brown, and A.F. Moorman, *Development and structures of the venous pole of the heart.* Developmental dynamics, 2006. **235**(1): p. 2-9.

18. Eisenberg, L.M. and R.R. Markwald, *Molecular regulation of atrioventricular valvuloseptal morphogenesis.* Circulation research, 1995. **77**(1): p. 1-6.

19. Markwald, R.R., T.P. Fitzharris, and F.J. Manasek, *Structural development of endocardial cushions.* Developmental Dynamics, 1977. **148**(1): p. 85-119.

20. Runyan, R.B. and R.R. Markwald, *Invasion of mesenchyme into three-dimensional collagen gels: a regional and temporal analysis of interaction in embryonic heart tissue.* Developmental biology, 1983. **95**(1): p. 108-114.

21. Tian, X., et al., *Subepicardial endothelial cells invade the embryonic ventricle wall to form coronary arteries.* Cell research, 2013. **23**(9): p. 1075.

22. Wessels, A. and J. Pérez-Pomares, *The epicardium and epicardially derived cells (EPDCs) as cardiac stem cells.* The anatomical record, 2004. **276**(1): p. 43-57.

23. Pérez-Pomares, J.M., et al., *The origin of the subepicardial mesenchyme in the avian embryo: an immunohistochemical and quail–chick chimera study.* Developmental biology, 1998. **200**(1): p. 57-68.

24. Kálmán, F., S. Virágh, and L. Módis, *Cell surface glycoconjugates and the extracellular matrix of the developing mouse embryo epicardium.* Anatomy and embryology, 1995. **191**(5): p. 451-464.

25. Spitz, F. and E.E. Furlong, *Transcription factors: from enhancer binding to developmental control.* Nature reviews. Genetics, 2012. **13**(9): p. 613.

26. Davidson, E.H. and D.H. Erwin, *Gene regulatory networks and the evolution of animal body plans.* Science, 2006. **311**(5762): p. 796-800.

27. Waardenberg, A.J., et al., *Genetic networks governing heart development.* Cold Spring Harbor perspectives in medicine, 2014. **4**(11): p. a013839.

28. Lyons, I., et al., *Myogenic and morphogenetic defects in the heart tubes of murine embryos lacking the homeo box gene Nkx2-5.* Genes & development, 1995. **9**(13): p. 1654-1666.

29. Prall, O.W., et al., *An Nkx2-5/Bmp2/Smad1 negative feedback loop controls heart progenitor specification and proliferation.* Cell, 2007. **128**(5): p. 947-959.

30. Stennard, F.A., et al., *Murine T-box transcription factor Tbx20 acts as a repressor during heart development, and is essential for adult heart integrity, function and adaptation.* Development, 2005. **132**(10): p. 2451-2462.

31. Watt, A.J., et al., *GATA4 is essential for formation of the proepicardium and regulates cardiogenesis.* Proceedings of the National Academy of Sciences of the United States of America, 2004. **101**(34): p. 12573-12578.

32. Chen, J.X., K. Plonowska, and S.M. Wu, *Somatic cell reprogramming into cardiovascular lineages.* Journal of cardiovascular pharmacology and therapeutics, 2014. **19**(4): p. 340-349.

33. Ieda, M., et al., *Direct reprogramming of fibroblasts into functional cardiomyocytes by defined factors.* Cell, 2010. **142**(3): p. 375-386.

34. Shashikant, C., et al., *Homeobox genes in mouse development.* Critical reviews in eukaryotic gene expression, 1991. **1**(3): p. 207-245.

35. Scott, M.P., J.W. Tamkun, and G.W. Hartzell, *The structure and function of the homeodomain.* Biochimica et Biophysica Acta (BBA)-Reviews on Cancer, 1989. **989**(1): p. 25-48.

36. Hayashi, S. and M.P. Scott, *What determines the specificity of action of Drosophila homeodomain proteins?* Cell, 1990. **63**(5): p. 883-894.

37. Rosenthal, N. and R.P. Harvey, *Heart development and regeneration*. Vol. 1. 2010: Academic Press.

38. McGinnis, W. and R. Krumlauf, *Homeobox genes and axial patterning.* Cell, 1992. **68**(2): p. 283-302.

39. Harvey, R.P., *NK-2homeobox genes and heart development.* Developmental biology, 1996. **178**(2): p. 203-216.

40. Tsao, D.H., et al., *Elongation of helix III of the NK-2 homeodomain upon binding to DNA: a secondary structure study by NMR.* Biochemistry, 1994. **33**(50): p. 15053-15060.

41. Smith, S.T. and J.B. Jaynes, *A conserved region of engrailed, shared among all en-, gsc-, Nk1-, Nk2-and msh-class homeoproteins, mediates active transcriptional repression in vivo.* Development, 1996. **122**(10): p. 3141-3150.

42. Tolkunova, E.N., et al., *Two distinct types of repression domain in engrailed: one interacts with the groucho corepressor and is preferentially active on integrated target genes.* Molecular and cellular biology, 1998. **18**(5): p. 2804-2814.

43. Gasperowicz, M. and F. Otto, *Mammalian Groucho homologs: redundancy or specificity?* Journal of cellular biochemistry, 2005. **95**(4): p. 670-687.

44. Masson, N., W.K. Greene, and T.H. Rabbitts, *Optimal activation of an endogenous gene by HOX11 requires the NH2-terminal 50 amino acids.* Molecular and cellular biology, 1998. **18**(6): p. 3502-3508.

45. Evans, S.M. *Vertebrate tinman homologues and cardiac differentiation*. in *Seminars in cell & developmental biology*. 1999. Elsevier.

46. Watada, H., et al., *Intramolecular control of transcriptional activity by the NK2-specific domain in NK-2 homeodomain proteins.* Proceedings of the National Academy of Sciences, 2000. **97**(17): p. 9443-9448.

47. Uhler, J., et al., *The Nk-2 box of the Drosophila homeodomain protein, Vnd, contributes to its repression activity in a Groucho-dependent manner.* Mechanisms of development, 2007. **124**(1): p. 1-10.

48. Kim, D.-W. and A.B. Lassar, *Smad-dependent recruitment of a histone deacetylase/Sin3A complex modulates the bone morphogenetic protein-dependent transcriptional repressor activity of Nkx3. 2.* Molecular and cellular biology, 2003. **23**(23): p. 8704-8717.

49. Elliott, D.A., et al., *A tyrosine-rich domain within homeodomain transcription factor Nkx2-5 is an essential element in the early cardiac transcriptional regulatory machinery.* Development, 2006. **133**(7): p. 1311-1322.

50. Evans, S.M., et al., *tinman, a Drosophila homeobox gene required for heart and visceral mesoderm specification, may be represented by a family of genes in vertebrates: XNkx-2.3, a second vertebrate homologue of tinman.* Development, 1995. **121**(11): p. 3889-3899.

51. Lints, T.J., et al., *Nkx-2.5: a novel murine homeobox gene expressed in early heart progenitor cells and their myogenic descendants.* Development, 1993. **119**(2): p. 419-431.

52. Stanley, E.G., et al., *Efficient Cre-mediated deletion in cardiac progenitor cells conferred by a 3'UTR-ires-Cre allele of the homeobox gene Nkx2-5.* International Journal of Developmental Biology, 2004. **46**(4): p. 431-439.

53. Christoffels, V.M., et al., *Formation of the venous pole of the heart from an Nkx2–5–negative precursor population requires Tbx18.* Circulation research, 2006. **98**(12): p. 1555-1563.

54. Tanaka, M., et al., *The cardiac homeobox gene Csx/Nkx2. 5 lies genetically upstream of multiple genes essential for heart development.* Development, 1999. **126**(6): p. 1269-1280.

55. Biben, C., et al., *Cardiac septal and valvular dysmorphogenesis in mice heterozygous for mutations in the homeobox gene Nkx2-5.* Circulation research, 2000. **87**(10): p. 888-895.

56. Azpiazu, N. and M. Frasch, *tinman and bagpipe: two homeo box genes that determine cell fates in the dorsal mesoderm of Drosophila.* Genes & Development, 1993. **7**(7b): p. 1325-1340.

57. Bodmer, R., *The gene tinman is required for specification of the heart and visceral muscles in Drosophila.* Development, 1993. **118**(3): p. 719-729.

58. Biben, C. and R.P. Harvey, *Homeodomain factor Nkx2-5 controls left/right asymmetric expression of bHLH gene eHand during murine heart development.* Genes & development, 1997. **11**(11): p. 1357-1369.

59. Mommersteeg, M.T., et al., *Molecular pathway for the localized formation of the sinoatrial node.* Circulation research, 2007. **100**(3): p. 354-362.

60. Mommersteeg, M.T., et al., *Pitx2c and Nkx2-5 are required for the formation and identity of the pulmonary myocardium.* Circulation research, 2007. **101**(9): p. 902-909.

61. Hatcher, C.J. and C.T. Basson, *Specification of the cardiac conduction system by transcription factors.* Circulation research, 2009. **105**(7): p. 620-630.

62. Moskowitz, I.P., et al., *A molecular pathway including Id2, Tbx5, and Nkx2-5 required for cardiac conduction system development.* Cell, 2007. **129**(7): p. 1365-1376.

63. Ferdous, A., et al., *Nkx2–5 transactivates the Ets-related protein 71 gene and specifies an endothelial/endocardial fate in the developing embryo.* Proceedings of the National Academy of Sciences, 2009. **106**(3): p. 814-819.

64. Wessels, M. and P. Willems, *Genetic factors in non-syndromic congenital heart malformations.* Clinical genetics, 2010. **78**(2): p. 103-123.

65. Fahed, A., et al., *Genetics of congenital heart disease: the glass half empty (vol 112, pg 707, 2013).* Circulation Research, 2013. **112**(12): p. E182-E182.

66. Van Der Bom, T., et al., *The changing epidemiology of congenital heart disease.* Nature Reviews Cardiology, 2011. **8**(1): p. 50-60.

67. Brickner, M.E., L.D. Hillis, and R.A. Lange, *Congenital heart disease in adults.* New England Journal of Medicine, 2000. **342**(4): p. 256-263.

68. Benson, D.W., et al., *Reduced penetrance, variable expressivity, and genetic heterogeneity of familial atrial septal defects.* Circulation, 1998. **97**(20): p. 2043-2048.

69. Elliott, D.A., et al., *Cardiac homeobox gene NKX2-5mutations and congenital heart disease.* Journal of the American College of Cardiology, 2003. **41**(11): p. 2072-2076.

70. Benson, D.W., *Genetic origins of pediatric heart disease.* Pediatric cardiology, 2010. **31**(3): p. 422-429.

71. Schott, J.-J., et al., *Congenital heart disease caused by mutations in the transcription factor NKX2-5.* Science, 1998. **281**(5373): p. 108-111.

72. Benson, D.W., et al., *Mutations in the cardiac transcription factor NKX2. 5 affect diverse cardiac developmental pathways.* Journal of Clinical Investigation, 1999. **104**(11): p. 1567.

73. König, K., et al., *Familial congenital heart disease, progressive atrioventricular block and the cardiac homeobox transcription factor gene NKX2. 5.* Clinical research in cardiology, 2006. **95**(9): p. 499-503.

74. Gutierrez-Roelens, I., et al., *Progressive AV-block and anomalous venous return among cardiac anomalies associated with two novel missense mutations in the CSX/NKX2-5 gene*. Human mutation, 2002. **20**(1): p. 75-76.

75. Posch, M.G., et al., *Molecular genetics of congenital atrial septal defects.* Clinical research in cardiology, 2010. **99**(3): p. 137-147.

76. Sarkozy, A., et al., *Spectrum of atrial septal defects associated with mutations of NKX2. 5 and GATA4 transcription factors.* Journal of Medical Genetics, 2005. **42**(2): p. e16-e16.

77. Gutierrez-Roelens, I., et al., *A novel CSX/NKX2-5 mutation causes autosomal-dominant AV block: are atrial fibrillation and syncopes part of the phenotype?* European journal of human genetics: EJHG, 2006. **14**(12): p. 1313.

78. Kasahara, H., et al., *Loss of function and inhibitory effects of human CSX/NKX2. 5 homeoprotein mutations associated with congenital heart disease.* Journal of Clinical Investigation, 2000. **106**(2): p. 299.

79. Kasahara, H. and D.W. Benson, *Biochemical analyses of eight NKX2. 5 homeodomain missense mutations causing atrioventricular block and cardiac anomalies.* Cardiovascular Research, 2004. **64**(1): p. 40-51.

80. Furtado, M.B., et al., *Point mutations in murine Nkx2-5 phenocopy human congenital heart disease and induce pathogenic Wnt signaling.* JCI insight, 2017. **2**(6).

81. Tanaka, M., et al. *A mouse model of congenital heart disease: cardiac arrhythmias and atrial septal defect caused by haploinsufficiency of the cardiac transcription factor Csx/Nkx2. 5*. in *Cold Spring Harbor symposia on quantitative biology*. 2002.

82. Moon, A., *Mouse models of congenital cardiovascular disease.* Current topics in developmental biology, 2008. **84**: p. 171-248.

83. Bruneau, B.G., *Mouse models of cardiac chamber formation and congenital heart disease.* Trends in Genetics, 2002. **18**(6): p. S15-S20.

84. Chen, Z., G.A. Friedrich, and P. Soriano, *Transcriptional enhancer factor 1 disruption by a retroviral gene trap leads to heart defects and embryonic lethality in mice.* Genes & development, 1994. **8**(19): p. 2293-2301.

85. Jacks, T., et al., *Tumour predisposition in mice heterozygous for a targeted mutation in Nf1*. Nature genetics, 1994. **7**(3): p. 353-361.

86. Fischer, A., et al., *The Notch target genes Hey1 and Hey2 are required for embryonic vascular development.* Genes & development, 2004. **18**(8): p. 901-911.

87. Xiang, F., et al., *Transcription factor CHF1/Hey2 suppresses cardiac hypertrophy through an inhibitory interaction with GATA4.* American Journal of Physiology-Heart and Circulatory Physiology, 2006. **290**(5): p. H1997-H2006.

88. Fischer, A., et al., *Hey basic helix-loop-helix transcription factors are repressors of GATA4 and GATA6 and restrict expression of the GATA target gene ANF in fetal hearts.* Molecular and cellular biology, 2005. **25**(20): p. 8960-8970.

89. Macchia, D.D., *Atrial natriuretic factor: a hormone secreted by the heart.* Pharmaceutisch Weekblad, 1987. **9**(6): p. 305-314.

90. Ogawa, T. and A.J. de Bold, *The heart as an endocrine organ.* Endocrine connections, 2014. **3**(2): p. R31-R44.

91. Lee, Y., et al., *The cardiac tissue-restricted homeobox protein Csx/Nkx2. 5 physically associates with the zinc finger protein GATA4 and cooperatively activates atrial natriuretic factor gene expression.* Molecular and cellular biology, 1998. **18**(6): p. 3120-3129.

92. Desplantez, T., *Cardiac Cx43, Cx40 and Cx45 co-assembling: involvement of connexins epitopes in formation of hemichannels and Gap junction channels.* BMC cell biology, 2017. **18**(1): p. 3.

93. Kirchhoff, S., et al., *Reduced cardiac conduction velocity and predisposition to arrhythmias in connexin40-deficient mice.* Current biology, 1998. **8**(5): p. 299-302.

94. King, T., et al., *Expression of Peg1 (Mest) in the developing mouse heart: involvement in trabeculation.* Developmental dynamics, 2002. **225**(2): p. 212-215.

95. Stefanovic, S., et al., *GATA-dependent regulatory switches establish atrioventricular canal specificity during heart development.* Nature communications, 2015. **5**.

96. Thomas, P.S., et al., *Elevated expression of Nkx-2.5 in developing myocardial conduction cells.* The Anatomical Record, 2001. **263**(3): p. 307-313.

97. Jay, P.Y., et al., *Nkx2-5 mutation causes anatomic hypoplasia of the cardiac conduction system.* Journal of Clinical Investigation, 2004. **113**(8): p. 1130.

98. Ponticos, M., et al., *Regulation of collagen type I in vascular smooth muscle cells by competition between Nkx2. 5 and δEF1/ZEB1.* Molecular and cellular biology, 2004. **24**(14): p. 6151-6161.

99. Cleaver, O.B., K.D. Patterson, and P.A. Krieg, *Overexpression of the tinman-related genes XNkx-2.5 and XNkx-2.3 in Xenopus embryos results in myocardial hyperplasia.* Development, 1996. **122**(11): p. 3549-3556.

100. Chen, J.-N. and M.C. Fishman, *Zebrafish tinman homolog demarcates the heart field and initiates myocardial differentiation.* Development, 1996. **122**(12): p. 3809-3816.

101. Cambier, L., et al., *Nkx2-5 regulates cardiac growth through modulation of Wnt signaling by R-spondin3.* Development, 2014. **141**(15): p. 2959-2971.

102. Zeisberg, E.M., et al., *Morphogenesis of the right ventricle requires myocardial expression of Gata4.* Journal of Clinical Investigation, 2005. **115**(6): p. 1522.

103. Shin, C.H., et al., *Modulation of cardiac growth and development by HOP, an unusual homeodomain protein.* Cell, 2002. **110**(6): p. 725-735.

104. Chen, H., et al., *BMP10 is essential for maintaining cardiac growth during murine cardiogenesis.* Development, 2004. **131**(9): p. 2219-2231.

105. Yang, Y.-Q., et al., *Novel GATA4 mutations in patients with congenital ventricular septal defects.* Medical science monitor: international medical journal of experimental and clinical research, 2012. **18**(6): p. CR344.

106. Bouveret, R., et al., *NKX2-5 mutations causative for congenital heart disease retain functionality and are directed to hundreds of targets.* Elife, 2015. **4**: p. e06942.

107. Rutenberg, J.B., et al., *Developmental patterning of the cardiac atrioventricular canal by Notch and Hairy-related transcription factors.* Development, 2006. **133**(21): p. 4381-4390.

108. Kokubo, H., et al., *Hesr1 and Hesr2 regulate atrioventricular boundary formation in the developing heart through the repression of Tbx2.* Development, 2007. **134**(4): p. 747-755.

109. Tsuchihashi, T., et al., *Hand2 function in second heart field progenitors is essential for cardiogenesis.* Developmental biology, 2011. **351**(1): p. 62-69.

110. McFadden, D.G., et al., *The Hand1 and Hand2 transcription factors regulate expansion of the embryonic cardiac ventricles in a gene dosage-dependent manner*. Development, 2005. **132**(1): p. 189-201.

Declaration of Research Integrity and Good Scientific Practice

I hereby certify that I have authored this Master's Thesis entitled "Characterization of a novel *Nkx2-5* mutant mouse model for Congenital Heart Disease" and without undue assistance from third parties. No other than the resources and references indicated in this thesis have been used. I have marked both literal and accordingly adopted quotations as such. They were no additional persons involved in the spiritual preparation of the present thesis. I am aware that violations of this declaration may lead to subsequent withdrawal of the degree.

Sydney, 10/08/2017

Ricardo Moreno Traspas